A Szilikátipari Tudományos Egyesület lapja

építőanyag

Journal of Silicate Based and Composite Materials

A TARTALOMBÓL:

2024/1

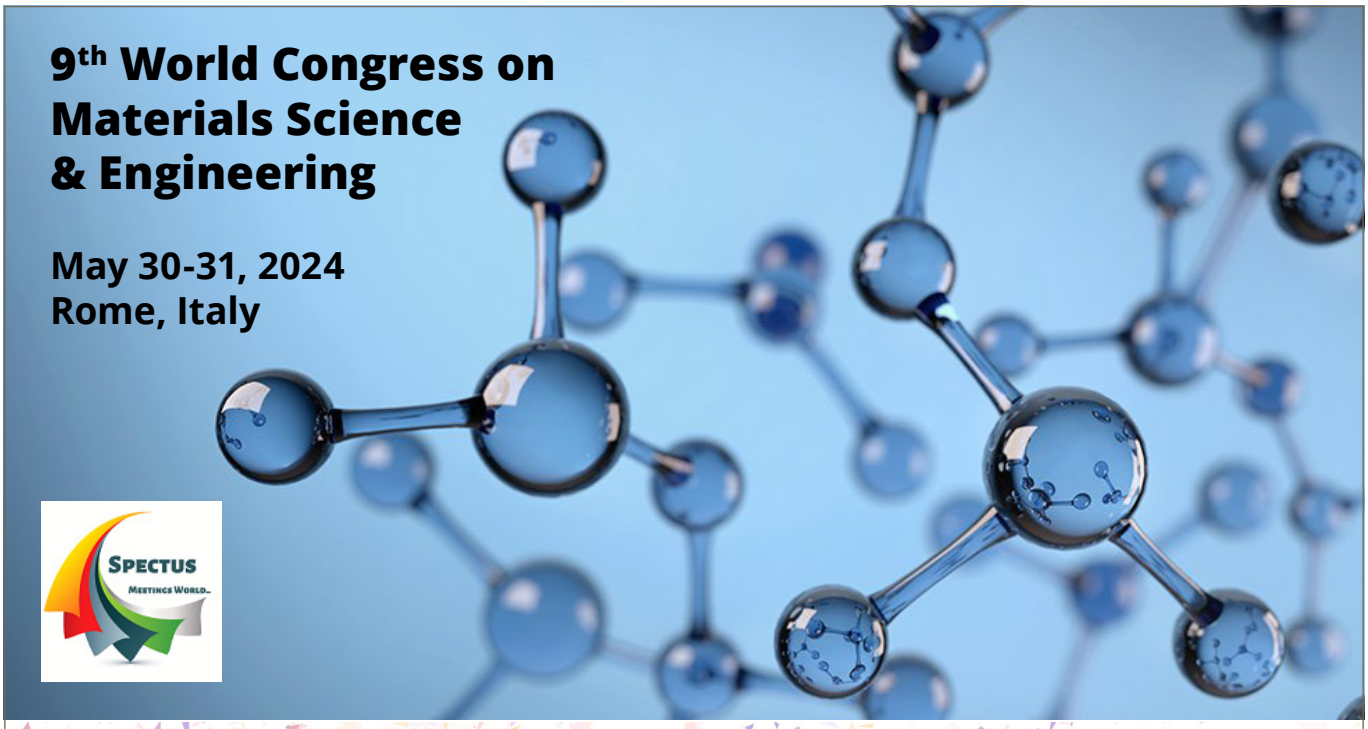

9th World Congress on Materials Science & Engineering

May 30-31, 2024
Rome, Italy

About the Conference

Material Science 2024 Heart fully welcomes every one of the members from everywhere the globe to join the 9th World Congress on Materials Science and Engineering. This year's event will be held on May 30-31, 2024 which is scheduled at the beautiful city of Rome, Italy. The main theme: Innovative Approach and Recent Developments in Materials Science and Engineering.

The MATCON 2024 will be a 2 days event that means to gather the key players of the Materials Science and Engineering community and related sectors. This event is launched with the aims to become an established event, attracting global participants, intent on sharing, exchanging and exploring new avenues of Materials Science and Engineering related scientific and commercial developments.

We will be really glad if you could join with us at Rome Italy or virtually from your place as it is hybrid event. Materials Science 2024 will be a platform of interactions for experts around the world and aims to accelerate scientific discoveries.

This conference includes keynote presentations, oral presentations, plenary talks, young research forums, poster presentations, student forum, technical workshop, symposia, start-up opportunities and meet the professors sessions. The scientific program features world-renowned experts and aspiring young researchers.

Looking forward to see you soon at Rome Italy during May 30-31, 2024.

spectusconferences.com/materials-science-conference

építőanyag

Journal of Silicate Based and Composite Materials

2024/1

TARTALOM

CONTENT

A finomkerámia-, üveg-, cement-, mész-, beton-, tégla- és cserép-, kő- és kavics-, tűzállóanyag-, szigetelőanyag-iparágak szakmai lapja
Scientific journal of ceramics, glass, cement, concrete, clay products, stone and gravel, insulating and fireproof materials and composites

A folyóiratot referálja · The journal is referred by:
ProQuest · Google Scholar · INDEX COPERNICUS INTERNATIONAL · THOMSON REUTERS

A folyóiratban lektorált cikkek jelennek meg.
All published papers are peer-reviewed.
Kiadó · Publisher: Szilikátipari Tudományos Egyesület (SZTE)
Elnök · President: ASZTALOS István
1034 Budapest, Bécsi út 120.
Tel.: +36-1/201-9360 ▪ E-mail: epitoanyag@szte.org.hu
Tördelő szerkesztő · Layout editor: NÉMETH Hajnalka
Címlapfotó · Cover photo: SIMON Andrea

WWW.EPITOANYAG.ORG.HU
EN.EPITOANYAG.ORG.HU

Online ISSN: 2064-4477
Print ISSN: 0013-970x
INDEX: 2 52 50 ▪ 76 (2024) 1-40

Vol. 76, No. 1

Thermophysical and mechanical properties plaster of Paris Ceilings modified with oil palm mesocarp fibre for application in buildings

Armstrong Udochukwu ANONABA ▪ Department of Industrial Physics, Faculty of Physical Sciences, Abia State University, Uturu, Abia State, Nigeria ▪ anonaba.armstrong@abiastateuniversity.edu.ng

Francis Chukwuemeka EZE ▪ Department of Physics, Faculty of Physical Sciences, Federal University of Technology, Owerri, Imo State, Nigeria

Israel Chukwuemeka NDUKWE ▪ Department of Physics, Faculty of Physical Sciences, Federal University of Technology, Owerri, Imo State, Nigeria

Chinedu IROEGBU ▪ Department of Physics, Faculty of Physical Sciences, Federal University of Technology, Owerri, Imo State, Nigeria

Érkezett: 2023. 06. 21. ▪ Received: 21. 06. 2023. ▪ https://doi.org/10.14382/epitoanyag-jsbcm.2024.1

Abstract

This study is aimed at assessing the practicability of harnessing the properties of the plaster of Paris (POP) ceiling to improve its use in thermal insulation by combining it with oil palm mesocarp fiber (OPMF). Various weight proportions of the OPMF were used to replace the POP during the fabrication of the samples. A drying process was applied to all the samples used for the study. The results obtained showed that the addition of filtered OPMF to the POP matrix improved from 0% to 40%, the change in mean values of water absorption, bulk density, thermal conductivity, specific heat capacity, thermal diffusivity, heat flow time, flakiness, and flexural strength (12.22 – 25.75) %, (1.768 – 1.407) 10^3 kgm^{-3}, (0.2245 – 0.1465) $Wm^{-1}K^{-1}$, (1.498 – 1.825) 10^3 $Jkg^{-1}K^{-1}$, (8.477 – 5.705) 10^{-8} m^2s^{-1}, (9.64 – 14.37) mins., (0.65 – 2.08) %, and (3.02 – 1.38) N/mm^2 respectively. The study showed that the addition of the OPMF to the POP matrix enhanced the efficiency of POP as a ceiling material with excellent heat-insulating ability and could be effective in buildings. If this model is effectively implemented, it would not only be useful as a good thermal insulator but also help mitigate the pollution usually experienced as a result of improper disposal of oil palm fiber.

Keywords: bulk density, flakiness, flexural strength, heat flow time, thermal insulation

Kulcsszavak: térfogatsűrűség, pelyhesedés, hajlítószilárdság, hőáramlási idő, hőszigetelés

Armstrong Udochukwu ANONABA
Lecturer II at the Department of Industrial Physics, Abia State University, Uturu, Abia State, Nigeria. His research interests include Solid State Physics and Materials Science.

Francis Chukwuemeka EZE
Professor at the Department of Physics, Federal University of Technology, Owerri, Imo State, Nigeria. A specialist in Experimental Solid State Physics and Materials Science.

Israel Chukwuemeka NDUKWE
Professor at the Department of Physics, Federal University of Technology, Owerri, Imo State, Nigeria. A specialist in Solid State Physics and Materials Science.

Chinedu IROEGBU
Reader at the Department of Physics, Federal University of Technology, Owerri, Imo State, Nigeria. A specialist in Solid State Physics and Materials Science.

1. Introduction

All buildings require a protective covering against heat generated from either the natural environment or human factors. One such covering is the ceiling. Globally, there are need for ceiling materials, at least, if not for the ecstasy to buildings, the protection against heat is very essential [1]. It has been the interest of researchers to convert raw materials into a finished product of interest. The production of ceilings from natural raw materials is no exception. Several raw materials such as sugarcane leaves [2], coconut leaflet [3], breadfruit seed coat [4], and cassava stalk [5] have been modified to generate ceilings. There have been several research on the production of sheets from a combined mixture of newspaper and coconut shell [6], residue from sugar beet [7], rattan particles [8], rice shell [9], and pineapple [10], etc possess desirable properties for use as ceilings in buildings. Again, ceilings produced from carton papers and tiger nut fiber [11], processed and unprocessed coconut shells [12], banana peels and leaves, and sawdust [13] have the potential to be converted to ceiling materials when the right compositions of the material are met. Ihueze et al [14] confirmed in their study that raw materials from the environment confer several benefits because of their ability to fit into several designs of the owner.

In situations nailing of the said panels is suspected to cause either significant damage during their installation or bring about an excessive rise in building construction cost, resorting to plaster of Paris (POP) is an option for consideration. This conventional ceiling is preferable because it poses no significant health risk, has resistance to heat, and shows no easy susceptibility to water from a leaked roof unlike in the case of using asbestos, polyvinyl chloride, and plywood respectively [15]. Unfortunately, emphasis on increased access to sufficient, safe, and inexpensive housing for the world's poorest people in slumbs by the year 2030 as provided in Goal II of the United Nations (UN) 2030 Agenda for Sustainable Development [16] appears to yield no result due to incessant rise in the cost of POP which has contributed a great deal to bane in sustainable housing development in developing countries [15]. So far, few studies reported on how to minimize the cost of applying POP ceiling some of which focussed on its modification with rice husk ash [17], groundnut seed coat and waste newspaper paste [18], rattan [19], and wood dust and waste paper ash [15] utilized as fillers. Findings from these studies have shown that recyclable solid wastes differ in their potential, thus warranting the quest for utilization of other such wastes.

This research is designed to modify POP ceilings with oil palm mesocarp fiber for application in buildings. The mesocarp fiber

is a typical biomass generated during palm oil extraction. Its use as boiler fuel [20 – 22], mulching medium [23] as well as for production of biogas [24] and acetoin [25] have been reported. Even at that, a vast amount of waste is generated and this could ensure sustainability in its applications. Unfortunately, it is majorly under-utilized, a situation that warrants its disposal by open burning or indiscriminate dumping thereby causing serious problems to the environment and public health [26]. Loh [27] noted that palm oil mills in Malaysia generate a total of 7.72 million tons of fibre yearly. As averred by Rizal et al [28], processing every 100,000 tons of oil palm fruit for oil could generate 15,700 tons of fiber. Based on their findings, Hambali and Rivai [29] remarked that due to increasing demand for crude palm oil would cause a continuous rise in fibre generation from 21,560,251 tons in 2020 to about 30,732,801 tons in 2030. This agrees with the assertion of Robert et al [30] solid waste volume may continue to accelerate throughout this century as ineffective solid waste management systems persist in Nigeria and other developing countries. Specifically, the thermophysical and mechanical properties of the new products will be evaluated to determine their suitability in building design.

2. Research methodology

2.1 Materials collection and description

Potable water (from bore hole), POP powder (from a building construction site), oil palm mesocarp fiber (from a palm oil mill), and detergent were utilized as major materials in this work. The materials were sourced in large quantities within Uturu, Abia State, Nigeria.

2.2 Processing and analysis of the fiber

In order to remove any remaining oil and enhance adhesion with the POP matrix, the fiber was washed with detergent and then water. After that, it was sun-dried until it became moisture-free. The dried material was pulverized by means of a local pepper grinder. This was followed by screening and the quantity of it that passed through a standard sieve having 2-mm openings was coded OPMF. Gradation of the OPMF was performed by sieve analysis [31]. Also, a reasonable quantity of it was analyzed for chemical composition [32].

2.3 Preparation of samples

The OPMF was utilized as filler at various weight replacement levels with the POP to produce ceiling samples. In each case, three representative samples were developed per formulation and the water-to-composite mix ratio was maintained at 2:5 by weight. *Fig. 1.* illustrates the sequence of the processes involved. Those meant for assessment of thermophysical properties were formed in circular molds measuring 110 mm in diameter and 7 mm in thickness whereas the ones prepared for investigation of mechanical properties were formed in molds of dimensions 160 mm x 120 mm x 14 mm. The cast mixtures were kept for 10 minutes under ambient conditions and then after, subjected to continuous sun-drying and weighing until there was further reduction in the mass of each of them. All the fabricated samples were tested as intended for them in this research.

Fig. 1 Pictorial illustration of the samples fabrication processes
1. ábra A minták gyártási folyamata

2.4 Tests implementation

Water absorption

This test was necessary in order gain an insight into the ability of the samples to absorb and retain water in the case of leakage from the roof of a building. The method of immersion was employed for its determination in this work [31]. Each sample was weighed before being immersed in water (initially at 28 °C). After 24 hours, the samples were removed from the water, allowed to surface-dry, and weighed separately again. Water absorption was calculated using the formula [18, 33]:

$$WA = \left(\frac{M_w \quad M_d}{M_d}\right) 100\% \tag{1}$$

where WA = water absorption of the sample, M_d = mass of the sample prior to immersion, and M_W = mass of the sample after immersion.

Bulk density

For this test, Modified water displacement method proposed by Robert et al [34] was applied to determine the bulk volume of each sample. The sealant used was wax and each sample was weighed by means of a digital scale having resolution of 0.1 g. Bulk volume was obtained as the difference between the volume of a sealed sample and that of the sealant on it. Based on the data obtained for each sample, bulk density ρ was computed thus [7, 12]:

$$\rho = \frac{M_S}{V} \tag{2}$$

where M_s = sample's mass, and V = bulk volume of sample.

Thermal conductivity

This test was implemented with the aid of Modified Lee – Charlton's Disc Apparatus technique [35]. During each testing process, an electric hotplate was employed as heat source

and the thickness of the sample under test was lagged using cotton wool. Aluminium block (cylindrical in shape) was used to separate the lower disc from the heating element of the hotplate [36]. For the purpose of modeling cooling rate function, Origin software (Version 2019) was used. The data obtained were applied to calculate thermal conductivity, k according to the relation [12]:

$$k = \left(\frac{Mcx}{A\Delta\theta}\right)\frac{dT}{dt} \quad (3)$$

where M = mass of the disc used, c = specific heat capacity of the disc, x = thickness of the sample, A = cross-sectional area of the sample, $\Delta\theta$ = temperature difference between the sample's surfaces, and $\frac{dT}{dt}$ = rate of cooling of the disc.

Specific heat capacity

SEUR'S apparatus was used for this test [37]. The measurement system in this case consisted of plywood plate (brown) and aluminium plate as additional heat exchange accessories to plate of the sample under test. Each plate measured 60 mm x 60 mm x 8 mm. By means of three digital thermometers (Model No. 305, calibrated and equipped with type-K probe), temperatures monitoring/measurement was actualized. When thermal balance was attained during heat exchange, the quantity, Q_p of heat gained by the plywood plate and the amount, Q_a of heat lost by the aluminium plate were calculated on assumption that energy was conserved in the system. The specific heat capacity, C of the sample was then determined by calculation using the formula [33]:

$$C = \left(\frac{Q_a - Q_p}{M_s \delta T}\right) \quad (4)$$

where δT = rise in temperature of the sample.

Thermal diffusivity and Heat flow time

Using the values of bulk density, specific heat capacity, and thermal conductivity already obtained for each sample, thermal diffusivity was determined as [11, 38 – 40]:

$$\lambda = \frac{k}{\rho C} \quad (5)$$

where λ = thermal diffusivity.

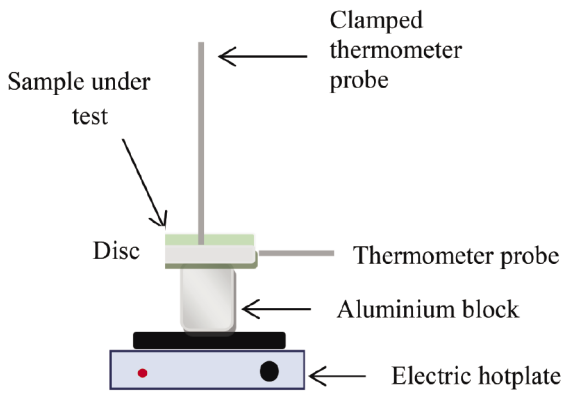

Fig. 2 Setup for measurement of heat flow time across sample's thickness
2. ábra A hőáramlási idő mérése a minta vastagságán keresztül

For measurement of heat flow time across the thickness of the sample, the setup earlier used for thermal conductivity test was employed with some modifications to ensure that the upper disc and lagging material were not applied as shown in *Fig. 2*. The lower disc was heat to the same temperature it attained at steady state. A sample that had cooled completely was placed on the disc and immediately, another thermometer was clamped ensuring that its probe tip made a firm contact with the upper surface of the sample. Timing of the process was done by means of a digital stopwatch. When the temperature reading given by the thermometer increased by about 0.2 °C with respect to the value registered at the commencement of the heating process, the time shown on the stopwatch was noted as the required heat flow time, T_x.

Flakiness

Since the test samples under consideration might undergo wear during their application and service life as building materials, an investigation of their flakiness was deemed necessary. In doing so, the initial mass of each sample was measured after which a 1.0 kg weight was attached to the top of a hard shoe brush to ensure application of uniform pressure during the test. Then the brush was rubbed against both cross-sectional surfaces of each sample until 100 strokes of forward and backward movements were made. The flaked samples were weighed and a decrease in the mass, ΔM of each of them was determined. Their flakiness, F_n was calculated as [41]:

$$F_n = \left(\frac{\Delta M}{M_i}\right)100\% \quad (6)$$

where M_i = mass of the sample before being flaked.

Flexural strength

A flexural strength test was conducted on the samples by using a three-point bending method in line with the standard procedure as stated in [42] and with the aid of an Electromechanical Universal Testing Machine (WDW – 10). During each test schedule, a sample was suspended as a single beam supported at two points and also loaded gradually in its middle. When it fractured, the process was discontinued immediately. The value of the load, P applied at that instant was used alongside the width, b and thickness of the sample to obtain the flexural strength [11, 43].

$$f_s = \frac{3PL}{2bx^2} \quad (7)$$

All the tests were conducted at 25.0 ± 1.0 °C. The results obtained for the triplicates were averaged per formulation and tabulated with their corresponding standard error value.

3. Results and Discussion

Table 1 shows the loose density and chemical constituents of the OPMF used as filler in this study. the loose density value of the filler indicates that it is light-weight. As can be seen, the proportion of cellulose is the highest followed by that of hemicelluloses and then lignin. Since cellulose is highly hydrophilic, it signifies that the filler has a strong affinity for water uptake. From *Fig. 3.*, it can be deciphered that the filler particles vary in size. This implies that inclusion of the filler in the POP matrix can create pores spaces of assorted areas.

The results of thermophysical and mechanical tests carried out on the samples are presented in *Table 2*. Water absorption of the samples increases as the proportion of the filler increases. This may be attributed to the fact that the filler is dominated by cellulose. As such, when the samples get in contact with water, their hydrophilicity becomes more pronounced as the fraction of the filler increases. A similar tendency was observed by Umoren et al [44] by utilizing *Lagenaria breviflora* rinds particle as filler to fabricate composite POP ceiling panels.

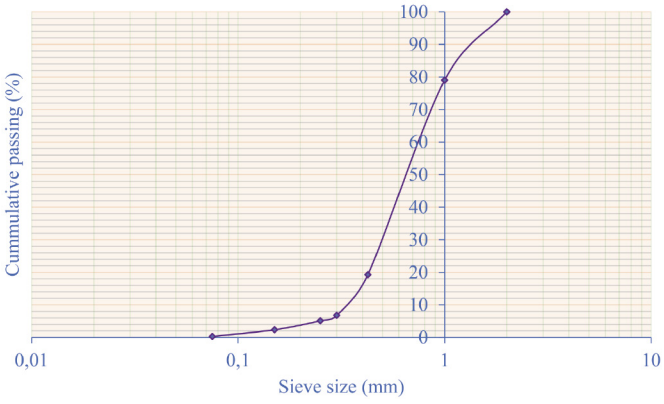

Fig. 3 Grading curve of the OPMF
3. ábra Az OPMF szemeloszlási diagramja

Parameters	Values for five determinations
Loose density (*kgm*$^{-3}$)	356.8 ± 0.4
Chemical constituents:	
Cellulose (%)	42.8 ± 0.9
Hemicellulose (%)	33.2 ± 0.6
Lignin (%)	22.6 ± 0.8

Table 1 Characteristics of the filler (OPMF)
1. táblázat A töltőanyag (OPMF) jellemzői

By utilizing 10%, 20%, 30% and 40% of the filler, the mean bulk density value of the resulting sample differs from that of pure POP by 220.0, 249.0, 280.0, and 361.0 (all in kgm^{-3}) respectively. The observed tendency is desirable for building design because there would be a reduction in the dead load of the building. This means that the filler application as a POP modifier has beneficial effects. Apart from enhancing the lightness of the composite ceiling formed, it can be seen as well that it improves the thermal conductivity of the products. Adepitan et al [45] reported thermal conductivity values of 0.4197 Wm^{-1}K^{-1} and 1.6499 Wm^{-1}K^{-1} for conventional ceilings like hardboard and polyvinyl chloride (PVC) respectively. Comparatively, it can be posited that all the samples are capable of ensuring thermal comfort better than the named ceilings if applied in buildings.

Fig. 4. reveals that the bulk density and thermal conductivity of the samples vary inversely with the proportion of the filler. Perhaps, this is due to the fact that the filler is lighter than the POP powder used. Also, its inclusion reduces the cohesiveness of the POP matrix by creating pores which are occupied by air only since the samples are completely dry.

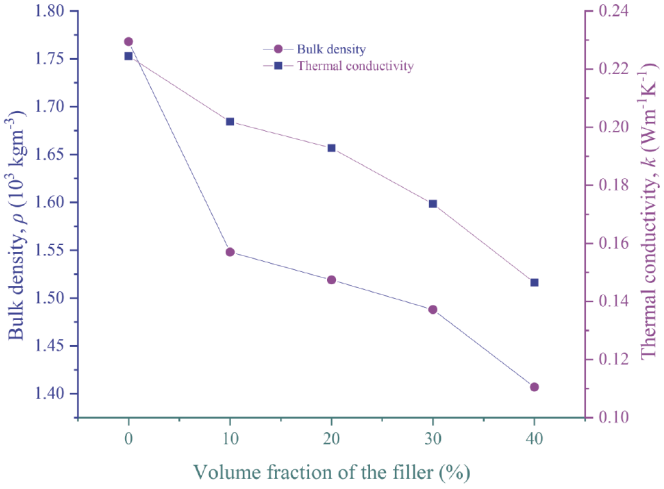

Fig. 4 Plots of bulk density and thermal conductivity against filler proportion
4. ábra Az ömlesztett sűrűség és a hővezető képesség változása a töltőanyag arányának függvényében

Consequently, the air volume increases in direct proportion to the filler content. Because air is a poor heat conductor, the ability of the samples to restrict heat transmission, therefore, increases with an increase in the percentage of the filler used.

Improvement in specific heat capacity is observed as the filler proportion increases. By increasing the filler content from 0% to 40%, the amount of heat the samples can store before the temperature of their unit mass changes by one Kelvin progressively increases from 1498 J to 1825 J. Robert et al [15] reported specific heat capacity of about 1540 Jkg^{-1}K^{-1} for POP modified with 18.3% of waste paper ash. For a composite ceiling developed using 25% of waste newspaper paste (WNP) with 75% of sawdust particles (SDP), a specific heat capacity of 1722.91 Jkg^{-1}K-1 has been reported [30]. Comparatively, these two values are almost similar to those obtained in this study by utilizing the filler at 10% and 30% levels. The implication is that the samples can exhibit the same performance tendency as the ash-modified POP ceiling as well as the composite WNP-SDP ceiling if subjected to the same conditions of application.

Filler fraction	WA (%)	ρ (10^3*kgm*$^{-3}$)	*k* (*Wm*$^{-1}$*K*$^{-1}$)	*C* (10^3*Jkg*$^{-1}$K^{-1})	λ (10^{-8}m^{2}s^{-1})	T_x (mins.)	F_n (%)	f_s (*N/mm*^{2})
0.0	12.22 ± 0.03	1.768 ± 0.003	0.2245 ± 0.0002	1.498 ± 0.003	8.477 ± 0.066	9.64 ± 0.03	0.65 ± 0.01	3.02 ± 0.02
10.0	13.12 ± 0.09	1.548 ± 0.003	0.2019 ± 0.0001	1.546 ± 0.002	8.436 ± 0.020	9.69 ± 0.01	0.88 ± 0.03	2.89 ± 0.02
20.0	16.49 ± 0.06	1.519 ± 0.002	0.1928 ± 0.0003	1.674 ± 0.002	7.582 ± 0.018	10.78 ± 0.02	1.24 ± 0.05	1.98 ± 0.02
30.0	20.53 ± 0.07	1.488 ± 0.004	0.1736 ± 0.0004	1.722 ± 0.003	6.775 ± 0.027	12.15 ± 0.04	1.86 ± 0.04	1.57 ± 0.04
40.0	25.75 ± 0.05	1.407 ± 0.004	0.1465 ± 0.0004	1.825 ± 0.003	5.705 ± 0.024	14.37 ± 0.02	2.08 ± 0.04	1.38 ± 0.03

Table 2 Thermophysical and mechanical properties of the samples
2. táblázat A minták termofizikai és mechanikai tulajdonságai

Decrease in thermal diffusivity with the filler content of the samples can be explained in terms of specific heat capacity. Since thermal diffusivity expresses the rate of heat spread for temperature propagation within a material, it is certain that the change in temperature of the samples is delayed as specific heat capacity increases. Consequently, heat diffusion within the sample is slowed down. All these occur by increasing the filler proportion used. A lower thermal diffusivity is an indicator of an improvement in thermal insulation because, in such cases, the propagation of thermal energy is restricted more. The least thermal diffusivity value obtained in this work is about 59.1% less than the mean value of (1.394 x 10^{-7} m^2s^{-1}) found by Ekpenyong et al [46] for composite boards prepared from groundnut shells.

The results of heat flow time lend credence to the thermal insulation performance of the samples. It correlates positively with the filler proportion in the samples, thereby supporting the fact that a reduction in thermal conductivity with an increase in specific heat capacity lowers the thermal diffusion rate within the samples. In turn, it increases the time heat takes to flow across the thickness of the samples. The marginal changes in heat flow time (0.05, 4.09, 1.37, and 2.22 mins.) as the filler content increases in steps of 10% from 0% to 40% in the samples simply indicates a non-linear relationship.

Regarding flakiness, the inclusion of the filler influences how flaky the samples could be in the course of their application in buildings. Except in the case of utilizing 40% of the filler, the flakiness values obtained for the samples are less than 2.0% which Berge [47] reported for asbestos ceiling. The meaning of this observation is that, if the samples are subjected to abrasion under same conditions in service, they would appear more durable compared to the asbestos. Plausibly, both the flakiness and flexural strength depend on the existing bonding strength between the filler and POP matrix. *Fig. 5.* illustrates how flakiness and flexural strength of the samples trend with the filler proportion. It could be understood that as more of the filler is introduced into the pure POP, the cohesiveness of POP powder and interlocking strength of the resulting sample are reduced. This eventually weakens the bond between the two materials thereby increasing the flaky concentration but decreasing the strength of the samples to withstand bending stress.

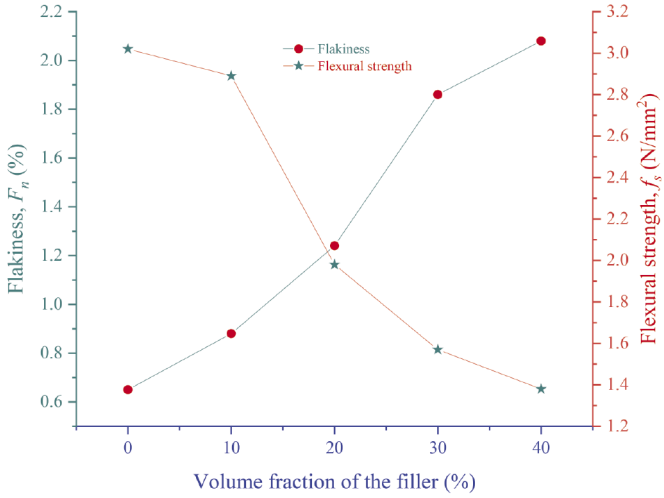

Fig. 5 Plots of flakiness and flexural strength against filler proportion
5. ábra A pelyhesedés és a hajlítószilárdság a töltőanyag arányának függvényében

4. Conclusions

The study has revealed the benefits of improving the thermal capacity of POP with OPMF when both materials are constitutively combined together. The addition of the OPMF increased the specific heat capacity, thermal conductivity, heat flow time, and release of heat absorption capacity. It also added flexibility to the product making it more malleable, resistant to microbial attack and easy to use. The implementation of this product in a large scale will help to save cost and improving the ecstasy of buildings and comfort of the safety. The conversion of OPMF to a finish product with POP will not only be useful in thermal insulation, it will also assist in the mitigation of waste in the environment; as well as reduce the cost of building.

References

[1] I.O. Ohijeagbon (2014) Retrofiting composite ceiling tiles. Res Gate, https://doi.org/10.13140/2.1.4847.872

[2] S.E. Etuk, U.W. Robert, O.E. Agbasi (2021) Investigation of heat transfer and mechanical properties of *Saccharum Officinarum* leaf boards. International Journal of Energy and Water Resources, 6(1); 95 – 102, https://doi.org/10.1007/s42108-021-00123-7

[3] U.W. Robert, S.E. Etuk, O.E. Agbasi, G.P. Umoren, N.J. Inyang (2021) Investigation of thermophysical and mechanical properties of board produced from coconut (*Cocos nucifera*) leaflet. Environmental Technology & Innovation, 24(1), 101869, https://doi.org/10.1016/j.eti.2021/101869

[4] O.N. Ezenwa, E.N. Obika, C. Umembamalu, F.C. Nwoye (2019) Development of ceiling board using breadfruit seed coat and recycled low density polyethylene. Heliyon, 5(11); e02712, https://doi.org/10.1016/j.heliyon.2019.e02712

[5] Felix A. Aisien; Andrew N. Amenaghawon; Kingsley C. Bienose (2015) Particle boards produced from cassava stalks: Evaluation of physical and mechanical properties. South African Journal of Science, 111(5-6), https://dx.doi.org/10.17159/sajs.2015/20140042

[6] U.W. Robert, S.E. Etuk, G.P. Umoren, O.E. Agbasi (2019) Assessment of Thermal and Mechanical properties of composite board produced from coconut (*cocos nucifera)* husks, waste newspapers and cassava starch. International Journal of Thermophysics, 40(9); 83, https://doi.org/10.1007/s10765-019-2547-8.

[7] S.E. Etuk, U.W. Robert, O.E. Agbasi, N.J. Inyang (2023) Evaluation of Thermophysical and Strength Properties of Composite Panels Produced from Sugarcane Bagasse and Waste Newspapers. Advances in Materials Science, 23(1); 19 – 31, https://doi.org/10.2478/adms-2023-0002

[8] I.O. Oladele, M.A. Okoro (2015) Development of rattan (*Calamus longipinna*) particulate reinforced paper pulp-based composite for structural application using waste papers. Leonardo Journal of Science, 14(27); 75 – 87

[9] C.O. Ataguba (2016) Properties of ceiling boards produced from a composite of waste paper and rice husk. International Journal of Advances in Science Engineering and Technology, Spl. Issue 2; 117 – 121

[10] Y. Zeleke, T. Feleke, W. Tegegn, Y. Atinaf (2022) Design and development of false ceiling board composite material using pineapple leaf Fibre reinforcement in unsaturated polyester matrix. International Journal of Sustainable Engineering, 15: 1, 146 - 154, https://doi.org/10.1080/19397038.2022.2097456

[11] U.S. Okorie, U.W. Robert, U.A. Iboh, G.P. Umoren (2020) Assessment of the suitability of tiger nut fibre for structural applications. Journal of Renewable Energy and Mechanics, 3(1); 32 – 39, https://doi.org/10.25299/rem.2020.vol3(01).4417

[12] N.E. Ekpenyong, G.P. Umoren, I.E. Udo, O.J. Yawo (2022) Assessment of Thermophysical and Mechanical Properties of Composite Panels Fabricated from Untreated and Treated Coconut Husk Particles for Structural Application. Brilliant Engineering, 2; 1 - 5, https://doi.org/10.36937/ben.2022.4547

[13] Y. Zeleke, G. K. Rotich (2021) Design and Development of False Ceiling Board Using Polyvinyl Acetate (PVAc) Composite Reinforced with False Banana Fibres and Filled with Sawdust. International Journal of Polymer Science, Volume 2021, Article ID 5542329, https://doi.org/10.1155/2021/5542329

[14] C. C. Ihueze, C. E. Okafor, C. I. Okoye (2015) "Natural fiber composite design and characterization for limit stress prediction in multiaxial stress state." Journal of King Saud University- Engineering Sciences, 27(2);193 – 206

[15] U.W. Robert, S.E. Etuk, O.E. Agbasi, S.A. Ekong, Z.T. Abdulrazzaq, A.U. Anonaba (2021) Investigation of Thermal and Strength Properties of Composite Panels fabricated with Plaster of Paris for Insulation in Buildings. Intl Journal of Thermophysics, 42(2):25, https://doi.org/10.1007/s10765-020-02780-y

[16] E.O. Ojoko, H.O. Abubakar, O. Ojoko, E. Ikpe (2016) Sustainable Housing Development in Nigeria: Prospect and Challenges. Journal of Multidisciplinary Engineering Science and Technology, 3(5); 4851 - 4860

[17] M.B. Ochang, P.R. Jubu, A.N. Amah, J.L. Oche (2018) Investigation of thermal properties of fabricated plaster of Paris – Rice husk ash composite with varying matrix-filler volume fractions for thermal insulation applications. American Journal of Engineering Research, 7(6); 215 – 222

[18] U.W. Robert, S.E. Etuk, U.A. Iboh, G.P. Umoren, O.E. Agbasi, Z.T. Abdulrazzaq (2020) Thermal and Mechanical properties of fabricated Plaster of Paris filled with groundnut seed coat and waste newspaper materials for structural application. Építőanyag-Journal of Silicate Based and Composite Materials, 72(2); 72 – 78. https://doi.org/10.14382/epĭtõanyag-jsbcm.2020.12

[19] T.E. Omoniyi, K.A. Ajobiewe (2020) Physico-mechanical properties of wood and non-wood plaster of Paris bonded composite ceiling boards. Journal of Engineering Studies and Research, 26(3); 148 - 153

[20] C.Y. Sing, M.S. Ariz (2013) A Study of Biomass Fuel Briquettes from Oil Palm Mill Residues. Asian Journal of Scientific Research, 6(3); 537 – 545, https://doi.org/10.3923/ajsr.2013.537.545

[21] B.K. Neoh, Y.M. Thang, M.Z.M. Zain, A. Junaidi (2011) Palm pressed fibre oil: A new opportunity for premium hardstock? *International Food Research Journal,* 18; 746 – 750

[22] Y.P. Teoh, D.M. Mat (2011) Kinetic model for the hydrolysis of sterilized palm press fibre. Chemical Engineering Science, 66; 3523 – 3530

[23] N.S.H. Md Yunos, A.S. Baharuddin, K.F. Md Yunos, M.N. Naim, H. Nishida (2012) Physiochemical property changes of oil palm mesocarp fibers treated with high-pressure steam. BioResources, 7(4); 5983 – 5994

[24] S. Chaikitkaew, P. Kongjan, S. O-Thong (2015) Biogas Production from Biomass Residues of Palm Oil Mill by Solid State Anaerobic Digestion. Energy Procedia, 79; 838 – 844, http://dx.doi.org/10.1016/j.egypro.2015.11.575

[25] M.Z.M. Yusoff, H. Akita, M.A. Hassan, S. Fujimoto, M. Yoshida, N. Nakashima, Z. Zen, C. Barlow, R. Gondowaristo, J.F. McCarthy (2016) Interventions to promote smallholder oil palm and socio-economic improvements in Indonesia, in: The Oil Palm Complex: Smallholders, Agribusiness and the State in Indonesia and Malaysia. NUS, Singapore, pp. 78 – 108

[26] U.W. Robert, S.E. Etuk, O.E. Agbasi, U.A. Iboh, S.S. Ekpo (2020) Temperature-Dependent Electrical Characteristics of Disc-shaped Compacts fabricated using Calcined Eggshell Nano powder and Dry Cassava starch. Powder Metallurgy Progress, 20(1); 12 – 20

[27] S.K. Loh (2017)The potential of the Malaysian oil palm biomass as a renewable energy source. Energy Conversation and Management, 141; 285 – 298

[28] N.F.A.A. Rizal, M.F. Ibrahim, M.R. Zakaria, S. Abd-Aziz, P.L. Yee, M.A. Hassan (2018) Pre-treatment of Oil Palm Biomass for Fermentable Sugars Production. Molecules, 23; 1381, https://doi.org/10.3390/molecules23061381

[29] E. Hambali, M. Rivai (2017) The Potential of Palm Oil Waste Biomass in Indonesia in 2020 and 2030. *IOP Conference Series: Earth and Environmental Science*, 65; 012050, https://doi.org/10.1088/1755-1315/65/1/012050

[30] U.W. Robert, S.E. Etuk, S.A. Ekong, O.E. Agbasi, S.S. Akpan, N.J. Inyang (2023) Paper – Sawdust Composites: Fabrication and Comparison in terms of Heat Transfer and Strength Properties. Structure and Environment, 15 (1); 38 - 48, https://doi.org/10.30540/sae-2023-005

[31] U.W. Robert, S.E. Etuk, O.E. Agbasi, U.S. Okorie, Z.T. Abdulrazzaq, A.U. Anonaba, O.T. Ojo (2021) On the hygrothermal properties of sandcrete blocks produced with sawdust as partial replacement of sand. Journal of the Mechanical Behavior of Materials, 30(1); 144 - 155. https://doi.org/10.1515/jmbm-2021-0015

[32] K. Mylsamy, I. Rajendran (2010) Investigation on Physio-chemical and mechanical properties of raw and alkali-treated Agave Americana fiber. Journal of Reinforced Plastics and Composites, 29(19); 2925 – 2935

[33] S.E. Etuk, U.W. Robert, O.E. Agbasi (2022) Thermophysical properties of oil empty fruit bunch peduncle for use as a mulching material. Journal of Oil Palm Research, https://doi.org/10.21894/jopr.2022.0065

[34] U.W. Robert, S.E. Etuk, O.E. Agbasi (2019) Modified Water Displacement Method and its Use for Determination of Bulk Density of Porous Materials. Journal of Renewable Energy and Mechanics, 1(1); 1 – 16, https://doi.org/10.25299/rem.2029.vol1(01).2292

[35] U.W. Robert, S.E. Etuk, O.E. Agbasi, U.S. Okorie (2021) Quick Determination of Thermal Conductivity of Thermal Insulators Using a Modified Lee – Charlton's Disc Apparatus Technique. International Journal of Thermophysics, 42; Article number 113, https://doi.org/10.1007/s10765-021-02864-3

[36] U. W. Robert, S. E. Etuk, O. E. Agbasi, U. S. Okorie, N. E. Ekpenyong, A. U. Anonaba (2022) On the Modification of Lee – Charlton's Disc Apparatus Technique for Thermal Conductivity Determination. Researchers Journal of Science and Technology, 2(3); 1 – 17

[37] S.E. Etuk, U.W. Robert, O.E. Agbasi (2020) Design and Performance evaluation of a device for determination of specific heat capacity of thermal insulators. Beni-Suef University Journal of Basic and Applied Sciences, 9(34); 1 – 7, https://doi.org/10.1186/s43088-020-00062-y

[38] S.E. Etuk, L.E. Akpabio, I.O. Akpan (2010) Comparative Study of Thermal transport in *Zea mays* straw and *Zea mays* heartwood (cork) boards. Thermal Science, 14(1); 31 – 38

[39] S.E. Etuk, O.E. Agbasi, Z.T. Abdulrazzaq, U.W. Robert (2018) Investigation of thermophysical properties of Alates (swarmers) termites wing as potential raw material for insulation. International Journal of Scientific World, 6(1); 1 – 7, https://doi.org/10.14419/ijsw.v6i1.8529

[40] N.J. George, V.I. Obianwu, G.T. Akpabio, I.B. Obot (2010) Comparison of thermal insulation efficiency of some select materials used as ceiling in building design. Archives of Applied Science Research, 2(3); 253 – 259

[41] U.W. Robert, S.E. Etuk, J.B. Emah, O.E. Agbasi, U.A. Iboh, (2022) Thermophysical and Mechanical Properties of Clay-Based Composites developed with Hydrothermally Cal-cined Waste Paper Ash Nano-material for Building Purposes. International Journal of Thermophysics, 43(5); 1 – 20, https://doi.org-/10.1007/s107650-22-02995-1

[42] ASTM C67/67M (2023) Standard Test Methods for Sampling and Testing Brick and Structural Clay Tile, ASTM International, West Conshohocken, PA

[43] U.W. Robert, S.E. Etuk, O.E. Agbasi, G.P. Umoren, S.S. Akpan, L.A. Nnanna (2021) Hydrothermally-calcined Waste Paper Ash Nanomaterial as an Alternative to Cement for Clay Soil Modification for Building Purposes. Acta Polytehnica, 6(6); 749 – 761, https://doi.org/10.14311/AP.2021.61.0749

[44] G.P. Umoren, A.O. Udo, I.E. Udo (2023) Suitability of *Lagenaria breviflora* Rind filled plaster of Paris ceilings for building design. Researchers Journal of Science and Technology, 3(2), 1 - 14

[45] J. O. Adepitan, F. O. Ogunsanwo, J. D. Ayanda, A. A. Okusanya, A. D. Adelaja, O. O. Oni, O. O. Odumosu (2019) Determination of thermal properties of some ceiling material commonly used in Ijebu-Ode, Nigeria. Nigeria Journal of Pure & Applied Physics, 9(1); 23 – 27, https://dx.doi.org/10.4314/njpap.v9i1.5

[46] N.E. Ekpenyong, S.A. Ekong, E.U. Nathaniel1, J.E. Thomas, U.S. Okorie, U.W. Robert, I.A. Akpabio, N.U. Ekanem (2023) Thermal Response and Mechanical Properties of Groundnut Shells' Composite Boards. Researchers Journal of Science and Technology, 3(1); 42 – 57

[47] H. Berge (1963) Asbestos Fundamentals, Origin and Properties. McGraw-Hill, London, p. 56

Ref.:
Anonaba, Armstrong Udochukwu – **Ndukwe**, Israel Chukwuemeka – **Eze**, Francis Chukwuemek: *Thermophysical and mechanical properties plaster of Paris Ceilings modified with oil palm mesocarp fibre for application in buildings*
Építőanyag – Journal of Silicate Based and Composite Materials, Vol. 76, No. 1 (2024), 4–9. p.
https://doi.org/10.14382/epitoanyag-jsbcm.2024.1

Calcined kaolinitic clay as a supplementary cementing material and its pozzolanic effect on concrete blends characteristics (Part II)

Nabil A. ABDULLAH
Consultant and Research Director in Aluminum Sulphate Co. of Egypt (ASCE).
Ph.D. in Environmental science, Faculty of Science, Ain Shams University, Egypt.

Hajer N. Abdullah
Research assistant in October University for Modern Science and Arts (MSA university), Faculty of Engineering, Civil Engineering Department, Egypt.

Nabil A. ABDULLAH ▪ Research & Development Dept. Director, Aluminum Sulphate Co. of Egypt ▪ nabilxp9@gmail.com
Hajer ABDULLAH ▪ Civil Engineering Dept., MSA university, Egypt ▪ Hnabdullah@msa.edu.eg

Érkezett: 2023. 11. 01. ▪ Received: 01. 11. 2023. ▪ https://doi.org/10.14382/epitoanyag-jsbcm.2024.2

Abstract
Part II included using of calcined kaolinitic clay (CKC) prepared by a fluidized bed kiln as a supplementary cementing blend and assessing its effect on the OPC and the durability of concrete. The experimental protocol included optimization of the mixes of CKC/OPC containing 10 and 15% CKC for the production of hardened concrete as determined in part I, and in this work, the durability against chlorides, sulfate, seawater, and heating was studied. The effect on the reinforcement steel was also assessed. It was found that the partial replacement of cement with CKC (10 and 15%) caused slight expansion of concrete within the limits and there was no significant effect on the alkaline silica reaction or alkalinity of the concrete medium. The ratio of 15% CKC/OPC achieved a higher percentage of CSH that enhanced the compactness of the concrete matrix. When using CKC in plain concrete, the ratio of 10% CKC/OPC resulted in better resistance against the aggressiveness of salt solution attack and the highest compressive strength under the different conditions, whereas it reached 24.6 and 21.5% for 10 and 15% CKC/OPC respectively compared with the control concrete after aging of 180 days. The ratio of 10% CPDK/OPC achieved high resistance to heating. The porosity for the concrete modified with CKC was minimal resulting in low permeability of concrete for the salt solutions causing protection of the reinforcing steel against corrosion.
Keywords: calcined kaolinitic clay, durability of concrete, concrete reinforced steel corrosion, anodic polarization of steel in concrete
Kulcsszavak: kalcinált kaolinites agyag, beton tartóssága, betonvasacél korróziója, acél anódos polarizációja betonban

1. Introduction

Manufacturing and use of concrete in construction are increasing due to its durability, and relatively low cost as compared with other construction materials [1-3]. The annual quota of concrete for each human on the earth is one ton [4]. There are numerous disadvantages of Portland cement, such as the huge energy requirement and the bad environmental impacts [5]. Too much quantity of carbon oxides are emitted during the production of cement resulting from two sources, one from the destruction of calcium carbonate stone to yield caustic lime and the other from the combustion of fuel [6, 7]. Portland cement is the main component in concrete; it requires water for hydration reactions forming binding compounds to fix the aggregates. Cement production exceeds four billion tons per year and the need is increasing, causing severe environmental pollution with carbon oxides which participate sharply in the biosphere warming [8].

The use of flown ash [9] fumed silica [10] waste glass [11] and ground granulated blast furnace slag as supplementary cementing materials[12] is one of the measures to mitigate this problem, as a partial replacement for cement in the cement industry. High compressive strength, better durability, no surface cracking, economic feasibility, and sustainability are advantages of adding cementitious ingredients to concrete. The quantity of the added materials that replace OPC is determined by their pozzolanic characteristics [13].

It was found that CKC can be used as a cementitious additive in concrete [14, 15]. The application of CKC as a cementitious ingredient in concrete production has gained interest and studies are still being conducted on adding pozzolanic materials to cement to enhance the concrete characteristics [16, 17]. As CKC is a very fine material it modifies the pore structure and fixes the calcium hydroxide of the hardened matrix of the concrete. The reactions of CKC with lime hydroxide produced during the hydration reactions of cement form secondary binding compounds such as calcium silicate hydrates (CSH) which modify the structure of concrete and make it more compact and highly durable against the aggressiveness of chemical attacks. The enhancement of concrete was confirmed by the physical characteristics such as; porosity, permeability, and chloride ion diffusion [18]. CKC particles are much smaller than cement particles but not finer than fumed silica [19]. Adding CKC to concrete upgraded the mechanical characteristics [20, 21].

Corrosion of steel of reinforced concrete represents one of the most important phenomena that lead to concrete cracks and its collapse, on explosion to chloride ion (Cl^-). Many modern studies are currently researching adding material that protects

the concrete mix and reinforcement steel. Therefore, the study discusses the effect of using the ratios 0, 10% and 15% CKC as partial replacement of cement in concrete. Anodic polarization is an electrochemical measurement that was used to estimate the extent of corrosion of reinforcement steel [22-29].

The kaolinitic clay (KC) collected from South Sinai quarries reduces cement content in concrete which can improve the environmental conditions. This research aims to study the use of the CKC prepared from low-grade kaolinitic clay for the production of durable concrete. CKC was first investigated physically and chemically. After that, the hydration, workability, mechanical characteristics, durability, and scan electron microscopy of CMC-modified concrete are thoroughly tested. The most relevant results and recommendations are recorded, which will aid in concrete application using CKC. The utilization of this material reduces carbon emissions by lowering the amount of the currently used ordinary Portland cement (OPC) [22]. CKC was added to ordinary Portland cement to enhance concrete performance [30]. The results and recommendations were reported, which will aid in the use of calcined kaolinite clays in the concrete industry.

Part I of the study, it was mentioned that the CKC produced by thermal treatment in a vertical fluidized bed kiln was considered a promising material that motivates the completion of the study to prove the potential use of this material for partial replacement of cement. The behavior of modified cement was investigated in the plain and reinforced concrete. It was found that the optimal replacement ratios for cement with CKC were 10% and 15%, which improved the compressive strength by an average of 120.8 and 118.7% respectively at the age of 28 days, compared to the control mix. Several studies indicate that 10% of CKC is the optimal ratio for substitution [31 -33] while other studies reported that 15% is optimal. The current study aims to investigate the durability of the modified concrete against chloride, sulfate solutions, and salty seawater and the impacts of these ratios on the compressive strength and protection of reinforcing steel in concrete against corrosion.

2. Material and methods

2.1 Materials

The kaolinitic clay samples were picked from the kaolin sedimentary rocks of abo Zienema, Sinai. The samples were crushed by a hummer crusher, sieved to be less than 3 mm by the sieve shaker attached to the crusher, and calcined in a fluidized bed furnace for 60 min. [34]. The chemical compositions of the KC and CKC are presented in *Table 1*. The CKC was ground by a ball mill to get an average diameter of 4.5 µm. The calcination at 750 °C process eliminated 10.3% of the bound water mass that deteriorates the crystal structure and activates the silicate and aluminate content to react easily with the hydration products of cement.

The reactive silica (SiO_2) that represents the reactive fraction of silica was 21.5% in CEM I 42.5 R Portland cement and 41.1% in CKC, the latter ratio supports the formation of calcium silicate hydrate during the hydration of the cement. The chemical composition of the cement is shown in *Table 1*.

Fine aggregates: Sand was used as a fine aggregate in both mortar and concrete mixtures. Tests for mechanical and physical properties of aggregates were carried out according to the standard specifications (EN 1097, EN 933). The specific gravity = 2.6 and the grain size averaged 2 mm.

The coarse aggregates are dolomite with a maximum particle size of 22 mm. Aggregates were obtained from local sources. The physical properties of the aggregates are presented in *Table 2*. The grading of the aggregate mixture was kept constant for all concrete mixtures.

Compound	Amount (wt %)		
	KC	CKC	CEM 1 42.5
SiO_2 (total)	50.6	61	21.5
SiO_2 (active)	37.6 = 0.627 M	41.1 = 0.685 M	21.5
Al_2O_3	32 = 0.314 M	35 = 0.32 M	3.5
SiO_2/Al_2O_3	2.0 M	2.14	-
Fe_2O_3	1.14	1.3	3.4
TiO_2	2.1	2.3	0.15
MgO	0.15	0.16	1.2
CaO	0.20	0.22	62
Na_2O	0.12	0.14	0.28
K_2O	0.13	0.13	0.32
SO_3	0.12	0.15	2.7
P_2O_5	0.09	0.10	0.04
SrO	-	0.05	-
Cl	0.04	0.05	0.12
L.O.I total	11.4	1.0	4.5
Total	98.1	99.6	99.71

Table 1 The chemical analysis of the kaolinitic clay, calcined kaolinitic clay and CEM 1 42.5
1. táblázat A kaolinites, a kalcinált kaolinites agyag és a CEM 1 42,5 kémiai elemzése

Parameter	Size 1	Size 2	The limits (Egyptian standard) ECCS203-2018
The specific gravity	2.65	2.65	-
The bulk density (ton/m³)	1.4	1.45	-
Water absorption (%)	1.8	1.65	Not more than 2.5
The dust and clay (%)	0.15	0.18	Not more than 2.5

Table 2 The physical properties of coarse aggregates
2. táblázat A durva adalékanyagok fizikai tulajdonságai

The chemical composition of coarse aggregates (dolomite) complies with Egyptian code (302/2018). (*Table 3*). The grain size averaged 16 mm.

For better mixing of the concrete mixtures Master Reobuild 3045 (Superplasticizer, SP) was added conforming to ASTM 494. Sulphonated naphthalene formaldehyde-based high-range water-reducing admixture with a specific gravity of 1.2 was added to get a slump of 140 mm for proper handling, placing, and consolidation in all concrete mixtures. For the characterization of the materials, XRD and XRF instruments were used for materials of interest and concrete.

Parameters	Coarse aggregates (wt %)	Limits	Fine aggregates (wt %)	Limits
SiO_2	1.90	-	94	-
Al_2O_3	0.07	-	1.8	-
Fe_2O_3	0.02	-	1.0	-
CaO	36	-	0.72	-
MgO	16.9	-	0.22	-
SO_3^{--}	0.14	< 0.4	0.25	< 0.4
Cl^-	0.01	< 0.04	0.06	< 0.06
Na_2O	0.03	-	0.32	-
K_2O	0.02	-	0.51	-
TiO_2	0.01	-	0.11	-
P_2O_5	0.01	-	0.05	-
MnO	0.01	-	0.04	-
L.O.I	44.5	-	0.70	-
Total	99.62	-	99.78	-

Table 3 Chemical analysis of coarse and fine aggregates
3. táblázat Durva és finom adalékanyagok kémiai elemzése

2.2 Test methods and equipment

The mineral composition of materials was determined using X-ray Diffraction (XRD) analysis PAN analytical X-Ray Diffraction equipment model X'Pert PRO with mono-chromate, Cu-radiation (λ=1.542Å) at 45 K.V., 35 mA. and scanning speed 0.03°/sec. were used. The reflection peaks between 2θ = 2° and 60°, and corresponding spacing (d, Å) and relative intensities (I/I°) were obtained. The chemical composition of raw materials was determined using Philips X-ray fluorescence (XRF) spectrometer Model PW/2404. SEM Microscope has been used to perform both SEM. Hitachi 3000N SEM Microscope was operated to examine cubed samples at low vacuum (VP-SEM)

The compressive test was carried out using a Non-Automatic Compression Range 200 KN-Hoek Cell Machine. The compressive strength was done following the ASTM C 109 Method (ASTM, 2016) [35]. Compressive strength standard test is the most widely test applied for assuring the quality of a building material [36, 37]. The measuring of compressive strength was obtained, at the age of, 7, 28, 56, 90, and 180 days. The average compressive strength of three specimens was considered for each age.

The morphology and microstructure of hardened concrete were examined by SEM [Inspect S-FEI Company, Netherlands]. Alkalinity (pH-value) test: 300 grams of cement or the mixture are stirred in 1,000 cm^3 of distilled water for 3 hours. The mixture is filtered and the pH is measured. Alkali-Silica reaction (ASR) was carried out according to ASTM: C 1567-07 [38].

Electrochemical techniques for measuring metallic corrosion of reinforcement steel were carried out according to RILEM TC-154-EMC: "Electrochemical techniques for measuring metallic corrosion" Test methods for on-site corrosion rate measurement of steel reinforcement in concrete using the polarization resistance method [39].

2.3 Experimental investigation

An experimental program was designed to produce high-strength concrete by adding several combinations of CKC. The materials used and the experimental procedures are described in the following sections.

2.3.1 Mix design

The details of the mixtures for the study are presented in *Table 4*. Three different mixtures (0% CKC, 10% CKC, and 15% CKC) were applied to test the effect of low water to binder ratio on concretes containing MK on the mechanical and durability properties. The control mixture (0% CKC) did not include CKC. In mixtures a 10% CKC and 15% CKC, cement content was partially replaced with 10, and 15% CKC (by mass) respectively. The binder consists of cement and CKC.

Components (kg/m^3)	CKC (wt. %)		
	0	10	15
OPC, 42.5N	400	360	340
CKC	-	40	60
Fine aggregate (sand)	632	632	632
Coarse aggregate (dolomite)	1264	1264	1264
Superplasticizer (SP)	8	8	8
Water	140	40	140

Table 4 The mix design for 1 m^3 of concrete
4. táblázat Keverék recept 1 m^3 betonra

2.3.2 Mixing and Casting of the concrete mixes

All the materials were mixed using a pan mixer with a maximum capacity of 100 L. The materials were fed into the mixer in the order of coarse aggregate, cement, CKC, and sand. The materials were mixed dry for 1.5 min. Subsequently, three-quarters of the water was added, followed by the SP and the remaining water while mixing continued for a further 5 minutes to obtain a homogenous mixture. Upon discharging from the mixer, the slump test was conducted on the fresh properties of each mixture.

2.3.3 Specimens and Curing

The following specimens were cast from each mixture: Three 100 × 100 × 100 mm cubes for the compressive strength. All the specimens were cast on a mechanical vibration table. After casting, all the specimens were covered with plastic sheets and water-saturated burlap and left at room temperature for 24 hours. The specimens were demolded after 24 hours of casting and were then cured in water at approximately 27 °C until the testing day.

According to the results, it was concluded that the replacement ratio of 10 and 15% CKC achieved better performance than the control mix with an enhancement in the compressive strength of 20.8 and 18.7% respectively at an age of 28 days. Therefore, the study was resumed with these ratios to assess the durability of the developed modified concrete mixes.

3. Results and discussions

3.1 The chemical composition of OPC paste

The chemical analysis of hardened Portland cement slurries containing the ratios; 0%, 10%, and 15% of the CKC is displayed in *Table 5* cured in tap water for 28 days. It is clear from the table that the percentage of reactive silica (SiO_2) and alumina (Al_2O_3) increased with increasing of CKC to 23.45% and 6.65% respectively for the added 10% of CKC, and 24.5 and 8.25% respectively for the added 15% CKC. Iron oxides and calcium oxides were dropped with increasing CKC ratios due to the dilution effect.

Oxides	CKC (wt. %)		
	0	10	15
SiO_2	21.5	23.46	24.50
Al_2O_3	3.5	6.65	8.25
Fe_2O_3	3.4	3.24	3.07
CaO	62	56.22	52.8
MgO	1.2	1.12	1.12
SO_3^-	2.7	2.49	2.35
Cl^-	0.12	0.11	0.15
Na_2O	0.28	0.27	0.35
K_2O	0.32	0.31	0.37
TiO_2	0.15	0.38	0.48
P_2O_5	0.04	0.05	0.05
MnO	-	-	-
L.O.I	4.5	4.22	3.92
Total	99.71	99.5	99.7

Table 5. The chemical composition of OPC contains 0, 10, and 15% CKC
5. táblázat A 0, 10 és 15% CKC-t tartalmazó OPC kémiai összetétele

3.2 XRD diffractogram for OPC incorporating 0, 10 and 15% CKC

Fig. 1 shows the results of the XRD chart for the OPC mixes containing 10 and 15% CKC compared with the plain cement after 28 days of immersion in water. The *Fig.* shows that an increase in the proportion of CKC in the mixture (15%) increases the rate of formation of calcium silicate hydrate (CSH) binder resulting from the added reactive silica as depicted in *Table 5*. There is a clear reduction of Portlandite mineral [$Ca(OH)_2$] that was consumed in binder formation.

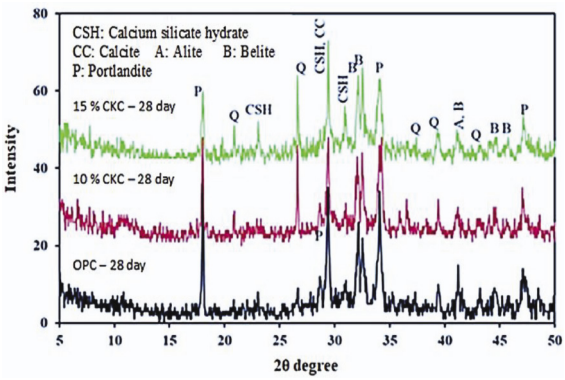

Fig. 1 XRD diffractogram for OPC incorporating 0, 10, and 15% CKC ratios after curing in water for 28 days
1. ábra A 28 napos 0, 10 és 15%-os CKC-arányt tartalmazó OPC röntgendiffraktogramja

3.3 Effect of CKC on the pH of the modified cement paste

The alkalinity of concrete medium is an important property for protecting the reinforcing steel from corrosion. At relatively low alkalinity below pH = 11.5, the steel becomes susceptible to corrosion attack resulting in cracks formation and concrete deterioration [40]. *Fig. 2* displays the pH profile for different doses of CKC, where slight reduction of the pH-value (12.82) as a result of CKC in the cement mix. At 10% the pH was 12.75, while at 15% CKC, the pH was 12.51 this is attributed to the relative reduction of alkaline species (Na_2O and K_2O) upon addition of CKC (*Table 5*).

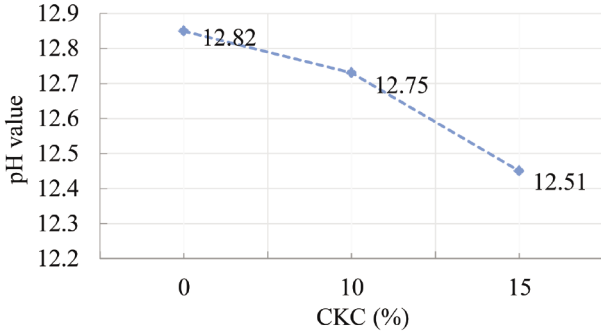

Fig. 2 pH of water extract for cement pastes incorporating 0, 10, and 15% CKC
2. ábra A 0, 10 és 15% CKC-t tartalmazó cementpépek vizes kivonatának pH-ja

3.4 Effect of alkali-silica reaction (ASR) of cement pastes containing 10 and 15% CKC on expansion

The high reactive of CKC resulted in catalyzing the reaction with the hydration products of OPC and forming excessive binding compounds, therefore it was necessary to investigate the expansion resulting from these new reactions with alkalis of cement. *Fig. 3* shows the results of the ASR test for Portland cement mixtures, which contain 0, 10%, and 15% of CKC. ASR tests were done according to ASTM: C1567-7. The values of expansion occurring as a result of the presence of 10 and 15% CKC were 0.037 and 0.015% respectively. These values are much less than the maximum allowed limit (0.1%). The alkali-silica reactions decreased at a ratio of 15% CKC and consequently the expansion decreased to 0.015%.

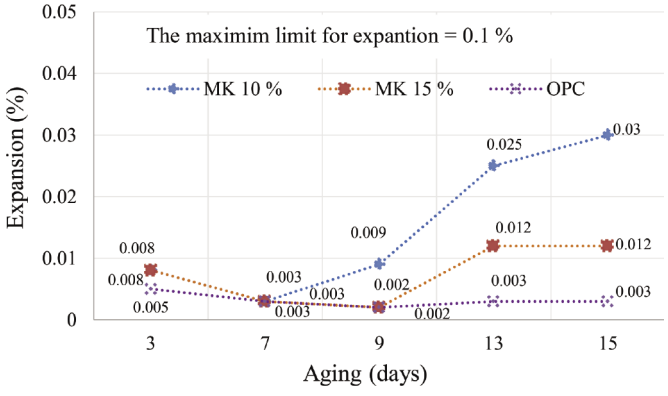

Fig. 3 Expansion values due to the alkali-silica reaction of cement pastes incorporating 10 and 15% CKC dosages relative to CKC-free cement paste
3. ábra A 10 és 15%-os CKC-adagolást tartalmazó cementpépek alkáli-kovasav reakcióból eredő tágulási értékei a CKC-mentes cementpéphez viszonyítva

The alkaline silica reaction (ASR) produces swelling gelatinous products. The soluble Ca^{++} and OH^{-}, active silica, and water are the main components in the paste matrix, and adding of CKC consumes the $Ca(OH)_2$ therefore any gelatinous products produced are not significant, and consequently no further expansion with 15% CKC and no cracks formed [41 - 43]. The high content of aluminum in CKC reduces the solubility of silica in alkaline solutions due to the formation of insoluble aluminum silicate binder restricting ASR expansion [43].

3.5 Scanning Electron Microscope (SEM)

Fig. 4 shows the SEM for samples of hardened cement mixtures, which contain the CKC ratios of 10% and 15%, after curing in water for 28 days, compared to a sample of Portland cement free of CMC. The images display the relative reduction of matrix whiteness with the addition of CKC confirming the conversion of calcium hydroxide to calcium silicate hydrate binder (CSH). When the CKC ratio increases, the size of micro cracks, capillary voids, and pores become relatively lower. This is attributed to that the calcined kaolin improves the structure of the matrix by reducing the interfacial spaces among the aggregates [44]. Therefore, the pozzolanic reaction and filling voids of CKC results in a denser structure which improves concrete strength and durability properties.

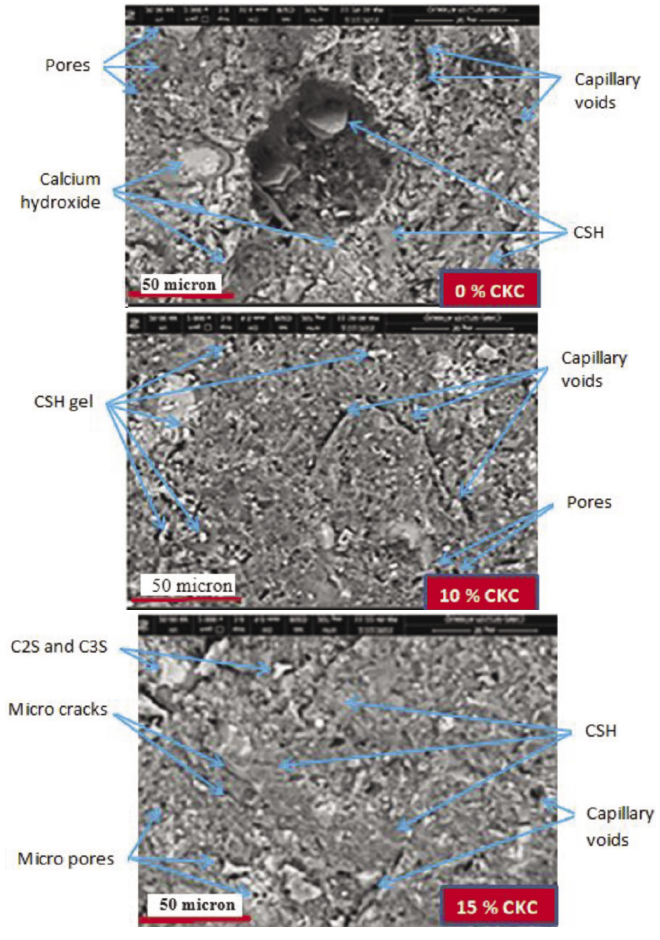

Fig. 4 SEM micrographs for cement pastes incorporating 0, 10, and 15% CKC after curing in tap water for up to 28 days
4. ábra SEM felvételek a 0, 10 és 15% CKC-t tartalmazó cementpépekről, miután 28 napig csapvízben szilárdultak

3.6 Durability tests

3.6.1 Compressive strength of concrete containing 10% and 15% CKC after curing in tap water for several durations of up to 3 months

The durability of concrete and its resistance to the aggressiveness of the environmental conditions was assessed by testing the compressive strength [45]. *Fig. 5* shows the values of the compressive strengths of concrete containing 0.0, 10, and 15% of CKC as a partial replacement of the cement after curing in tap water for several durations up to 90 days. It was found that the concrete mixes containing 10% CKC recorded higher compressive strength than the control mix by values of 24, 26.3, 25.4, and 24.6% at 7, 28, 60, 90, and 180 days respectively, and also higher than the concrete mixes containing 15% CKC whereas they achieved 14.3, 16.2, 21.7, 19.2 and 21.5% after 7, 28, 60, 90 and 180 days respectively. These results show that the CKC ratio of 10% is the optimal ratio as a replacement ratio for agreeing with that reported by other research [12]. The relative reduction in compressive strength for the 15% CKC ratio in concrete compared to 10% CKC could be explained as the result of the cement dilution effect.

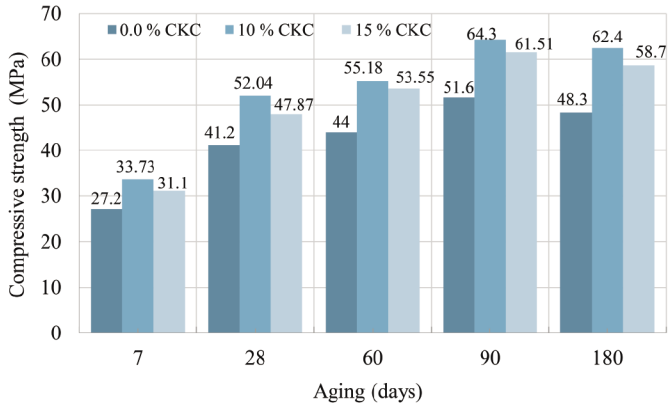

Fig. 5 Compressive strength of concrete containing different percentages of CKC cured in water for 7, 28, 60, 90, and 180 days
5. ábra A különböző százalékos CKC-tartalommal rendelkező 7, 28, 60, 90 és 180 napig vízben szilárdított betonok nyomószilárdsága

3.6.2 Compressive strength of concrete containing 0.0, 10, and 15% CKC after curing in NaCl (5%) for 7, 28, 60, 90 and 180 days

Fig. 6 shows that the compressive strength of concrete containing 0, 10, and 15% CKC after curing in NaCl (5%) for 7, 28, 60, 90, and 180 days. It was found that the concrete mixes containing 10% CKC recorded higher compressive strength than the control mix by values of 31.18, 25, 27.38, 24.08, and 28.5% at 7, 28, 60, 90, and 180 days respectively, and also higher than the concrete mixes containing 15% CKC whereas they achieved 25, 12.3, 17.2, 15 and 14.7% after 7, 28, 60, 90 and 180 days respectively.

The compressive strength increases up to 90 days, then decreases, but it is still higher than that of CKC-free concrete. The compressive strength values increased due to the pozzolanic effect of the amorphous silica, which supports the hydration reactions of cement [13; 45 - 47]. The formed products reduce the chloride ions permeability and sorptivity

of concrete, by blocking the porosity [47] and increasing the resistance of Cl^- ions diffusion [48, 50]. The deterioration of strength refers to the soluble calcium chloride formed from the reaction of calcium hydroxide with NaCl forming $CaCl_2$ which reacts with calcium aluminate forming Calcium chloro-aluminate (Freidel's salt, $(3CaO{\cdot}Al_2O_3{\cdot}CaCl_2 \cdot 10H_2O)$ [51]. Freidel's salt (FS) resulted from the ratio of 15% CKC by the excess active alumina which helped the reaction with $CaCl_2$ as shown in the diffractogram (*Fig. 7*).

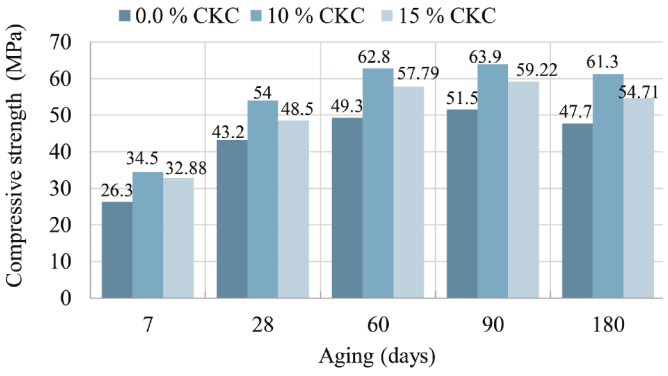

Fig. 6 Compressive strength of concrete containing 0, 10 and 15% of CKC cured in sodium chloride solution (5%) for up to 180 days
6. ábra A 0, 10 és 15% CKC-t tartalmazó beton nyomószilárdsága nátrium-klorid oldatban (5%) történő szilárdítás után

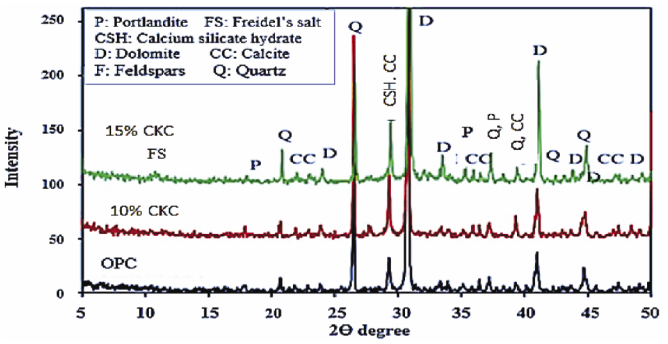

Fig. 7 XRD diffractogram for a concrete containing 0, 10, and 15% of CKC cured in sodium chloride solution for 6 months
7. ábra A nátrium-klorid oldatban 6 hónapig szilárdított 0, 10 és 15% CKC-t tartalmazó beton röntgendiffraktogramja

3.6.3 Compressive strength of concrete containing 0.0, 10% and 15% CKC after curing in magnesium sulfate solution (5%) for 7, 28, 60, and 90 days

The deterioration of subsurface concrete structures is caused by sulfate salts in subsurface water, soil, and seawater, in combination with alkali and alkaline earth metals such as sodium, magnesium, and calcium [52-56]. Most subsurface concrete structures are subject to corrosion attack for several reasons rather than only sulfate attack. Magnesium and sulfate ions are the most active ions that affect negatively the internal mechanical structures of concrete [57 - 61].

Magnesium sulfate-induced cracking, exposure of aggregates; compressive strength loss, and expansion of concrete were recorded [62 – 65]. Magnesium sulfate solution reacts with cement hydration products to form magnesium hydroxide (brucite mineral), calcium aluminum sulfate hydrate (ettringite), calcium sulfate (gypsum), and magnesium oxide (magnesia) [66 - 68]. Brucite decomposes to gypsum and damage concrete [69]. Several claims reported that magnesium sulfate environments caused more severe concrete degradation than sodium sulfate environments [70, 71–73]. The reason is that the combination of sulfate and magnesium attack destroys hydrated calcium silicate forming gypsum and ettringite minerals [74, 75, 76–81]. The mechanism of this attack was essentially controlled by magnesium which forms gypsum and hydrated magnesium silicate hydrate (not cementing material) [82]. Degradation caused by the formation of thaumasite was also noted when the temperature was less than 15 C [83]. Magnesium sulfate attack leads to decreased pH, speeding up the formation of gypsum and consequent intensification of concrete degradation [84].

Fig. 8 shows the compressive strengths of concrete samples containing 10 and 15% of CKC, after immersion in a $MgSO_4$ solution (5%) for 7, 28, 56, 90, and 180 days. The compressive strength increased up to 56 days, then decreased, but it is still higher than that of the control mix. It was found that the concrete mixes containing 10% CKC recorded higher compressive strength than the control mix by values of 23, 20.6, 21.5, 12.9, and 16.6% at 7, 28, 60, 90, and 180 days respectively, and also higher than the concrete mixes containing 15% CKC whereas they achieved 17, 10.6, 13.1, 11.4 and 13.6% after 7, 28, 60, 90 and 180 days respectively.

The increase in the compressive strength is attributed to the cementing effect of the amorphous silica, which causes acceleration in the reaction of the cement with water [85, 86]. The regression of the strength caused by the formation of gypsum as in the following equation:

$$Ca(OH)_2 + MgSO_4{\cdot}7H_2O \rightarrow CaSO_4{\cdot}2H_2O \text{ (gypsum)} + Mg(OH)_2 + 5H_2O$$

The formed gypsum reacts with calcium aluminate (product of cement hydration) and ettringite mineral $3CaO{\cdot}Al_2O_3{\cdot}\ 3CaSO_4{\cdot}31H_2O$ is formed as indicated in *Fig. 9* which causes relative expansion and cracking.

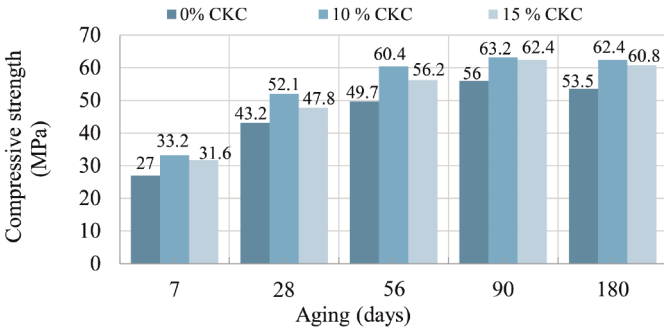

Fig. 8 Compressive strength of concrete mixes containing different percentages of CKC cured in magnesium sulfate solution for 6 months
8. ábra A különböző százalékos CKC-tartalmú betonkeverékek nyomószilárdsága magnézium-szulfát oldatban történő szilárdítás után

Curing in seawater for 7, 28, 60, 90, and 180 days of concrete containing 10 and 15% of CKC

Several trials were performed using sea water as it is highly salty (more than 40 g/l). The compressive strengths of concrete containing 0, 10, and 15% of CKC were determined after periods of immersion in seawater for up to 3 months (*Fig. 10*). It was found that from that the compressive strength of concrete

takes the same behavior when exposed to seawater, where the compressive strengths are relatively higher for concrete samples containing CKC compared to the untreated concrete with CKC.

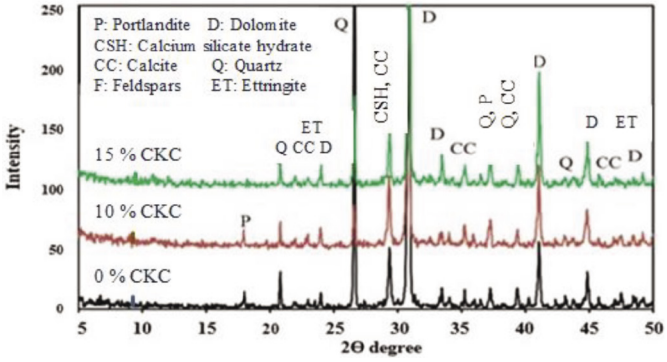

Fig. 9 XRD diffractogram for a concrete containing 0, 10, and 15% of CKC cured in magnesium sulfate solution for 180 days
9. ábra magnézium-szulfát oldatban 180 napig szilárdított 0, 10 és 15% CKC-t tartalmazó beton röntgendiffraktogramja

It was found that the concrete mixes containing 10% CKC recorded higher compressive strength than the control mix by values of 27.4, 18.6, 18.2, and 19, at 28, 60, 90, and 180 days respectively, and also higher than the concrete mixes containing 15% CKC whereas they achieved 15, 16, 13.7, and 13.4% after 28, 60, 90 and 180 days respectively.

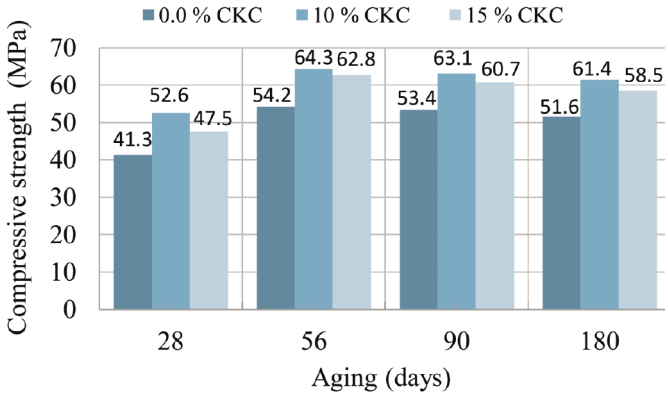

Fig. 10 Compressive strength of concrete containing different percentages of CKC after curing in seawater for up to 180 days
10. ábra A különböző százalékos CKC-tartalmú betonkeverékek nyomószilárdsága tengervízben történő szilárdítás után

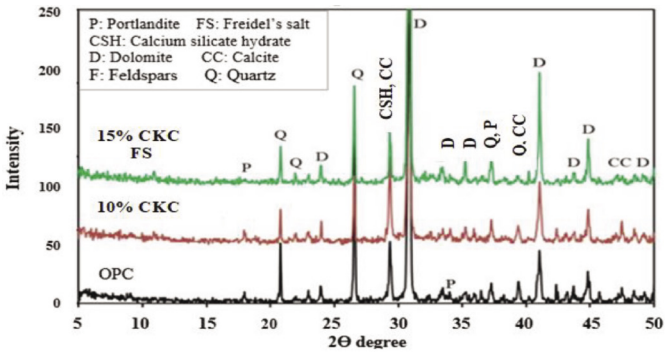

Fig. 11 XRD diffractogram for concrete containing 0, 10, and 15% of CKC cured in seawater for 180 days
11. ábra A tengervízben 180 napig szilárdított 0, 10 és 15% CKC-t tartalmazó beton röntgendiffraktogramja

The compressive strength went slightly down after 3 months, but it was still higher than the CKC-free concrete. The increase in compressive strength is due to the decrease in the percentage of calcium hydroxide (Portlandite), which reduces the formation of gypsum and ettringite minerals, in addition to that there is another reason related to the morphology of pores, as they are not interconnected as a result there was no way for passage of sulfates to the concrete bulk agreeing with what was reported [50]. The decreasing strength may be attributed to the formation of weak easily soluble calcium chloride salt from the reaction of calcium hydroxide with NaCl yielding $CaCl_2$ which reacts with calcium aluminate hydrate forming calcium chloro-aluminate (Freidel's salt) [51] (*Fig. 11*).

3.6.4 Exposure of concrete modified with CKC to heat

3.6.4.1 Effect of heat on the compressive strength

High temperatures have a bad effect on concrete; the short-time exposure to elevated temperatures slightly affects it's the performance when initially exposed to fire [87, 88]. However, relatively long-time exposure would inevitably change the chemical composition and physical and mechanical properties severely. Thermal-induced cracks usually induce material degeneration and further threaten the safety and serviceability of whole structures [88, 89]. The concrete strength deteriorates, leading to loss of cohesion, causing collapse [BS EN 1992–1–2 (2004) and ACI Committee 216]. The reduction of the strength of the specimens exposed to 200 °C temperature may be attributed to the loss of the physically adsorbed water and the destruction of hydrated binder [91]. The addition of CKC increases the heat-bearing strength of concrete. *Fig. 12* shows the effect of exposure to increasing temperatures from 25 to 700 °C for concrete containing 10 and 15% of CKC relative to CKC-free concrete. In general, the compressive strength values of concrete decrease with the continuation of the temperature increase until 700 °C.

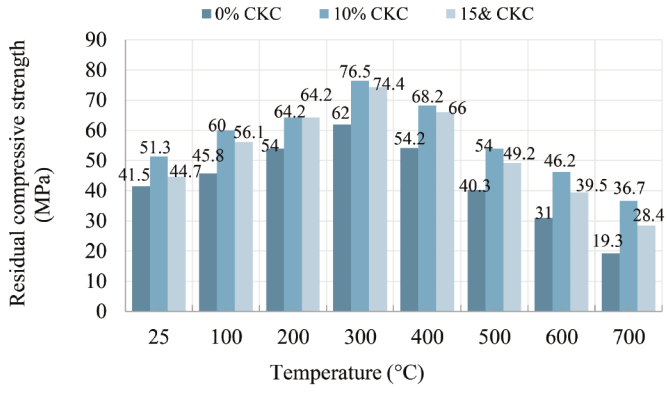

Fig. 12 Effect of heat on the compressive strength of concrete containing 10 and 15% of CKC
12. ábra A hőmérséklet hatása a 0, 10 és 15% CKC-t tartalmazó betonok nyomószilárdságára

The concrete which contains 10% CKC retains compressive strength values more than those containing 15% CKC and the free of CKC for all temperatures. At 700 °C the compressive strength of concrete containing CKC 10% reduced to 36.7 MPa relative to the compressive strength value at room temperature (25 °C) which was 51.3 MPa with a reduction percentage of

28.5%, while the compressive strength value of the containing concrete 15% reduced to 28.4 MPa with a percentage reduction of 36.5%. *Fig. 12* shows that 10% MK is the best ratio of thermal endurance and high compressive strength retention compared to concrete containing 15% MK or the free mix.

3.6.4.2 Effect of heat on the weight of concrete modified with CKC

Fig. 13 gives weight loss values for concrete containing 0, 10, and 15% of CKC when exposed to temperatures from 200-700 °C. The results show that the concrete containing 10% CKC is the lowest in weight loss with a temperature rise from 200 to 700 °C, rather than the concrete containing 15% of CKC. The loss in weight for concrete containing 10% CKC was 7.89%, while the loss in weight for concrete containing 15% was 8.42%, and the loss in concrete without CKC = 10.4%.

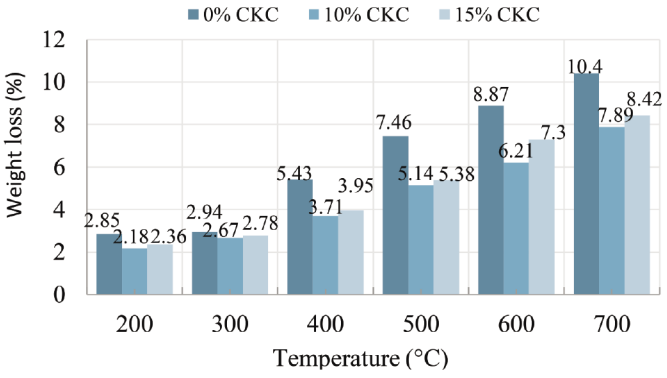

Fig. 13 *Effect of heat on the weight loss of concrete containing 10 and 15% of CKC*
13. ábra *A hőmérséklet hatása a 0, 10 és 15% CKC-t tartalmazó beton tömegveszteségére*

3.6.4.3 Effect of heat on the porosity of concrete

It was found that the porosity of concrete increased with increasing of temperature. The higher porosity at elevated temperatures may be attributed to the increase in pore volume due to moisture elimination from the concrete matrix. Above 400 °C, the voids and micro-cracks start to appear due to bound water escape. Over 500 °C, micro cracks were developed, causing more increase in the porosity.

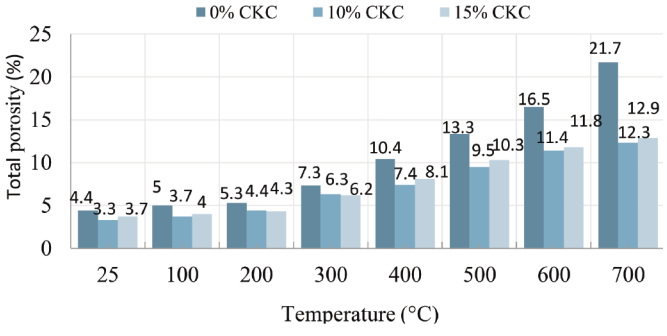

Fig.14 *The total porosity of concrete containing 0, 10 and 15% CKC exposed to heat up to 700 °C*
14. ábra *A 0, 10 és 15% CKC-t tartalmazó beton teljes porozitásának változása a hőmérséklet emelésének következtében 700 °C-ig*

Fig. 14 shows that the total porosity of concrete containing 10 and 15% of CKC is lower than that of the control mix at all temperatures in the range from 200 to 700 °C. At 700 °C the porosity reached 12.3% at 10% CKC compared to concrete containing 15%, where the porosity was 12.9%, and the porosity of CKC-free concrete was 21.7%. It should be noted that the low porosity of concrete containing 10% of CKC at room temperature 3.3% is one of the important characteristics of concrete in terms of low permeability that prevents the entry of aggressive chemicals from the medium surrounding the concrete.

3.6.5 Effect of CKC as a partial cement replacement in reinforced concrete on steel corrosion

Several electrochemical measurements are used for evaluating the risk of steel corrosion in concrete. The anodic polarization measurement is one of the important methods this method proved to be a reliable test for predicting the corrosive or inhibitive nature of the medium surrounding the steel reinforcement. Several research studies reported the limits for maintaining the steel passivity in concrete in the surrounding environment as the passivation potential > 600 mV (SCE) [91, 92]. The anodic polarization results as illustrated in *Fig. 15* for reinforcement steel in the concrete containing 0, 10, and 15% CKC after curing in water for 28 days. The following limits for estimating the strength of reinforcement steel in concrete are the passivation Potential > 600 mV to reach zero passivation, and the highest time for achieving that potential is 15 min. From these results, it was clear that the concrete modified with CKC 15% achieved the highest value of passivation potential (698 mV), in the shortest time (5.7 min.), while the concrete that contains 10% achieved 685 mV at a time of 6.4 min and the 0% CKC reached 645 mV at a time 8.2 min. therefore, 10 and 15% of CKC reached passivation higher than zero CKC concrete.

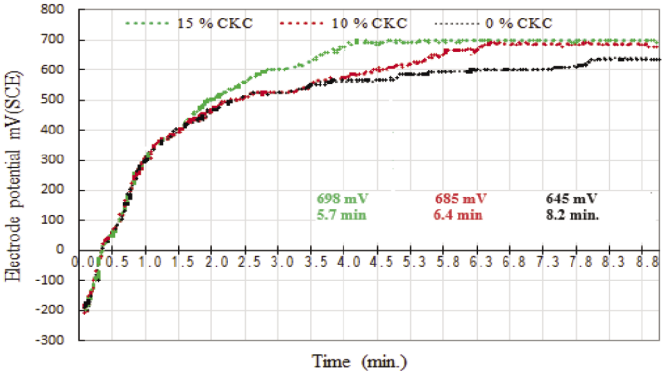

Fig. 15 *Anodic polarization behavior of steel in concrete, after curing in tap water for 28 days*
15. ábra *Az acél anódos polarizációs viselkedése betonban, miután 28 napig csapvízben érlelődött*

By using seawater as the ambient conditions for concrete it was found that the continuity of rising passivation potential for concrete that contains 15% CKC was 660 mV in 6.2 min. while the concrete that contains 10% achieved 645 mV at a time of 6.4 min and the 0% CKC reached 627 mV at a time of 7.8 min. therefore, 10 and 15% of CKC reached passivation higher than zero CKC concrete. So, 15% CKC is the best ratio for protecting steel against corrosion as shown in *Fig. 16*.

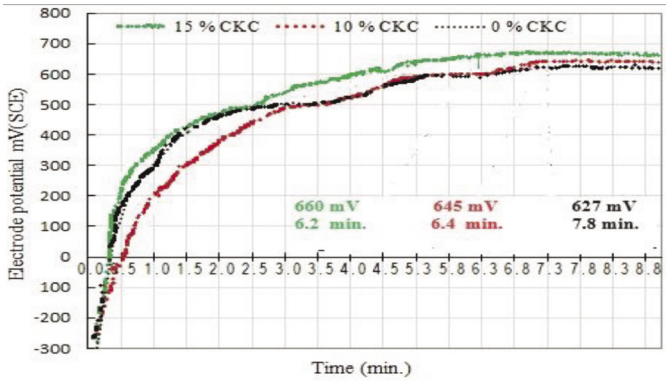

Fig.16 Anodic polarization behavior of steel in concrete, after curing in seawater for 28 days

16. ábra Az acél anódos polarizációs viselkedése betonban, tengervízben történő 28 napos szilárdulás után

These measurements show that 15% MK is the better ratio as a replacement percentage for cement in concrete that preserves steel against corrosion as a result of the penetration of harmful elements from water to concrete.

4. Conclusions

1. It was concluded that the partial replacement of cement with CKC (10 and 15%) caused slight expansion of concrete within the limits and there was no significant effect on the alkaline silica reaction or alkalinity of the concrete medium. Therefore there is no negative impact on the hydration products of cement and formation of the binding materials.
2. For the concrete mixes cured in tap water it was found that the concrete mixes containing 10% CKC recorded higher compressive strength than the control mix by values of 24, 26.3, 25.4, and 24.6% at 7, 28, 60, 90, and 180 days respectively, and also higher than the concrete mixes containing 15% CKC whereas they achieved 14.3, 16.2, 21.7, 19.2 and 21.5% after 7, 28, 60, 90 and 180 days respectively.
3. For samples cured in NaCl solution (5%), it was found that the concrete mixes containing 10% CKC recorded higher compressive strength than the control mix by values of 31.18, 25, 27.38, 24.08, and 28.5% at 7, 28, 60, 90, and 180 days respectively, and also higher than the concrete mixes containing 15% CKC whereas they achieved 25, 12.3, 17.2, 15 and 14.7% after 7, 28, 60, 90 and 180 days respectively.
4. For concrete mixes cured in $MgSO_4$ solution (5%), the compressive strength increased up to 56 days, then decreased, but it is still higher than that of the control mix. It was found that the concrete mixes containing 10% CKC recorded higher compressive strength than the control mix by values of 23, 20.6, 21.5, 12.9, and 16.6% at 7, 28, 60, 90, and 180 days respectively, and also higher than the concrete mixes containing 15% CKC whereas they achieved 17, 10.6, 13.1, 11.4 and 13.6% after 7, 28, 60, 90 and 180 days respectively.
5. A substituted ratio of 10% OPC with calcined kaolinitic clay in the concrete is the best in terms of resistance to wear and tear due to the thermal endurance and maintaining high compressive strength relative to the concrete containing 15% or the free concrete. At 700 °C the compressive strength of concrete containing CKC 10% reduced by 28.5%, while the compressive strength value of the containing concrete 15% reduced by 36.5%.
6. 10% replacement of cement resulted in the lowest total porosity of concrete, which minimized the permeability of concrete and the penetration of aggressive elements from the environment, so, the improved concrete structure endures in the near marine areas.
7. The replacements of 10 and 15% of cement with calcined kaolinitic clay protect the steel from corrosion.

Acknowledgment

This work was supported by the Aluminum Sulphate Co. of Egypt.

References

[1] Smirnova, O.M.; Menéndez Pidal de Navascués, I.; Mikhailevskii, V.R.; Kolosov, O.I.; Skolota, N.S. 2021. "Sound-Absorbing Composites with Rubber Crumb from Used Tires". Appl. Sci., 11, 7347. https://doi.org/10.3390/app11167347

[2] Alvee, A.R.; Malinda, R.; Akbar, A.M.; Ashar, R.D.; Rahmawati, C.; Alomayri, T.; Raza, A.; Shaikh, F.U.A. 2022. "Experimental Study of the Mechanical Properties and Microstructure of Geopolymer Paste Containing Nano-Silica from Agricultural Waste and Crystalline Admixtures". Case Stud. Constr. Mater., 16, e00792. https://doi.org/10.1016/j.cscm.2021.e00792

[3] Althoey, F. 2021. "Compressive Strength Reduction of Cement Pastes Exposed to Sodium Chloride Solutions: Secondary Ettringite Formation". Constr. Build. Mater., 299, 123965. https://doi.org/10.1016/j.conbuildmat.2021.123965

[4] Marie, I.; Quiasrawi, H. 2012. "Closed-Loop Recycling of Recycled Concrete Aggregates". J. Clean. Prod., 37, 243–248. https://doi.org/10.1016/j.jclepro.2012.07.020

[5] Ahmad, J.; Aslam, F.; Martinez-Garcia, R.; De-Prado-Gil, J.; Qaidi, S.M.A.; Brahmia, A. 2021. "Effects of Waste Glass and Waste Marble on Mechanical and Durability Performance of Concrete". Sci. Rep., 11, 21525. https://doi.org/10.1038/s41598-021-00994-0

[6] Rahmawati, C.; Aprilia, S.; Saidi, T.; Aulia, T.B. 2021."Current Development of Geopolymer Cement with Nanosilica and Cellulose Nano-crystals". In Journal of Physics: Conference Series, Proceedings of the Annual Conference on Science and Technology Research (ACOSTER), Medan, Indonesia, 20–21 June 2021; IOP Publishing: Bristol, UK; pp. 1–8. https://doi.org/10.1088/1742-6596/1783/1/012056

[7] Ahmad, J.; Tufail, R.F.; Aslam, F.; Mosavi, A.; Alyousef, R.; Faisal Javed, M.; Zaid, O.; Khan Niazi, M.S. 2021. "A Step towards Sustainable Self-Compacting Concrete by Using Partial Substitution of Wheat Straw Ash and Bentonite Clay Instead of Cement". Sustainability, 13, 824. https://doi.org/10.3390/su13020824

[8] Singh, M.; Choudhary, K.; Srivastava, A.; Sangwan, K.S.; Bhunia, D. 2017. "A Study on Environmental and Economic Impacts of Using Waste Marble Powder in Concrete". J. Build. Eng., 13, 87–95. https://doi.org/10.1016/j.jobe.2017.07.009

[9] Taskin, A.; Fediuk, R.; Grebenyuk, I.; Elkin, O.; Kholodov, A. 2020. "Effective Cement Binders on Fly and Slag Waste from Heat Power Industry of the Primorsky Krai, Russian Federation. Int. J. Sci. Technol. Res., 9, 3509–3512.

[10] Abdelgader, H.; Fediuk, R.; Kurpi´ nska, M.; Elkhatib, J.; Murali, G.; Baranov, A.V.; Timokhin, R.A. 2019. "Mechanical Properties of Two-Stage Concrete Modified by Silica Fume". Mag. Civ. Eng., 89, 26–38. https://creativecommons.org/licenses/by/4.0

[11] Ahmad, J.; Martínez-García, R.; De-Prado-Gil, J.; Irshad, K.; El-Shorbagy, M.A.; Fediuk, R.; Vatin, N.I. 2022. "Concrete with Partial Substitution of Waste Glass and Recycled Concrete Aggregate". Materials, 15, 430.

[12] Dinakar, P.; Sethy, K.P.; Sahoo, U.C. 2013. "Design of Self-Compacting Concrete with Ground Granulated Blast Furnace Slag". Mater. Des., 43, 161–169. https://doi.org/10.1016/j.matdes.2012.06.049

[13] Sabir, B.B.; Wild, S.; Bai, J. 2001. "Metakaolin and Calcined Clays as Pozzolana for Concrete: A Review". Cem. Concr. Compos., 23, 441–454.

[14] Lee, G.; Ling, T.-C.; Wong, Y.-L.; Poon, C.-S. 2011. "Effects of Crushed Glass Cullet Sizes, Casting Methods and Pozzolanic Materials on ASR of Concrete Blocks. Constr. Build. Mater., 25, 2611–2618.

[15] Vizcayno, C.; de Gutiérrez, R.M.; Castello, R.; Rodriguez, E.; Guerrero, C.E, 2010. "Pozzolan Obtained by Mechano-chemical and Thermal Treatments of Kaolin". Appl. Clay Sci., 49, 405–413. https://doi.org/10.1016/j.clay.2009.09.008

[16] Siddique, R.; Klaus, J., 2009. "Influence of Metakaolin on the Properties of Mortar and Concrete: A Review". Appl. Clay Sci., 43, 392–400. https://doi.org/10.1016/j.clay.2008.11.007

[17] Güneyisi, E.; Geso˘ glu, M.; Karao˘ glu, S.; Mermerda¸ S, K., 2012. "Strength, Permeability and Shrinkage Cracking of Silica Fume and Metakaolin Concretes". Constr. Build. Mater., 34, 120–130. https://doi.org/10.1016/j.conbuildmat.2012.02.017

[18] Badogiannis, E.; Tsivilis, S. 2009. "Exploitation of Poor Greek Kaolins: Durability of Metakaolin Concrete". Cem. Concr. Compos., 128–133. https://doi.org/10.1016/j.cemconcomp.2008.11.001

[19] Ding, J.-T.; Li, Z., 2002. "Effects of Metakaolin and Silica Fume on Properties of Concrete". Mater. J., 99, 393–398.

[20] Bai, J. ;Wild, S.; Sabir, B.B., 2002. "Sorptivity and Strength of Air-Cured and Water-Cured PC–PFA–MK Concrete and the Influence of Binder Composition on Carbonation Depth". Cem. Concr. Res., 32, 1813–1821. https://doi.org/10.1016/S0008-8846(02)00872-4

[21] Güneyisi, E.; Mermerda¸ S, K., 2007. "Comparative Study on Strength, Sorptivity, and Chloride Ingress Characteristics of Air-Cured and Water-Cured Concretes Modified with Metakaolin". Mater. Struct., 40, 1161–1171.

[22] Tian, B., Cohen, M.D., 2000. "Does gypsum formation during sulfate attack on concrete lead to expansion? Cement and Concrete Research, 30 (1), pp. 117-123. https://doi.org/10.1016/S0008-8846(99)00211-2

[23] Skaropoulou, A., Tsivilis, S., Kakali, G., Sharp, J.H., Swamy, R.N., 2009. "Long-term behavior of Portland limestone cement mortars exposed to magnesium sulfate attack". Cement and Concrete Composites, 31 (9), pp. 628-636. https://doi.org/10.1016/j.cemconcomp.2009.06.003

[24] Gutt, W.H. and Harrison, W.H., 1977. "Chemical resistance of concrete", Concrete, 11, 35 – 37.

[25] Ramachandran, V.S., Feldman, R.F. and Beaudoin, J.J., 1981. "Concrete Science", Heyden & Sons. Inc., Philadelphia, USA.

[26] Manisha M, S.K. Bhattacharyya, SK, V. Barai, 2020. "Thermal and mechanical properties of concrete and its constituents at elevated temperatures: A review, Construction and Building Materials, Vol. 270, 8 February 2021, 121398.
https://doi.org/10.1016/j.conbuildmat.2020.121398

[27] Regourd, M., 1981. "Chemical durability of concrete", Contemporary European Concrete Research Confr., Stockholm, 1.

[28] Javellana, M. P. and Jawed, I. (1982) Extraction of the free lime in Portland Cement and Clinker by Ethylene Glycol", Cement and Concrete Research, Vol. 12, 1982, pp. 309-403.

[29] Palomo, A., Blanco-Varela, M.T., Granizo, M.L., Puertas, F., Vazquez, T., and Grutzeck, M.W.," Chemical Stability of Cementitious Materials Based on Metakaolin", Cement and Concrete Research, 29, 997 (1999). https://doi.org/10.1016/S0008-8846(99)00074-5

[30] Güneyisi, E.; Geso˘ glu, M.; Mermerda¸ S, K., 2008. "Improving Strength, Drying Shrinkage, and Pore Structure of Concrete Using Metakaolin. Mater. Struct., 41, 937–949. https://doi.org/10.1617/s11527-007-9296-z

[31] Danish, P.; Ganesh, M.G., 2020. "Behavior of Self-Compacting Concrete Using Different Mineral Powders Additions in Ternary Blends. Rev. Rom. Mater., 50, 232–239.

[32] Nazir, U., Jandiyal, A., Salotra, S. and Sharma, R., 2016. "Incorporation of metakaolin in concrete: A Review" Inter. J., Civil Engineering and Technology, 7, 17.

[33] Shelokar A.P. and Jadhao P.D., 2013. "Strength appraisal of high grade concrete by using high reactive metakaolin", Inter. J. of Innovative Research in Science, Engineering and Technology", 2, 657-663.

[34] Dinakar P., Pradosh K.S. and Sriram G., 2013. "Effect of metakaolin content on the properties of high strength concrete", Inter. J. of Concrete Structures and Materials, 7, 215-223.

[35] Hoda S. Eldin, Nabil, A. Abdullah, Ismail Mahmoud F., Hashem Ahmed I. (2022) *Preparation of meta phase of kaolinite as a precursor for geopolymer adsorbent fabrication* Epitőanyag– Journal of Silicate Based and Composite Materials, Vol. 74, No. 3 (2022), 82–87. p.
https://doi.org/10.14382/epitoanyag-jsbcm.2022.13

[36] ASTM C. Standard test method for compressive strength of hydraulic cement mortars (using 2-in. or [50-mm] cube specimens). Annual Book of ASTM Standards. 2016;4.

[37] Rushing TS, Stynoski PB, Barna LA, Al-Chaar GK, Burroughs JF, Shannon JD, Kreiger MA, Case MP. Investigation of concrete mixtures for additive construction. In3D Concrete Printing Technology 2019 Jan 1 (pp. 137-160). Butterworth-Heinemann.
https://doi.org/10.1016/B978-0-12-815481-6.00007-5

[38] Krishnan P, Jewaratnam J. Recovery of water treatment residue into clay bricks. Chemical Engineering Transactions. 2017 Mar 20; 56:1837-1842. https://doi.org/10.3303/CET1756307

[39] ASTM C1567-07 "Standard test method for determining the potential alkali –silica reactivity of combinations of cementations materials and aggregate "(Accelerated mortar-bar method) (2007).

[40] Rilem TC 154-EMC, "Electrochemical techniques for measuring metallic corrosion, test methods for on-site corrosion rate measurement of steel reinforcement in concrete by means of thepolarization resistance method", Materials and Structures/ Materiauxet Constructions, 37, , 623-643,(2004).

[41] Gouda, V.K., Adul Azim, A.A. and El-Sayed, H.A., 1974. "Some aspects of reinforcement corrosion in Egyptian structures", British corrosion J., 9, 185 – 189.

[42] Shekarchi M., Bonakdar A., Bakhshi, Mirdamadi A. and Mobasher B., 2010. "Transport properties in metakaolin blended concrete", Construction and Building Materials", 24, 2217-2223.

[43] Kostush, J.A., Walters, V. and Jones T.R., 1993. "High-Performance Concretes Incorporating Metakaolin: A Review, Proc. of Conference concrete 2000 Economic and Durable Construction through Excellence, 1799-1811.

[44] Maria C.G.J. and Rafat S., 2015. "Recent advances in understanding the role of supplementary cementitious materials in concrete", Cement and Concrete Research, 78, 71-80.

[45] Jones, M.R., Mc Carthy, M.J. and Dhir, R.K., 1993. "Chloride resistant concrete", Concrete 2000 Economic and durable construction through Excellency, Proc. of Inter. Confr., Scotland, UK, 1429-1444.

[46] Badogiannis, E.; Tsivilis, S., 2009. "Exploitation of Poor Greek Kaolins: Durability of Metakaolin Concrete". Cem. Concr. Compos., 31, 128–133.

[47] Jian-Tong, D. and Zongjin, Li, 2002. "Effects of metakaolin and silica fume on properties of concrete", ACI Mater, J., 99, 393-398.

[48] Xianmingi Shi, Ning Xie, Keith, F. and Jing G., 2012. "Durability of steel reinforced concrete in chloride environments; An overview", Const. and Build. Mater., 30, 125-138.

[49] Valipour, M., Pargar, F., Shekarchi, M. and Khani, S., 2013. "Comparing a natural pozzolan, zeolite, to metakaolin and silica fume in terms of their effect on the durability characteristics of concrete: A laboratory study, Const. and Build. Mater., 41, 879-888.

[50] Shatat, M.R., Maroof, M.A., El-Sayed, A.Y., Abo-Elenein, S.A. and Heikal, E.S., 2016. "Physico-chemical properties of the hardened blended cement pastes made of OPC-MK blends CKD", Chemistry of Advanced Materials, 1, 17-26.

[51] Mohammed, T.U., Ostsuki, N. and Hamada, H., 2003. "Corrosion of steel bars in cracked concrete under marine environment", J. of Materials in Civil Engineering, ASCE, 15, 460-469.

[52] Ouyang, C., Nanni, A., Chang, W.F., 1988. "Internal and external sources of sulfate ions in Portland cement mortar: two types of chemical attack, *Cement and Concrete Research*, 18 (5), pp. 699-709. https://doi.org/10.1016/0008-8846(88)90092-0

[53] Wee, T.H., Suryavanshi, A.K., Wong, S.F., Anisur Rahman, A.K.M., 2000. "Sulfate resistance of concrete containing mineral admixtures. *ACI Structural Journal*, 97 (5), pp. 536-549.

[54] Zhao, G., Li, J., 2018. "Study on degradation in axial bearing capacity of a cast-in-situ pile caused by sulfate attack in saline area", pp. 253-264. Geo Shanghai International Conference, May 26-29, Shanghai.

[55] Rasheeduzzafar., "Influence of Cement Composition on Concrete Durability", ACI Materials Journal, Vol. 89 (6), 1992, pp. 574-585.
[56] Cohen, Menashi D., Mather, Bryant Sulfate attack on concrete. (1991) *ACI Materials Journal*, 88 (1), pp. 62-69.
[57] Behfarnia, K., Farshadfar, O. The effects of pozzolanic binders and polypropylene fibers on durability of SCC to magnesium sulfate attack (2013) Construction and Building Materials, 38, pp. 64-71. Cited 62 times. https://doi.org/10.1016/j.conbuildmat.2012.08.035
[58] Zhao, H., Xiong, R., Guan, B.-W. Fatigue damage property of cement concrete under magnesium sulfate corrosion condition (2014) *Applied Mechanics and Materials*, Part I 638-640, pp.1153-1157.ISBN:978-303835258-7 https://doi.org/10.4028/www.scientific.net/AMM.638-640.1153
[59] Brown, P.W., Doerr, A. Chemical changes in concrete due to the ingress of aggressive species (2000) *Cement and Concrete Research*, 30 (3), pp. 411-418. Cited 96 times. https://doi.org/10.1016/S0008-8846(99)00266-5
[60] Jiang, L., Niu, D., 2016. "Study of deterioration of concrete exposed to different types of sulfate solutions under drying-wetting cycles". *Construction and Building Materials*, 117, pp.88-98. https://doi.org/10.1016/j.conbuildmat.2016.04.094
[61] Al-Amoudi, Omar Saeed Baghabra, Maslehuddin, Mohammed, Saadi, Mahmoud M., 1995. "Effect of magnesium sulfate and sodium sulfate on the durability performance of plain and blended cements". *ACI Materials Journal*, 92 (1), pp. 15-24.
[62] Higgins, D.D., Crammond, N.J., 2003. "Resistance of concrete containing ggbs to the thaumasite form of sulfate attack". Cement and Concrete Composites, 25 (8), pp. 921-929. https://doi.org/10.1016/S0958-9465(03)00149-5
[63] Al-Dulaijan, S.U., 2007. "Sulfate resistance of plain and blended cements exposed to magnesium sulfate solutions". *Construction and Building Materials*, 21 (8), pp. 1792-1802. Cited 73 times. https://doi.org/10.1016/j.conbuildmat.2006.05.017
[64] Al-Amoudi, O.S.B., Maslehuddin, M., Abdul-Al, Y.A.B., 1995. "Role of chloride ions on expansion and strength reduction in plain and blended cements in sulfate environments". *Construction and Building Materials*, 9 (1), pp. 25-33. https://doi.org/10.1016/0950-0618(95)92857-D
[65] Karakoç, M.B., Türkmen, I., Maraş, M.M., Kantarci, F., Demirbola, R., 2016. *Ceramics International*, PartB 42 (1), pp.1254-1260. https://doi.org/10.1016/j.ceramint.2015.09.058
[66] Cohen, Menashi D., Bentur, Arnon,, 1988. "Durability or Portland cement-silica fume pastes in magnesium sulfate and sodium sulfate solutions". *ACI Materials Journal*, 85 (3), pp. 148-157.
[67] Lee, S. J., Park, J.M., 2017. "A study on the magnesium sulfate resistance of garnet fiber concrete". *Key Engineering Materials*, 730 KEM, pp. 389-394. https://doi.org/10.4028/www.scientific.net/KEM.730.389
[68] Santhanam, M., Cohen, M.D., Olek, J., 2003. "Mechanism of sulfate attack: A fresh look - Part 2. Proposed mechanisms". *Cement and Concrete Research*, 33 (3), pp. 341-346. https://doi.org/10.1016/S0008-8846(02)00958-4
[69] Jiang, L., Niu, D., Study of deterioration of concrete exposed to different types of sulfate solutions under drying-wetting cycles, Constr. Build. Mater. 117 (2016) 88–98.
[70] Santhanam, M., Cohen, M. D., Olek, J., Mechanism of sulfate attack: a fresh look: Part 1: Summary of experimental results, Cem. Concr. Res. 32 (6) (2002) 915– 921.
[71] Park, Y. S., Suh, J. K., Lee, J. H., Shin, Y. S., Strength deterioration of high strength concrete in sulfate environment, Cem. Concr. Res. 29 (9) (1999) 1397–1402.
[72] Neville, A., The confused world of sulphate attack on concrete, Review, Cem. Concr. Res. 34 (2004) 1275–1296.
[73] Al-Amoudi, O. S. B., Maslehuddin, M., M.M. Saadi, M. M., Effect of magnesium sulfate and sodium sulfate on the durability performance of plain and blended cements, ACI Mater. J. 92 (1) (1995) 15–24
[74] H. Siad, M. Lachemi, S.K. Bernard, M. Sahmaran, A. Hossain, Assessment of the long-term performance of SCC incorporating different mineral admixtures in a magnesium sulphate environment, Constr. Build. Mater. 80 (C1) (2015) 141– 154.
[75] Y. Tan, H. Yu, H. Ma, Y. Zhang, C. Wu, Study on the micro-crack evolution of concrete subjected to stress corrosion and magnesium sulfate, Constr. Build. Mater. (2017) 453–460.
[76] W.G.V. Saavedra, D.E. Angulo, R.M.D. Gutiérrez, Fly ash slag geopolymer concrete: resistance to sodium and magnesium sulfate attack, J. Mater. Civil. Eng. 28 (12) (2016) 04016148.
[77] M. Basista, W. Weglewski, Chemically assisted damage of concrete: a model of expansion under external sulfate attack, Int. J. Damage Mech. 18 (2) (2009) 155–175.
[78] D. Mostofinejad, F. Nosouhian, H. Nazari-Monfared, Influence of magnesium sulphate concentration on durability of concrete containing micro-silica, slag and limestone powder using durability index, Constr. Build. Mater. 117 (2016) 107–120. [
[79] G.G. Liu, A.B. Ma, C.M. Pang, P. Zhang, H.G. Qin, L. Wang, Corrosion behavior of F30S30 concrete under wet-dry cycles in simulated seawater with magnesium salt and sulfate, Adv. Mater. Res. 936 (2014) 1366–1372.
[80] S.A. Hartshorn, J.H. Sharp, R.N. Swamy, The thaumasite form of sulfate attack in Portland-limestone cement mortars stored in magnesium sulfate solution, Cem. Concr. Compos. 24 (3) (2002) 351–359.
[81] Rasheeduzzafar, O.S.B. Al-Amoudi, S.N. Abduljauwad, M. Maslehuddin, Magnesium-sodium sulfate attack in plain and blended cements, ASCE J. Mater. Civil. Eng. 6 (2) (1994) 201–222.
[82] A. Skaropoulou, K. Sotiriadis, G. Kakali, S. Tsivilis, Use of mineral admixtures to improve the resistance of limestone cement concrete against thaumasite form of sulfate attack, Cement Concr. Compos. 37 (2013) 267–275.
[83] P.W. Brown, H.F.W. Taylor, The role of ettringite in external sulfate attack, Materials science of concrete: sulfate attack mechanisms (1999) 73–97.
[84] Bonen, D., Cohen, M. D., 1992. "Magnesium sulfate attack on portland cement paste-I. Microstructural analysis". *Cement and Concrete Research*, 22 (1), pp. 169-180. https://doi.org/10.1016/0008-8846(92)90147-N
[85] Siad, H., Lachemi, M., Bernard, S.K., Sahmaran, M., Hossain, A., 2015. "Assessment of the long-term performance of SCC incorporating different mineral admixtures in a magnesium sulfate environment". *Construction and Building Materials*, 80, pp.141-154. https://doi.org/10.1016/j.conbuildmat.2015.01.067
[86] H. Hajiloo and M. F. Green, "Post-fire residual properties of GFRP reinforced concrete slabs: a holistic investigation," *Composite Structures*, vol. 201, pp. 398–413, 2018.
[87] D. S. Ellis, H. Tabatabai, and A. Nabizadeh, "Residual tensile strength and bond properties of GFRP bars after exposure to elevated temperatures," *Materials*, vol. 11, no. 3, p. 346, 2018.
[88] E. R. K. Chandrathilaka, J. C. P. H. Gamage, and S. Fawzia, "Mechanical characterization of CFRP/steel bond cured and tested at elevated temperature," *Composite Structures*, vol. 207, pp. 471–477, 2019.
[89] Q. Ma, R. Guo, Y. Sun, K. C. He et al., "Behavior of modified lightweight aggregate concrete after exposure to elevated temperatures," *Magazine of Concrete Research*, vol. 70, no. 5, pp. 1–14, 2017.
[90] Saca, N., Georgescu, M., 2014. "Behavior of ternary blended cements containing limestone filler and fly ash in magnesium sulfate solution at low temperature". *Construction and Building Materials*, 71, pp. 246-253. https://doi.org/10.1016/j.conbuildmat.2014.08.037
[91] El-Sayed, H. A., A. H. Ali, and A. M. Sharara. "Resistance of pastes of sulphate-resisting cement to salt attack and concomitant effects on corrosion of embedded reinforcement." CEMENTO 92 (1995): 175-188.
[92] J.A. González, J. A., C. Andrade, C., Alonso, C. Feliu, S., Comparison of rates of general corrosion and maximum pitting penetration on concrete embedded steel reinforcement, Cem. Concr. Res. 25 (1995) 257–264. https://doi.org/10.1016/0008- 8846(95)00006-2

Ref.:
Abdullah, Nabil A. – **Abdullah**, Hajer: *Calcined kaolinitic clay as a supplementary cementing material and its pozzolanic effect on concrete blends characteristics (Part 2)*
Építőanyag – Journal of Silicate Based and Composite Materials, Vol. 76, No. 1 (2024), 10–20 p.
https://doi.org/10.14382/epitoanyag-jsbcm.2024.2

Durability of concrete modified with acid leached calcined kaolinitic clay

Nabil A. ABDULLAH
Consultant and Research Director in Aluminum Sulphate Co. of Egypt (ASCE). Ph.D. in Environmental science, Faculty of Science, Ain Shams University, Egypt.

Hajer N. Abdullah
Research assistant in October University for Modern Science and Arts (MSA university), Faculty of Engineering, Civil Engineering Department, Egypt..

Nabil A. ABDULLAH ▪ Research & Development Dept. Director, Aluminum Sulphate Co. of Egypt ▪ nabilxp9@gmail.com
Hajer ABDULLAH ▪ Civil Engineering Dept., MSA university, Egypt ▪ Hnabdullah@msa.edu.eg

Érkezett: 2023. 12. 15. ▪ Received: 15. 12. 2023. ▪ https://doi.org/10.14382/epitoanyag-jsbcm.2024.3

Abstract
Calcined or thermally treated kaolinitic clay (CKC) was leached by sulphuric acid to extract aluminum in the manufacturing of aluminum sulfate coagulant. The residual of this process is called low alumina calcined kaolinitic clay or Acid-Leached Calcined Kaolinitic Clay (ALCKC). ALCKC was investigated as a supplementary cementing material by mixing with Ordinary Portland Cement (OPC) and the durability of the concrete was assessed. The experimental protocol included optimization of the mixes of ALCKC/OPC containing 0, 10, and 15 ALCKC for the production of hardened concrete, and in this work, the durability against chlorides, sulfates solutions, heating, and seawater was studied. It was found that the addition of ALCKC to cement/concrete caused slight expansion of concrete within the limits and there was no significant effect on the alkaline silica reaction or alkalinity of the concrete medium. When using ALCKC in plain concrete, the ratio of 10% ALCKC/OPC achieved higher resistance against the negative effect of salt solutions attack. The ratio 10% of ALCKC to OPC is the optimum ratio that achieved high-performance plain concrete with compressive strength greater than the reference OPC by 24.7% and the ratio of 15% achieved 17.9% after aging of 90 days and this performance was better than that achieved by the ratio of 20% therefore for this reason this ratio was excluded. The ratio of 10% LACKC/OPC achieved high resistance to heat exposure keeping high compressive strength. The total porosity for the concrete vaccinated with ALCKC was minimal, resulting in protecting the concrete from aggressive solutions. Passivation potential measurements proved the vaccination gained by inoculation of ALCKC.
Keywords: calcined kaolinitic clay, durability of concrete, partial dealuminated kaolin, aluminum sulfate manufacturing solid waste
Kulcsszavak: kalcinált kaolinitos agyag, beton tartóssága, részben dealuminált kaolin, alumínium-szulfát gyártási szilárd hulladék

1. Introduction

Concrete fabrication and application in construction have increased due to its durability, and economic characteristics compared with other construction materials [1-4]. One ton of concrete is made up yearly for each human on the earth [5]. The production of Portland cement has several disadvantages, including intensive energy demand and acute negative environmental impacts [6]. The calcination process emits huge amounts of carbon oxides due to the heating of calcium carbonate stone and the firing of fuels for the production of cement [7, 8]. Cement is the main ingredient in concrete since it requires water to be hydrated forming binding compounds to fix the fine and coarse aggregates. Cement production was over 4 billion tons per year in 2018 and the demand is increasing, emitting a great quantity of carbon oxides into the biosphere participating in the warming of the earth's atmosphere [9].

The use of supplementary cementing materials (CMs) such as flown ash [10] fumed silica [11] waste glass [12] and ground granulated blast furnace slag [13] is one solution to this problem while manufacturing concrete or as a partial substitution for cement in the cement industry. High strength, better durability, no surface cracking, economic feasibility, and sustainability are benefits of adding cementitious ingredients to concrete. The quantity of the added materials that replace OPC is limited by their pozzolanity [14].

Several researchers have reported that ALCKC can be used as a cementitious additive in concrete [15, 16]. The use of high-reactivity calcined kaolin as a cementitious ingredient in the concrete industry has gained popularity and the studies are still interested in adding pozzolanic materials to cement to improve the concrete performance [17, 18]. ALCKC is a very fine material fabricated by calcining kaolinite clay at a temperature of about 700 °C to remove chemically bonded water and to deteriorate the crystalline structure, and then it was treated with sulphuric acid (60%) to leach alumina and form an aluminum sulfate product. By adding ALCKC to replace partially OPC, it modifies the pore structure and immobilizes the lime hydroxide of the hardened matrix of the concrete. The reactions of ALCKC [low alumina high silica (AS_2)] with lime hydroxide produced during the hydration reactions of cement form secondary binding compounds such as calcium silicate hydrates (CSH) which modify the internal matrix of the structure of concrete and make it more competent and durable against the aggressive conditions. Depending on the amount of CH and alumina A available, the following equations may happen [19]:

$$AS_2 + 3CH + 6H \rightarrow CSH + C_2ASH_8$$
$$AS_2 + 5CH + 3H \rightarrow 2CSH + C_3AH_6$$
$$AS_2 + 6CH + 9H \rightarrow 2CSH + C_4AH_{13}$$

Where AS_2 is ALCKC (SiO_2 and low alumina); CH is calcium hydroxide ($Ca(OH)_2$; H is water, CSH is Calcium Silicate Hydrate; C_2ASH_8 is hydrated stratlingite; C_3AH_6 is tricalcium aluminum hydrate and C_4AH_{13} is tetracalcium aluminate hydrate.

The improvement was confirmed by some physical characteristics such as; porosity, permeability, and chloride ion

diffusion [20]. ALCKC particles are much smaller than cement particles but not finer than fumed silica [21]. Adding CKC to concrete has a significant positive effect on the mechanical characteristics as determined by [22, 23].

The use of ALCKC reduces cement content in concrete relatively which can assist in mitigating environmental impacts. Based on the above, the purpose of this research work is to study the use of the local ALCKC for the production of durable concrete. The qualities of ALCKC are first discussed, which mostly involve physical and chemical characteristics. After that, the hydration, workability, mechanical characteristics, durability, and scan electron microscopy of ALCKC-modified concrete are thoroughly investigated. Furthermore, the most relevant results and recommendations are offered, which will aid future concrete investigations using ALCKC. This material is ecologically benign since it reduces carbon emissions into the atmosphere by lowering the amount of the currently used ordinary Portland cement [24]. ALCKC as CKC can be added to ordinary Portland cement to improve concrete characteristics [25]. The relevant findings were reported, which will aid in the utilization of the ALCKC in concrete fabrication in the future.

The ALCKC produced by thermal treatment in a fluidized bed kiln was considered a promising material that motivates the completion of the study to prove the validity of this material for use within the pozzolanic materials. The behavior of this mixture was investigated when used in normal and reinforced concrete. Several studies indicate that 10% of calcined pozzolana is the optimal ratio for substitution [26 - 28], while other studies reported that 15% is optimal. The current study aims to investigate the durability of the ALCKC-modified concrete against chlorides, sulfate, and sea-water and the effect of these ratios in concrete on the strength and protection of reinforcing steel in concrete against corrosion using the ratios of 10, and 15% compared with the plain concrete. The ratio of 20% wasn't promising according to a past study [29].

2. Material and methods

2.1 Materials

ALCKC samples were collected from the siliceous residuals of aluminum sulfate industry. The ALCKC samples were washed, ground, sieved, and dehydrated at 105 °C in an oven till complete dehydration. pH of the sample after washing was tested [30] using this experiment by the Hanna edge® pH HI2002 and Hanna digital pH electrode HI11310, with a resolution of 0.01 pH and accuracy of ±0.01 pH. The instrument has automatic temperature compensation [31].

The chemical composition of the KC, metakaolin (MK), and ALCKC was determined using an X-ray Fluorescence -1800 wavelength-dispersive spectrometer, Shimadzu (*Table 1*). The calcination process was done at 700 °C for 90 minutes to remove 11.5% of bound water that deteriorates the crystal structure resulting in active silicate and aluminate. These active species react easily with the hydration products of cement as that of the pure metakaolin [32]. Reactive silica became 40% after thermal treatment of KC supporting the silicate binder formation by reaction with cement hydration products. Alumina (34.2%) of ALCKC supports the formation of the binder calcium aluminum silicate hydrate upon addition to cement.

Compound	Amount (weight %)			
	KC	CKC	ALCKC	CEM 1 42.5
SiO_2 (total)	51.3	59.4	82.5	21.5
SiO_2 (active)	37.6	40	55.4	21.16
Al_2O_3	32	34.2	6.5	3.5
Fe_2O_3	1.3	1.44	0.43	3.4
TiO_2	2.3	2.6	3.54	0.15
MgO	0.15	0.17	0.11	1.2
CaO	0.20	0.23	0.14	62
Na_2O	0.13	0.15	0.09	0.28
K_2O	0.11	0.13	0.07	0.32
SO_3	0.12	0.15	1.2	2.7
P_2O_5	0.09	0.11	0.14	0.04
SrO	-	0.05	-	-
Cl	0.05	0.07	-	0.12
LOI total (Loss of Ignition)	11.5	0.7	4.91	4.5
Total	99.25	99.4	99.63	99.71

Table 1 The chemical composition of the kaolinitic, calcined kaolinitic clay and CEM 1 42.5
1. táblázat A kaolinites, kalcinált kaolinites agyag és a CEM 1 42,5 kémiai összetétele

Table 1 shows a high content of reactive SiO_2 (21.16%); reactive silica represents the fraction of silica that participates in the reactions with the hydration products of cement forming the binders.

CEM I 42.5 R Portland cement has a specific gravity of 3.14 and Blaine fineness of 327 m^2/kg utilized in concrete mixtures. The chemical composition of the cement is shown in *Table 2*.

Fine aggregates; Sand was used as a fine aggregate in both mortar and concrete mixtures. Sand tests were carried out according to the standard specifications (EN 1097, EN 933). The specific gravity = 2.6 and the grain size averaged 2 mm.

Compound	SiO_2	Al_2O_3	Fe_2O_3	CaO	MgO	SO_3	Na_2O	K_2O	Cl^-	LOI
%	21.16	5.32	3.52	63.8	1.32	2.01	0.2	0.13	0.02	2.52

Table 2 Chemical composition of Ordinary Portland cement (OPC)
2. táblázat A hagyományos portlandcement (OPC) kémiai összetétele

The properties	Size 1	Size 2	The limits ECCS203-2018 Egyptian standard
The specific gravity	2.65	2.65	-
The bulk density (ton/m^3)	1.4	1.45	-
Water absorption (%)	1.8	1.65	Not more than 2.5
The dust and clay (%)	0.15	0.18	Not more than 2.5

Table 3 The physical properties of coarse aggregates
3. táblázat A durva adalékanyagok fizikai tulajdonságai

The coarse aggregates are dolomite with a maximum particle size of 22 mm. Aggregates were obtained from local sources. The physical properties of the aggregates are presented in *Table 3*. Grading of the aggregate mixture was kept constant for all concretes.

The chemical composition of coarse aggregates (dolomite) complies with Egyptian code No. 302/2018. (*Table 4*). The grain size averaged 16 mm.

Compound	Coarse aggregates (Dolomite)	Limits	Fine aggregates (sand)	Limits
SiO_2	1.90	-	94	-
Al_2O_3	0.07	-	1.8	-
Fe_2O_3	0.02	-	1.0	-
CaO	36	-	0.72	-
MgO	16.9	-	0.22	-
SO_3^{--}	0.14	< 0.4	0.25	< 0.4
Cl^-	0.01	< 0.04	0.06	< 0.06
Na_2O	0.03	-	0.32	-
K_2O	0.02	-	0.51	-
TiO_2	0.01	-	0.11	-
P_2O_5	0.01	-	0.05	-
MnO	0.01	-	0.04	-
L.O.I	44.5	-	0.70	-
Total	99.62	-	99.78	-

Table 4 Chemical analysis of coarse and fine aggregates
4. táblázat Durva és finom adalékanyagok kémiai elemzése

Master Reobuild 3045 was added to achieve good mixing of the concrete mixtures, as a water-reducing agent. It conforms to ASTM 494. Sulphonated naphthalene formaldehyde-based high-range water-reducing admixture with a specific gravity of 1.19 was employed to achieve a slump of 14 cm for ease of handling, placing, and consolidation in all concrete mixtures. XRD and XRF instruments were used for the identification of the chemical and mineral composition of concrete.

2.2 Experimental investigation

2.2.1 Mix design

The mix proportions of the concrete are indicated in *Table 5*. Three different mixtures (0%, 10%, and 15% LACKC) were applied to test the effect of low water-to-binder ratio on concretes containing MK on the mechanical and durability properties. The control mixture (0% ALCKC) did not include LACKC. In mixtures of 10% LACKC and 15% LACKC, cement content was partially replaced with 10, and 15% LACKC (by mass) respectively. The binder consists of cement and LACKC.

2.2.2 Mixing and Casting of the concrete mixes

All the materials were mixed using a pan mixer with a maximum capacity of 100 L. The materials were fed into the mixer in the order of coarse aggregate, cement, LACKC, and sand. The materials were mixed dry for 1.5 min. Subsequently, three-quarters of the water was added, followed by the SP and the remaining water while mixing continued for a further 5 minutes to obtain a homogenous mixture. Upon discharging from the mixer, the slump test was conducted on the fresh properties of each mixture.

2.2.3 Curing

The following specimens were cast from each mixture: Three 100 × 100 × 100 mm cubes for the compressive strength. All the specimens were cast on a mechanical vibration table. After casting, all the specimens were covered with plastic sheets and water-saturated burlap and left at room temperature for 24 hours. The specimens were demolded after 24 hours of casting and were then cured in water at approximately 27 °C until the testing day.

Components (kg/m³)	0% ALCKC	10% ALCKC	15% ALCKC
OPC, 42.5N	400	360	340
ALCKC	-	40	60
Fine aggregate (sand)	632	632	632
Coarse aggregate (dolomite)	1264	1264	1264
Superplasticizer	8	8	8
Water	140	140	140

Table 5 The mix components of the concrete for 1 m³
5. táblázat 1 m³ beton keverék összetétele

Based on the obtained results it was found that the replacement ratio of 10 and 15% ALCPC achieved better results than the control mix with an improvement in the compressive strength of 20.8 and 18.7% respectively at an age of 28 days. Therefore in the complementary current study, the ratios 10 and 15% were studied to assess each ratio for the durability of the developed concrete mixes.

3. Results and discussions

3.1 The chemical composition of OPC paste

Table 6 gives the chemical analysis of hardened Portland cement slurries containing the ratios are 10% & 15% of the LACKC compared to Portland cement free of ALCKC, after immersing in water for 28 days. It is clear from the table that the percentage of silica (SiO_2) and alumina (Al_2O_3) increased with increasing of LACKC to 17.7% and 5.5% respectively for the pastes contained 10% LACKC, and 20 and 6.7% respectively for pastes containing 15% ALCKC. Iron oxides and calcium oxides were dropped with increasing LACKC ratios.

Oxides (%)	0% ALCKC	10% ALCKC	15% ALCKC
SiO_2 (Qz)	0.0	2.67	4.0
SiO_2(amorphous)	21.16	24.48	26.2
Al_2O_3	5.32	5.45	5.52
Fe_2O_3	3.52	3.21	3.05
CaO	63.8	57.43	54.3
MgO	1.32	1.2	1.12
SO_3	2.01	1.93	2.80
Cl^-	0.2	0.19	0.19
Na_2O	0.13	0.13	0.12
K_2O	0.13	0.12	0.11
TiO_2	≤ 0.1	0.35	0.53
L.O.I	2.52	2.6	2.5
Total	99.73	99.75	99.44

Table 6 The chemical composition of OPC contains 0, 10, and 15% ALCKC
6. táblázat A 0, 10 és 15% ALCKC-t tartalmazó OPC kémiai összetétele

3.2 The mineralogical composition

Fig. 1 shows the results of the scattered X-ray examination for the OPC mixes containing 10, and 15% ALCKC compared with the plain cement after 28 days of immersion in water. The figure shows that an increase in the proportion of LACKC in the mixture (15%) increases the rate of formation of calcium silicate hydrate (CSH) and reduction of Portlandite mineral [$Ca(OH)_2$].

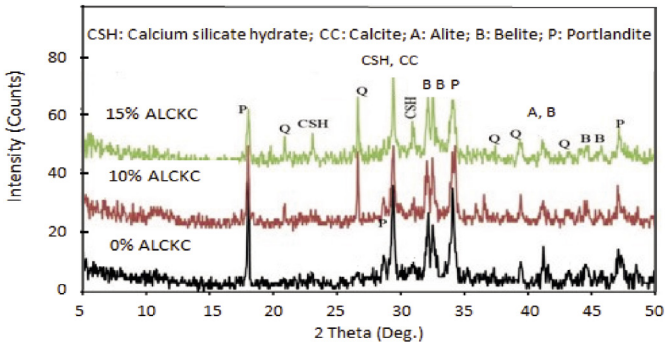

Fig. 1 XRD diffractogram for OPC incorporating 0, 10, and 15% ALCKC ratios compared to plain OPC after tap water curing for 28 days
1. ábra A 0, 10 és 15%-os ALCKC-arányt tartalmazó OPC XRD-diffraktogramja a sima OPC-hez viszonyítva 28 napos csapvízes kezelés után

Expansion due to alkali-silica reaction (ASR) of cement pastes incorporating 10 and 15% ALCKC

Due to the high reactivity of ALCKC to interact with cement hydration products and form new compounds, it was necessary to test the expansion that resulted from the reaction of ALCKC with lime in the ambient medium. *Fig. 2* shows the results of the ASR test for Portland cement mixtures, which contain percentages of ALCKC 15%, 10%, and ALCKC free cement. This test was performed according to ASTM: C1567-7. It was noticed that the shrinkage that occurs at an early-age (7 days) can arise from either external or internal water loss. The external water loss due to evaporation can result in plastic shrinkage and even some early drying shrinkage (which occurs in the hardened concrete during the first few days), while the internal water loss can result in autogenously shrinkage [33].

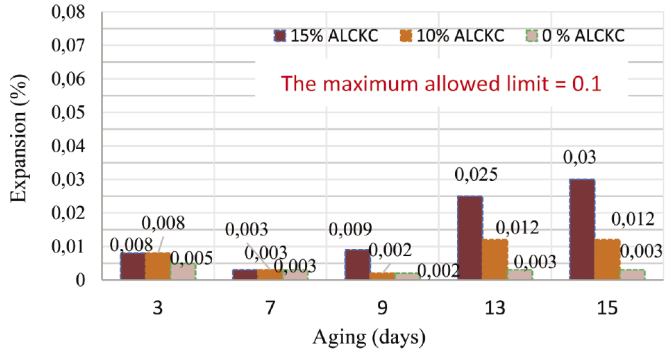

Fig. 2 Expansion values due to the alkali-silica reaction of cement pastes containing 10 and 15% of ALCKC dosages relative to ALCKC-freæement paste
2. ábra A 10 és 15% ALCKC-t tartalmazó cementpépek alkáli-szilícium-dioxid reakciójából adódó tágulási értékei az ALCKC-mentes cementpéphez viszonyítva

The values of expansion were 0.033 and 0.0128% for 10 and 15% of ALCKC respectively. These values are much less than the maximum allowed limit (0.1%). The resistance to alkali reaction increases at a ratio of 15% ALCKC/ OPC and consequently, the expansion decreases to 0.012%.

It was known that the alkaline silica reaction (ASR) produces a swelling gel. The essential ingredients in the paste matrix are soluble Ca^{++}, OH^-, active silica, and water, and adding ALCKC reduces the concentrations of $Ca(OH)_2$ in the cement paste to the lowest level and any ASR gel produced is not significant and therefore no further expansion and no cracking can be detected [34 -35]. Also, it has been found that aluminum ion in ALCKC reduces the solubility of silica in alkaline solutions reducing the ASR expansion [35].

3.3 Change the pH in cement paste due to cement replacement by ALCKC

Maintaining of alkalinity of the medium around the reinforcing steel in the concrete is important, as the steel becomes susceptible to corrosion at relatively low alkalinity (pH ≤ 11.5), and thus internal stresses are created in the concrete causing cracks [37]. *Fig. 3* gives the results pH measurements; it shows a slight decrease in the pH value as a result of the presence of ALCKC in the cement mix. When the cement contains 10% ALCKC slight decrease in pH (12.7) happened while when it contains 15% ALCKC the pH became 12.4 this is attributed to the rise of the percentage of alkalies (K_2O & Na_2O) in ALCKC/OPC.

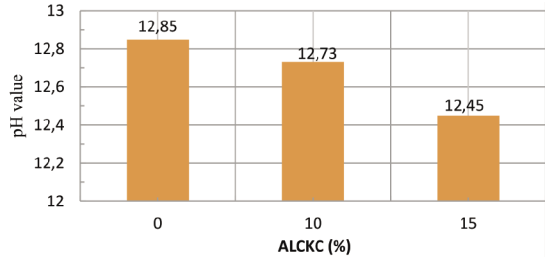

Fig. 3 pH of water extract for cement pastes incorporating 0, 10, and 15% CKC.
3. ábra 0, 10 és 15% CKC-t tartalmazó cementpépek vízkivonatának pH-értéke

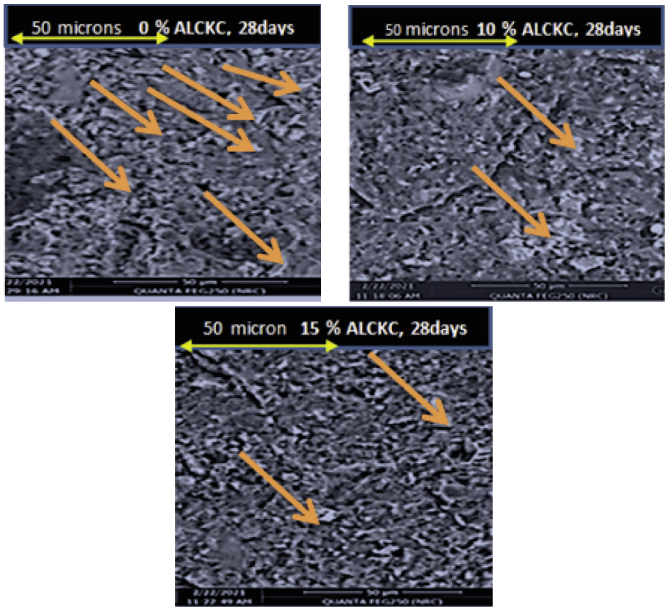

Fig. 4 SEM images for cement pastes incorporating 0, 10, and 15%ALCKC after curing in tap water for up to 28 days
4. ábra A 28 napig csapvízben szilárdult 0, 10 és 15% ALCKC-t tartalmazó cementpépek SEM felvételei

3.4 Scanning Electron Microscope (SEM)

Fig. 4 SEM images of cement mixtures, which contain the ratios ALCKC 10%, and 15%, after curing in water for 28 days, compared to a sample of Portland cement free of ALCMC. The white spots of portlandite mineral were reduced as indicated by the brown arrows with the increasing of the ALCKC ratio in the mixture, this was attributed to the consumption of a part of calcium hydroxide it in the pozzolanic reaction and the formation of CSH binder.

3.5 Durability tests

3.5.1 Chemical resistance of concrete containing 10 and 15% ALCKC

The compressive strength is the main property that tends to be used to assess concrete durability [38]; therefore it was used to evaluate the ability of concrete containing ALCKC 10% and 15% to counteract the effects of the aggressive environment.

3.5.1.1 Compressive strength of concrete containing 10% and 15% ALCKC after curing in tap water for several periods up to 180 days

The compressive strength was tested according to BS EN 12390-2:2009. *Table 7* and *Fig. 5* give the results of the compressive strength of concrete containing 10 and 15% ALCKC as a partial replacement of the cement after curing in tap water for several periods up to 180 days. It was clear from the results that the concrete containing 10% ALCKC has higher compressive strength than the control mix with a values of 22.8, 27.7, 26.6, and 24.6% at 7, 28, 60, and 90 days respectively, and also higher than that containing 15% ALCKC that achieved 15, 15.3, 22.3, and 17.9% after 7, 28, 60, and 90 days respectively. These results show that the ALCKC ratio of 10% is the optimal ratio as a replacement ratio agreeing with that reported by the research [13]. The reduction in compressive strength for a 15% ALCKC ratio in concrete compared to 10% ALCKC could be explained as the result of the cement dilution effect and reduction of CSH illustrated in *Fig. 6*.

Mixes/increase in compressive strength	Aging (days)				
	7	28	60	90	180
	Compressive strength, (MPa)				
0% ALCKC	27.2	41.2	44	51.6	49.3
10% ALCKC	33.4	52.6	55.7	64.3	62.5
% increase compared to OPC	22.8	27.7	26.6	24.6	26.8
15% ALCKC	31.3	47.5	53.8	60.3	61.2
% increase compared to OPC	15	15.3	22.3	17.9	24.1

Table 7 *Compressive strength of concrete containing different AlCKC ratios after curing in tap water*
7. táblázat *Különböző AL CKC arányt tartalmazó beton nyomószilárdsága csapvízben történő szilárdulás után*

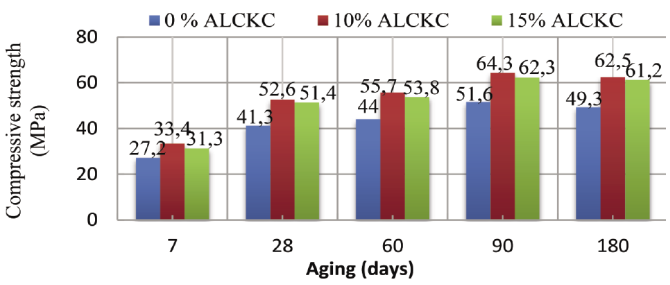

Fig. 5 *Compressive strength of concrete containing different percentages of ALCKC cured in water for 7, 28, 60, 90 and 180 days*
5. ábra *Különböző százalékos ALCKC-t tartalmazó beton nyomószilárdsága 7, 28, 60, 90 és 180 napig történő vízben érlelés után*

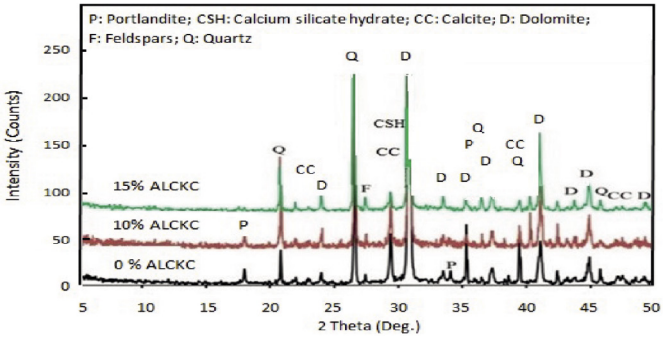

Fig. 6 *XRD for a concrete containing 0, 10, and 15% of ALCKC cured in water for 28 days*
6. ábra *A 28 napig vízben szilárdított 0, 10 és 15% ALCKC-t tartalmazó betonok röntgendiffraktogramja*

3.5.1.2 Compressive strength of concrete containing 10% and 15% ALCKC as cement replacement after curing in NaCl (5%) for 7, 28, 60, 90 and 180 days

The results of the compressive strength measurements of concrete samples containing 10 and 15% of ALCKC, after treatment in a 5% sodium chloride (NaCl) solution for 7, 28, 60, 90, and 180 days were shown in *Table 7* and *Fig. 7*. The compressive strength rises up to 90 days, then a slight set back occurs, but it is still higher than that of ALCKC-free concrete. The increase in the compressive strength values can be explained by the pozzolanic effect of the active silica, which causes acceleration in the reaction of the cement with water as reported by [14, 38 - 40] ALCKC reduces the chloride permeability and sorptivity of concrete, by decreasing the mean pore size and improving the uniformity of the pore size distribution [40], and increases the penetration resistance of Cl^- ions [42, 43]. The decreasing strength may be attributed to the formation of weak easily soluble calcium chloride from the reaction of calcium hydroxide with NaCl and the resulting $CaCl_2$ reacts with calcium aluminate forming Freidel's salt (Calcium chloro aluminate according to equations (1) and (2) [44]:

$$Ca(OH)_2 + 2\ NaCl \rightarrow CaCl_2 + 2\ NaOH \quad (1)$$

$$CaCl_2 + 3CaO{\cdot}Al_2O_3 + 10H_2O \rightarrow 3CaO{\cdot}Al_2O_3{\cdot}CaCl_2{\cdot}10H_2O \text{ (Freidel's salt)} \quad (2)$$

Freidel's salt (FS) appeared with 15% ALCKC, this may be attributed to the excess active alumina which facilitate the reaction with $CaCl_2$ as illustrated in *Fig. 8*.

Mixes/increase in compressive strength	Aging (days)				
	7	28	60	90	180
	Compressive strength (MPa)				
0% ALCKC	27	42	50	50.6	48.3
10% ALCKC	33	53	63.5	65	60
Increase of strength	22.2	26.2	27	28.5	24.2
15% ALCKC	33.5	47.3	59	57.7	55.7
Increase of strength	24	11.2	18	14	15.3

Table 8 *Compressive strength of concrete containing different percentages of ALCKC after curing in sodium chloride solution (5%) up to 180 days*
8. táblázat *Különböző százalékos ALCKC-t tartalmazó betonok nyomószilárdsága 180 napig (5%-os) nátrium-klorid oldatban történő érlelés után*

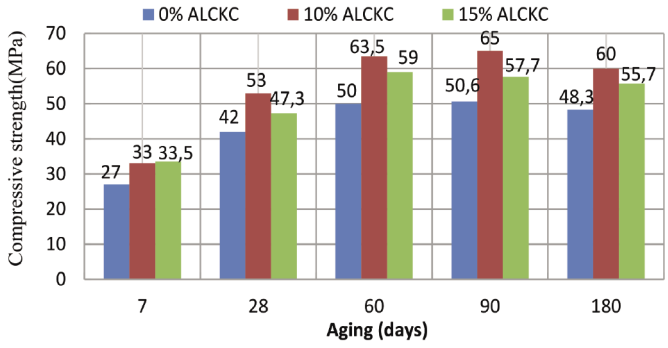

Fig. 7 Compressive strength of concrete containing 10 and 15% of ALCKC cured in sodium chloride solution (5%) for up to 180 days

7. ábra 10 és 15% ALCKC-t tartalmazó beton nyomószilárdsága, legfeljebb 180 napig (5%-os) nátrium-klorid oldatban történő érlelés után

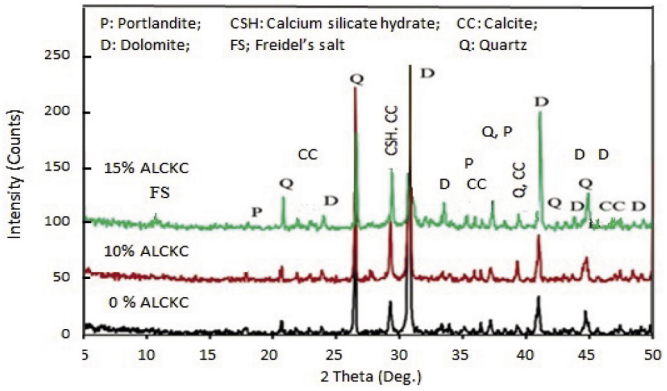

Fig. 8 XRD for concrete containing 0, 10, and 15% of ALCKC cured in sodium chloride solution (5%) for 180 days

8. ábra A 0, 10 és 15% ALCKC-t tartalmazó beton röntgenfelvételei 180 nap (5%-os) nátrium-klorid oldatban történő érlelést követően

3.5.1.3 Curing in magnesium sulfate ($MgSO_4$) solution (5%) for 7, 28, 56, 90, and 180 days

The results of the compressive strength measurements of concrete samples containing 10 and 15% of ALCKC, after treatment in a $MgSO_4$ solution (5%) for 7, 28, 56, 90, and 180 days (*Table 9*) and (*Fig. 9*) showed the compressive strength rises up to 56 days, then decreasing occurs, but it is still higher than that of the control mix. The increase in the compressive strength can be explained by the cementing effect of the amorphous silica, which causes acceleration in the reaction of the cement with water [45]. The regression of compressive strength with 15% attributed to the formation of gypsum that resulted from the reaction of sulfate ion with calcium ion of portlandite (P) resulting in its disappearance and the low relative intense peak of CSH (*Fig. 10*). Gypsum consumes a part of the CSH binder causing relative reduction of compressive strength according to equation (3) and (4).

$$Ca(OH)_2 + MgSO_4 \cdot 7H_2O \rightarrow CaSO_4 \cdot 2H_2O \text{ (gypsum)} + Mg(OH)_2 + 5H_2O \quad (3)$$

Gypsum reacts with calcium aluminate (product of cement hydration) forming ettringite mineral which causes relative expansion and cracks formation [44, 45], according to the following equation:

$$3CaO \cdot Al_2O_3 \cdot 2H_2O + 3(CaSO_4 \cdot 2H_2O) + 13H_2O \rightarrow 3CaO \cdot Al_2O_3 \cdot 3CaSO_4 \cdot 31H_2O \text{ (ettringite)} \quad (4)$$

Mixes/increase in compressive strength	Aging (days)				
	7	28	60	90	180
	Compressive strength (MPa)				
0% ALCKC	26.4	42	50.3	55.3	51.2
10% ALCKC	33.4	51.5	61	64	61.7
Increase of strength	26.5	22.6	21.3	15.7	20.5
15% ALCKC	32	46	57.6	63.4	57.5
Increase of strength	21.2	9.5	14.5	14.6	12.3

Table 9 Compressive strength of concrete containing different percentages of ALCKC after curing in magnesium sulfate solution for up to 180 days

9. táblázat Különböző százalékos ALCKC-t tartalmazó betonok nyomószilárdsága legfeljebb180 napig magnézium-szulfát oldatban történő érlelés után

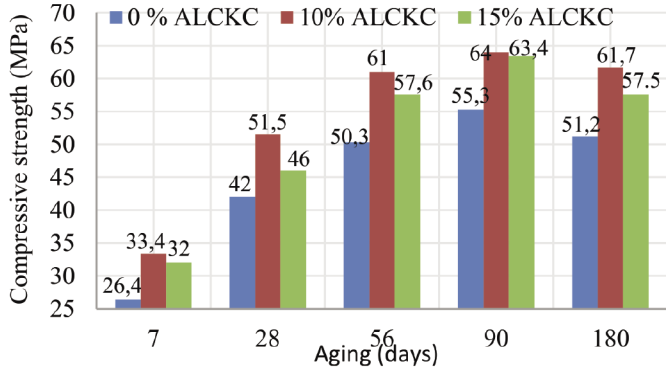

Fig. 9 Compressive strength of concrete containing different percentages of ALCKC after curing in magnesium sulfate solution (5%) for 6 months

9. ábra Különböző mennyiségű ALCKC-t tartalmazó betonok nyomószilárdsága, legfeljebb 6 hónapig (5%-os) magnézium-szulfát-oldatban történő érlelés után

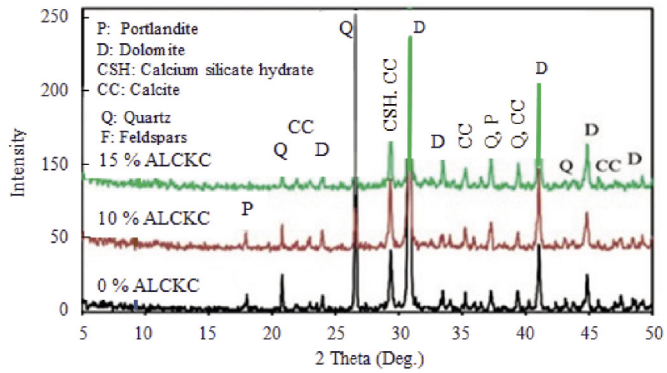

Fig. 10 XRD for a concrete containing 0, 10, and 15% of ALCKC cured in magnesium sulphate solution (5%) for up to 180 days

10. ábra A 0, 10 és 15% ALCKC-t tartalmazó beton röntgenfelvételei 180 nap (5%-os) magnézium-szulfát oldatban történő érlelést követően

3.5.1.4 Curing in sea water for 7, 28, 60, 90, and 180 days of concrete containing 10 and 15% of ALCKC

The experiments were carried out using seawater as it has the highest salinity (4.3%). The compressive strength of concrete containing 10 and 15% of ALCKC was determined after periods of curing in seawater that lasted for 180 days, as shown in *Table 9*. It was noted from the measurements that the compressive strength of concrete takes the same behavior when exposed to sea water, where the compressive strengths are relatively higher in the case of containing ALCKC compared to concrete without it.

The compressive strength decreased after 90 days and then slightly declined, but it was still higher than the ALCKC-free

concrete (*Fig. 11*). The increase in compressive strength is due to the decrease in the percentage of calcium hydroxide (Portlandite), which reduces the formation of gypsum and ettringite minerals, in addition to that there is another reason related to the structure of the pores, as they do not allow the entry of sulfates into the concrete through the pores, by what was recorded [43]. The decreasing of strength may be attributed to the formation of weak easily soluble calcium chloride from the reaction of calcium hydroxide with NaCl yielding $CaCl_2$ which reacts with calcium aluminate hydrate forming Freidel's salt (Calcium chloro aluminate (*Fig. 12*) [44]. Freidel's salt stabilizes chloride ions.

Mixes/increase in compressive strength	Aging (days)			
	28	60	90	180
	Compressive strength (MPa)			
OPC	40.5	53.2	55.3	51.6
10% ALCKC	53.2	65	62.5	60.8
Increase of strength	31.4	22.2	17	17.8
15% ALCKC	48.3	63.5	61.3	60.4
Increase of strength	19.3	19.4	14.8	17.1

Table 10 Compressive strength of concrete containing different percentages of ALCKC after seawater curing for up to 180 days
10. táblázat Különböző százalékos ALCKC-t tartalmazó betonok nyomószilárdsága legfeljebb180 napig tengervízben történő érlelés után

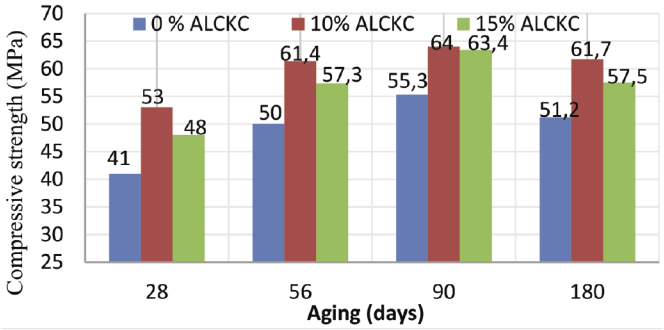

Fig. 11 Compressive strength of concrete containing different percentages of ALCKC after curing in sea water for up to 180 days
11. ábra Különböző mennyiségű ALCKC-t tartalmazó betonok nyomószilárdsága, legfeljebb 180 napig tengervízben történő érlelés után

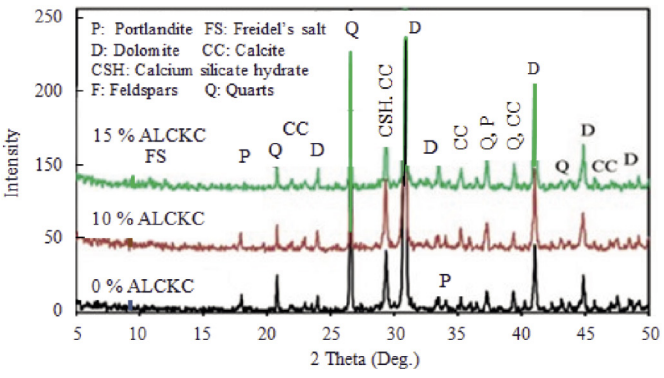

Fig. 12 XRD for a concrete containing 0, 10, and 15% of ALCKC cured in seawater for 180 days
12. ábra A 0, 10 és 15% ALCKC-t tartalmazó beton röntgenfelvételei 180 nap tengervízben történő érlelést követően

3.5.2 Exposure of concrete to heat

3.5.2.1 Effect of heat on the compressive strength

When concrete is exposed to high temperatures, its strength deteriorates, which leads to a loss of cohesion and endurance, leading to collapse agreeing with that reported by [BS EN 1992–1–2 (2004) and ACI Committee 216]. The reduction of strength of the specimens exposed to 200 °C temperature may be referred to two causes. The 1st one: in the range of 150–200 °C, concrete begins to lose its strength due to the desorption of the physically adsorbed water, which may cause strength loss [47]. The 2nd one: is that cement gel layers move closer due to the moisture loss resulting in increased van der wall forces, which in turn causes strength gain. The addition of ALCKC increases the heat-bearing strength of concrete. *Fig. 13* shows the effect of exposure to temperatures from 25 up to 700 °C for concrete containing 10 and 15% of ALCKC relative to ALCKC- free concrete. In general, the compressive strength values of concrete decrease with the continuation of the temperature increase until 700 °C.

Concrete containing 10% ALCKC retains compressive strength values above that containing ALCKC 15% and those free of ALCKC for all temperatures. At 700 °C the loss in compressive strength of concrete containing ALCKC 10% reaches 23% relative to the compressive strength value at room temperature (25 °C), while the percentage of loss in the compressive strength value of the containing concrete 15% was 36.5%. *Fig. 14* shows that 10% ALCKC is the best ratio of thermal endurance and high compressive strength retention compared to concrete containing 15% ALCKC or the free mix.

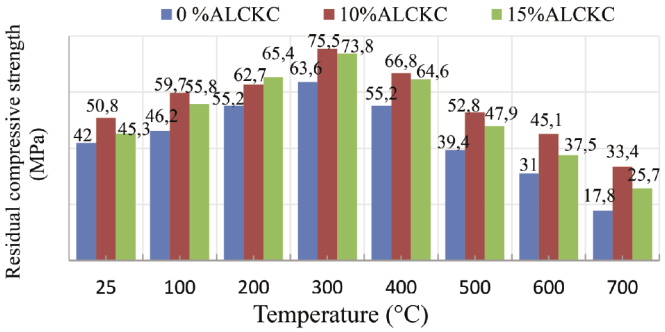

Fig. 13 Effect of heat on the compressive strength of concrete containing 10 and 15% of ALCKC
13. ábra A hőmérséklet hatása a 0, 10 és 15% ALCKC-t tartalmazó betonok nyomószilárdságára

3.5.2.2 Effect of heat on the weight of concrete

Fig. 14 gives weight loss values for concrete containing 10, and 15% of ALCKC when exposed to temperatures from 200-700 °C. The results show that the concrete containing 10% of AlCKC is the lowest in weight with a temperature rise from 200 to 700 °C, compared to the concrete containing 15%. The loss in weight for concrete containing 10% ALCKC was 8.02%, and the loss in weight for concrete containing 15% was 8.54%, while the loss in concrete without ALCKC = 10.8%. The weight loss is attributed to the evaporation of water in concrete that is relatively higher in the concrete containing 15%.

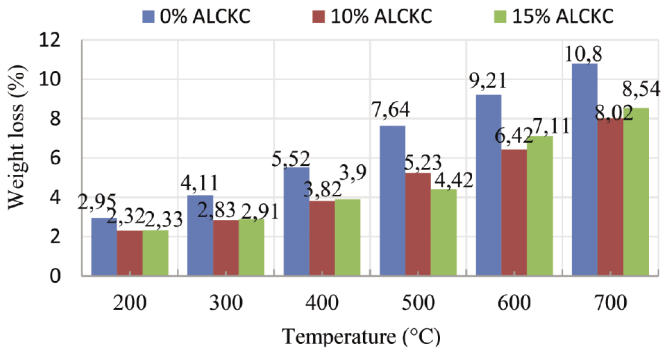

Fig. 14 Effect of heat on the weight loss of concrete containing 10 and 15% of ALCKC
14. ábra A hőmérséklet hatása a 0, 10 és 15% ALCKC-t tartalmazó beton tömegveszteségére

3.5.2.3 Effect of heat on the porosity of concrete

It is a direct relationship between the porosity of concrete and temperature rising. Increasing porosity at high temperatures is attributed to moisture evaporation from the concrete matrix. Beyond 400 °C, voids and micro-cracks began to appear in the mortar region due to bound water elimination. Beyond 500 °C, the concrete showed the development of micro cracks, causing a further increase in the porosity [47].

Fig. 15 shows that the total porosity of concrete containing 10, and 15% of ALCKC is lower than that of the control mix at all temperatures in the range from 200 to 700 °C. At 700 °C the porosity reached 12% at 10% ALCKC compared to concrete containing 15%, where the porosity was 13.2%, and the porosity of ALCKC-free concrete was 23%. It should be noted that the low porosity of concrete containing 10% of ALCKC at room temperature of 3.3% is one of the important characteristics of concrete in terms of low permeability that prevents the penetration of aggressive chemicals into the concrete.

Mixes	Temperature (°C)							
	25	100	200	300	400	500	600	700
	Total porosity (%)							
0% ALCKC	4.0	5.0	5.5	7.3	11	13	18.6	23
10% ALCKC	3.0	3.6	4.0	6.0	7.8	10	11	12.5
15% ALCKC	4.0	4.0	4.5	6.2	8.3	10.5	11.9	13.8

Table 11 The total porosity of concrete containing 0, 10, and 15% ALCKC exposed to heat
*11. táblázat A hőnek kitett 0, 10 **és** 15% ALCKC-t tartalmazó beton teljes porozitása*

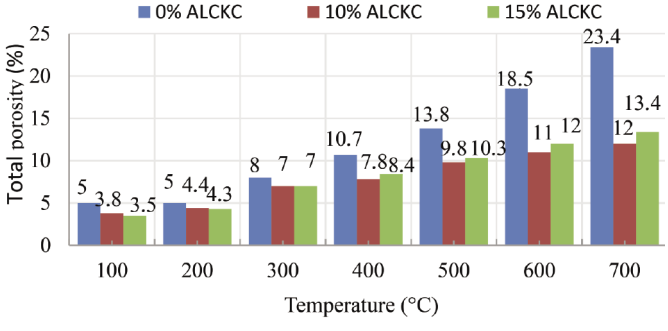

Fig. 15 The total porosity of concrete containing 0, 10, and 15% ALCKC exposed to heat up to 700 °C
15. ábra A 0, 10 és 15% ALCKC-t tartalmazó beton teljes porozitásának változása a hőmérséklet emelésének következtében 700 °C-ig

3.5.3 Effect of ALCKC as a partial cement replacement in reinforced concrete oncorrosion of steel reinforcement

The corrosion of steel reinforcement of concrete represents one of the most important factors that lead to concrete cracks and its premature collapse, especially if the concrete is exposed to chloride (Cl^-). Many modern studies are currently conducting research on adding material that protects the concrete mix and reinforcement steel. Therefore, the study will discuss the effect of using the ratios 0, 10%, and 15% ALCKC as partial replacement of cement in concrete. Anodic polarization is one of the electrochemical measurements that are used to estimate the extent of corrosion of reinforcement steel [48-50].

Fig. 16 gives the anodic polarization results for reinforcement steel in the concrete containing 0, 10, and 15% ALCKC after curing in water for 28 days. The following limits for estimating the strength of reinforcement steel in concrete are: Passivation Potential > 600 mV to reach zero passivation, and the maximum time for achieving that potential is 15 min. From these results it is clear that the concrete containing MK 15% achieve the maximum value of passivation potential of 700 mV, and it reaches this value in the shortest time (5.5 min.), while the concrete that contains 10% achieved 687 mV at a time 6.5 min and the 0% ALCKC reached 640 at a time 8 min. therefore, 10 and 15% of ALCKC reached passivation higher than zero ALCKC concrete.

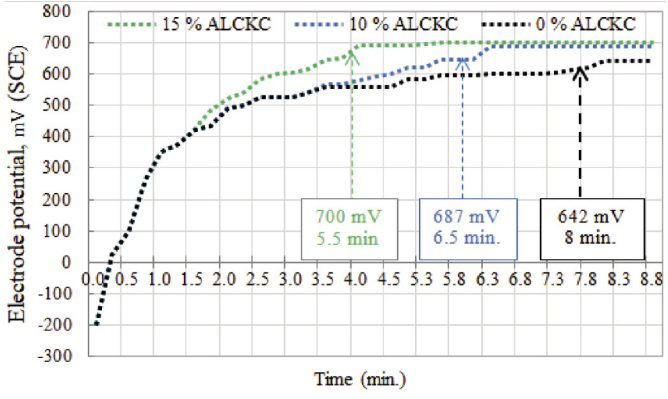

Fig. 16 Anodic polarization behavior of steel in concrete, after curing in tap water for 28 days
16. ábra Az acél anódos polarizációs viselkedése betonban, miután 28 napig csapvízben érlelődött

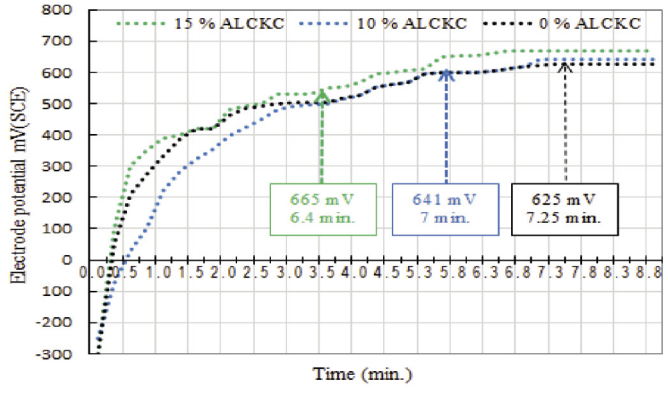

Fig. 17 Anodic polarization behavior of steel in concrete, after curing in seawater for 28 days
17. ábra Az acél anódos polarizációs viselkedése betonban, tengervízben történő 28 napos érlelés után

Performing these measurements using seawater as the ambient conditions for concrete (*Fig. 17*), shows the continuity of rising of passivation potential for concrete that contains 15% ALCKC to 665 mV in 6.4 min. So, 15% ALCKC is the best ratio for protecting steel against corrosion.

These measurements show that 15% ALCKC is the better ratio as a replacement percentage for cement in concrete - in preserving steel against corrosion as a result of the penetration of harmful elements from water to concrete.

4. Conclusions

- The use of acid-leached calcined kaolinitic clay for partial cement replacement causes slight expansion of the concrete as a result of alkali-silica reaction but it is still far from the limits; therefore there is no effect on the hydration products of cement and formation of the binding compounds.
- There was no significant effect on the alkalinity (pH) of concrete.
- The ratio of acid-leached calcined kaolinitic clay to OPC is 10% achieving the optimum ratio for high-performance plain concrete with compressive strength greater than the reference OPC by 24.7% and the ratio of 15% achieved by 17.9% after aging of 90 days. This percentage enhances the concrete's resistance to the effects of chloride, sulfate solutions (5%), and seawater.
- The ratio of acid-leached calcined kaolinitic clay to OPC of 10% in concrete is the best in terms of resistance to wear and tear due to the thermal endurance and maintaining high compressive strength relative to the concrete containing 15% or the free concrete.
- 10% replacement of cement resulted in the lowest total porosity of concrete, which will reduce the permeability of concrete to penetration of aggressive elements from the environment, so this improved concrete can endure in the near marine areas.
- 10 and 15% replacements of cement with acid-leached calcined kaolinitic clay protect steel from corrosion. The ratio of 15% ALCKC is the better ratio as a replacement percentage for cement in concrete – in preserving steel against corrosion as a result of the penetration of harmful elements from water to concrete.

Acknowledgment

This work was supported by Aluminum Sulphate Co. of Egypt, (ASCE) industrial sharing company, Cairo and the analysis, mix design and results was performed in the center of building and housing research, Egypt.

References

[1] Nawy EG. Fundamentals of High Strength High Performance Concrete. In: Concrete Design and Construction Series. Longman; 1996, 335 pp.

[2] Smirnova, O.M.; Menéndez Pidal de Navascués, I.; Mikhailevskii, V.R.; Kolosov, O.I.; Skolota, N.S. Sound-Absorbing Composites with Rubber Crumb from Used Tires. Appl. Sci. 2021, 11, 7347. https://doi.org/10.3390/app11167347

[3] Alvee, A.R.; Malinda, R.; Akbar, A.M.; Ashar, R.D.; Rahmawati, C.; Alomayri, T.; Raza, A. (2022); Shaikh, F.U.A. Experimental Study of the Mechanical Properties and Microstructure of Geopolymer Paste Containing Nano-Silica from Agricultural Waste and Crystalline Admixtures. Case Stud. Constr. Mater., 16, e00792. https://doi.org/10.1016/j.cscm.2021.e00792

[4] Althoey, F. Compressive Strength Reduction of Cement Pastes Exposed to Sodium Chloride Solutions: Secondary Ettringite Formation. Constr. Build. Mater. 2021, 299, 123965. https://doi.org/10.1016/j.conbuildmat.2021.123965

[5] Marie, I.; Quiasrawi, H. (2012) Closed-Loop Recycling of Recycled Concrete Aggregates. J. Clean. Prod. 2012, 37, 243–248. https://doi.org/10.1016/j.jclepro.2012.07.020

[6] Ahmad, J.; Aslam, F.; Martinez-Garcia, R.; De-Prado-Gil, J.; Qaidi, S.M.A.; Brahmia, A. (2021) Effects of Waste Glass and Waste Marble on Mechanical and Durability Performance of Concrete. Sci. Rep.11, 21525. https://doi.org/10.1038/s41598-021-00994-0

[7] Rahmawati, C.; Aprilia, S.; Saidi, T.; Aulia, T.B. (2021) Current Development of Geopolymer Cement with Nanosilica and Cellulose Nanocrystals. In Journal of Physics: Conference Series, Proceedings of the Annual Conference on Science and Technology Research (ACOSTER), Medan, Indonesia, 20–21 June 2021; IOP Publishing: Bristol, UK, pp. 1–8. https://doi.org/10.1088/1742-6596/1783/1/012056

[8] Ahmad, J.; Tufail, R.F.; Aslam, F.; Mosavi, A.; Alyousef, R.; Faisal Javed, M.; Zaid, O.; Khan Niazi, M.S. A Step towards Sustainable Self-Compacting Concrete by Using Partial Substitution of Wheat Straw Ash and Bentonite Clay Instead of Cement. Sustainability 2021, 13, 824. https://doi.org/10.3390/su13020824

[9] Singh, M.; Choudhary, K.; Srivastava, A.; Sangwan, K.S.; Bhunia, D. A Study on Environmental and Economic Impacts of Using Waste Marble Powder in Concrete. J. Build. Eng. 2017, 13, 87–95. https://doi.org/10.1016/j.jobe.2017.07.009

[10] Taskin, A.; Fediuk, R.; Grebenyuk, I.; Elkin, O.; Kholodov, A. Effective Cement Binders on Fly and Slag Waste from Heat Power Industry of the Primorsky Krai, Russian Federation. Int. J. Sci. Technol. Res. 2020, 9, 3509–3512.

[11] Abdelgader, H.; Fediuk, R.; Kurpi´ nska, M.; Elkhatib, J.; Murali, G.; Baranov, A.V.; Timokhin, R.A. Mechanical Properties of Two-Stage Concrete Modified by Silica Fume. Mag. Civ. Eng. 2019, 89, 26–38.

[12] Ahmad, J.; Martínez-García, R.; De-Prado-Gil, J.; Irshad, K.; El-Shorbagy, M.A.; Fediuk, R.; Vatin, N.I. Concrete with Partial Substitution of Waste Glass and Recycled Concrete Aggregate. Materials 2022, 15, 430. https://doi.org/10.3390/ma15020430

[13] Dinakar, P.; Sethy, K.P.; Sahoo, U.C. Design of Self-Compacting Concrete with Ground Granulated Blast Furnace Slag. Mater. Des. 2013, 43, 161–169. https://doi.org/10.1016/j.matdes.2012.06.049

[14] Sabir, B.B.; Wild, S.; Bai, J. Metakaolin and Calcined Clays as Pozzolans for Concrete: A Review. Cem. Concr. Compos. 2001, 23, 441–454. https://doi.org/10.1016/S0958-9465(00)00092-5

[15] Lee, G.; Ling, T.-C.; Wong, Y.-L.; Poon, C.-S. Effects of Crushed Glass Cullet Sizes, Casting Methods and Pozzolanic Materials on ASR of Concrete Blocks. Constr. Build. Mater. 2011, 25, 2611–2618.

[16] Vizcayno, C.; de Gutiérrez, R.M.; Castello, R.; Rodriguez, E.; Guerrero, C.E. (2010) Pozzolan Obtained by Mechanochemical and Thermal Treatments of Kaolin. Appl. Clay Sci., 49, 405–413. https://doi.org/10.1016/j.clay.2009.09.008

[17] Siddique, R.; Klaus, J. (2009) Influence of Metakaolin on the Properties of Mortar and Concrete: A Review. Appl. Clay Sci., 43, 392–400. https://doi.org/10.1016/j.clay.2008.11.007

[18] Güneyisi, E.; Geso˘ glu, M.; Karao˘ glu, S.; Mermerda¸s, K. (2012) Strength, Permeability and Shrinkage Cracking of Silica Fume and Metakaolin Concretes. Constr. Build. Mater., 34, 120–130. https://doi.org/10.1016/j.conbuildmat.2012.02.017

[19] Murat M. Hydration reaction and hardening of calcined clays and related minerals—I. Preliminary investigation on metakaolinite. Cem. Concr. Res. 1983;13:259–266. https://doi.org/10.1016/0008-8846(83)90109-6

[20] Badogiannis, E.; Tsivilis, S. (2009) Exploitation of Poor Greek Kaolins: Durability of Metakaolin Concrete. Cem. Concr. Compos., 128–133. https://doi.org/10.1016/j.cemconcomp.2008.11.001
[21] Ding, J.-T.; Li, Z. Effects of Metakaolin and Silica Fume on Properties of Concrete. Mater. J. 2002, 99, 393–398.
[22] Bai, J.;Wild, S.; Sabir, B.B. (2002) Sorptivity and Strength of Air-Cured and Water-Cured PC–PFA–MK Concrete and the Influence of Binder Composition on Carbonation Depth. Cem. Concr. Res. 20, 32, 1813–1821. https://doi.org/10.1016/S0008-8846(02)00872-4
[23] Güneyisi, E.; Gesoˇ glu, M.; Mermerda¸ S, K. (2008) Improving Strength, Drying Shrinkage, and Pore Structure of Concrete Using Metakaolin. Mater. Struct., 41, 937–949. https://doi.org/10.1617/s11527-007-9296-z
[24] Danish, P.; Ganesh, M.G. Behavior of Self-Compacting Concrete Using Different Mineral Powders Additions in Ternary Blends. Rev. Rom. Mater. 2020, 50, 232–239.
[25] Nazir, U., Jandiyal, A., Salotra, S. (2016) and Sharma, R., "Incorporation of metakaolin in concrete: A Review" Inter. J., Civil Engineering and Technology (IJCIET), 7, 17.
[26] Shelokar A.P. and Jadhao P.D., (2013) "Strength appraisal of high-grade concrete by using high reactive metakaolin", Inter. J. of Innovative Research in Science, Engineering and Technology", 2, 657-663.
[27] Dinakar P., Pradosh K.S. and Sriram G., (2013) "Effect of metakaolin content on the properties of high strength concrete", Inter. J. of Concrete Structures and Materials, 7, 215-223.
[28] Hoda S. Eldin, Nabil, A. Abdullah, Ismail Mahmoud F., Hashem Ahmed I. (2022) Preparation of meta phase of kaolinite as a precursor for geopolymer adsorbent fabrication. Építőanyag – Journal of Silicate Based and Composite Materials, Vol. 74, No. 3 (2022), 82–87. p. https://doi.org/10.14382/epitoanyag-jsbcm.2022.13
[29] Abdullah, Nabil A. – Abdullah, Hajer: Compressive strength, setting time, and flowability of OPC mortar mixtures modified with a composite of Nano carbon and partially de-aluminated metakaolin Építőanyag – Journal of Silicate Based and Composite Materials, Vol. 75, No. 3 (2023), 118–126. p. https://doi.org/10.14382/epitoanyag-jsbcm.2023.17
[30] Loh, P.Y.; Shafigh, P.; Katman, H.Y.B.; Ibrahim, Z.; Yousuf, S. pH Measurement of Cement-Based Materials: The Effect of Particle Size. Appl. Sci. 2021, 11, 8000. https://doi.org/10.3390/app11178000
[31] Hanna Instruments. pH. In General Catalog; Hanna Instruments Inc.: Woonsocket, RI, USA, 2020; Volume 34, pp. 2.1–2.170.
[32] Shekarchi M., Bonakdar A., Bakhshi, Mirdamadi A. and Mobasher B., "Transport properties in metakaolin blended concrete", Construction and Building Materials, 24, 2217-2223 (2010)
[33] Kurup, D. S., Mohan, M. K., Van Tittelboom, K., De Schutter, G., Santhanam, M., & Rahul, A. (2023). Early-age shrinkage assessment of cementitious materials: A critical review. Cement and Concrete Composites, 145, 105343. https://doi.org/10.1016/j.cemconcomp.2023.105343
[34] Kostush, J.A., Walters, V. and Jones T.R., "High Performance Concretes Incorporating Metakaolin: A Review, Proc. of Conference Concrete 2000 Economic and Durable Construction Through Excellence, 1799-1811 (1993). https://doi.org/10.12691/ajcea-6-6-4
[35] Maria C.G.J. and Rafat S., "Recent advances in understanding the role of supplementary cementitious materials in concrete", Cement and Concrete Research, 78, 71-80 (2015)
[36] Gouda, V.K., Adul Azim, A.A. and El-Sayed, H.A., "Some aspects of reinforcement corrosion in Egyptian structures", British corrosion J.,9, 185 – 189 (1974)
[37] Jones, M.R., Mc Carthy, M.J. and Dhir, R.K.,1993) "Chloride resistant concrete", Concrete 2000 Economic and durable construction through excellency, Proc. of Inter. Confr., Scotland, UK, 1429-1444.
[38] Badogiannis, E.; Tsivilis, S. (2009) Exploitation of Poor Greek Kaolins: Durability of Metakaolin Concrete. Cem. Concr. Compos. 2009, 31, 128–133.
[39] Jian-Tong, D. and Zongjin, Li, (2002) "Effects of metakaolin and silica fume on properties of concrete", ACI Mater., J., 99, 393-398.
[40] Xianmingi Shi, Ning Xie, Keith, F. and Jing G., (2012) "Durability of steel reinforced concrete in chloride environments; An overview", Const. and Build. Mater., 30, 125-138. https://doi.org/10.1016/j.conbuildmat.2011.12.038
[41] Valipour, M., Pargar, F., Shekarchi, M. and Khani, S., (2013) "Comparing a natural pozzolan, zeolite, to metakaolin and silica fume in terms of their effect on the durability characteristics of concrete: A laboratory study, Const. and Build. Mater., 41, 879-888. https://doi.org/10.1016/j.conbuildmat.2012.11.054
[42] Shatat, M.R., Maroof, M.A., El-Sayed, A.Y., Abo-Elenein, S.A. and Heikal, E.S., (2016) "Physico-chemical properties of the hardened blended cement pastes made of OPC-MK blends CKD", Chemistry of Advanced Materials, 1, 17-26.
[43] Mohammed, T.U., Ostsuki, N. and Hamada, H, "Corrosion of steel bars in cracked concrete under marine environment", J. of Materials in Civil Engineering, ASCE, 15, 460-469 (2003) https://doi.org/10.1061/(ASCE)0899-1561(2003)15:5(460)
[44] Gutt, W.H. and Harrison, W.H., (1977)"Chemical resistance of concrete", Concrete, 11, 35 – 37 (1977)
[45] Ramachandran, V.S., Feldman, R.F. and Beaudoin, J.J., (1981). "Concrete Science", Heyden & Sons. Inc., Philadelphia, USA.
[46] Malik M, Bhattacharyya S. K, Barai S. V. (2021). Thermal and mechanical properties of concrete and its constituents at elevated temperatures: A review, Construction and Building Materials, 270 (2020), 121398. https://doi.org/10.1016/j.conbuildmat.2020.121398
[47] Khoury, G.A., Majorana, C.E., Pesavento, F. and Schrefler, B.A. (2002) Modeling of Heated Concrete. Magazine of Concrete Research, 54, 77. https://doi.org/10.1680/macr.54.2.77.40895
[48] Rilem TC 154-EMC, "Electrochemical techniques for measuring metallic corrosion, test methods for on-site corrosion rate measurement of steel reinforcement in concrete by means of the polarization resistance method", Materials and Structures/ Materiauxet Constructions, 37, , 623-643,(2004)
[49] Millard, S. G., Law D., Bungey, J. H. and Cairns, J., "Environmental influences on linear polarization corrosion rate measurement in reinforced concrete", NDT & E Int., 34, 409-17, (2001)
[50] Elshami, A., "Efficiency of corrosion inhibitors used for structures in an aggressive environment", Ph. D. Thesis, in Materials Science for Engineers, Nantes University, (2012)

Ref.:
Abdullah, Nabil A. – **Abdullah**, Hajer: *Durability of concrete modified with acid leached calcined kaolinitic clay*
Építőanyag – Journal of Silicate Based and Composite Materials, Vol. 76, No. 1 (2024), 21–30 p.
https://doi.org/10.14382/epitoanyag-jsbcm.2024.3

Impact of Printing Directions and Printing Paths on the Compressive Strength of 3D Printed Concrete

Marwah M. THAJEEL ▪ Department of Construction Materials and Technologies, Budapest University of Technology and Economics, Hungary ▪ thajeel.marwah@edu.bme.hu
Sándor SÓLYOM ▪ Department of Construction Materials and Technologies, Budapest University of Technology and Economics, Hungary ▪ solyom.sandor@emk.bme.hu
György L. BALÁZS ▪ Department of Construction Materials and Technologies, Budapest University of Technology and Economics, Hungary ▪ balazs.gyorgy@emk.bme.hu

Érkezett: 2023. 12. 15. ▪ Received: 15. 12. 2023. ▪ https://doi.org/10.14382/epitoanyag-jsbcm.2024.4

Abstract

3D concrete printing, also known as 3D CP, offers an advantage in creating intricate and unique shapes using a printer equipped with a pump, hose pipe and nozzle. The speed at which the printing process occurs is crucial for construction. It depends on factors such as the size and complexity of the printed element, the pump rate and the quality of the concrete used. To achieve precision during printing, it is essential to use high-performance construction materials. Unlike cast methods, 3D CP does not require support formwork. Thus, certain factors like the fresh properties of the material being used, the orientation in which it is printed and how long it is printed can significantly affect the capacity of the printed objects. The layering involved in printing concrete can introduce weaknesses in joints, which affect all mechanical characteristics of 3D printed elements. This study examines how the printing direction and printing paths influence the compressive strength of 3D printed specimens. Additionally, conventional mould cast specimens were tested for comparison purposes. The findings indicate that both the printing directions and paths impact the strength of these printed specimens.

Keywords: 3D concrete printing, printing directions, printing paths, compressive strength
Kulcsszavak: 3D betonnyomtatás, nyomtatási irány, nyomtatási vonal, nyomószilárdság

Marwah M. THAJEEL
Civil Engineer (MSc in structural engineering), PhD student at the Department of Construction Materials and Technologies, Budapest University of Technology and Economics. Main fields of interest: reinforced concrete, concrete technology, construction materials, 3D concrete printing and sustainability.

Sándor SÓLYOM
Assistant professor at the Department of Construction Materials and Technologies, Faculty of Civil Engineering, Budapest University of Technology and Economics. Research interest: FRP (Fibre Reinforced Polymer), FRC (Fibre Reinforced Concrete), bond of reinforcement to concrete, 3D concrete printing, concrete technology, and durability.

György L. BALÁZS
Civil Engineer, PhD, Dr.-habil., Professor of structural engineering at the Department of Construction Materials and Technologies of Budapest University of Technology and Economics (BME). His main fields of activities are experimental investigation and modelling of RC, PC, FRC, FRP, HSC, HPC, LWC, fire resistance and fire design, durability, sustainability, bond and cracking. He is chairman of several commissions and task groups of fib. He is president of Hungarian Group of fib, Editor-in-chief of the Journal "Concrete Structures". He was elected as President of fib for the period of 2011-2012. Since then, he is Honorary President of fib. Chairman of fib Com 9 Dissemination of knowledge

1. Introduction

The possibilities of 3D concrete printing in the construction industry are undeniably transformative. This approach involves designing a three-dimensional representation of an object using computer-aided design (CAD) software. Subsequently, this model is divided into layers, generating a G-code that directs the computer-guided motion of the printing nozzle to deposit the concrete [1, 2]. The concrete employed in 3D printing is pumped, extruded through the nozzle, and precisely placed in consecutive layers. This process constructs a three-dimensional element that can bear its load and maintain its form without requiring additional formwork [3, 4]. The process of extruding concrete layer by layer is also known as concrete additive manufacturing or printing with concrete ink [5].

Integrating 3D concrete printing technology into the construction field is seen as a new era for the industry, given its capacity to transform traditional construction methods [6, 7]. Its unique characteristics include construction without formwork, minimal human involvement, reduced material waste, and mass customisation [8, 9]. The technology eliminates formwork costs, reduces labour costs by 50-80%, and lowers construction materials waste at the site by 30-60% [10]. Furthermore, it enhances efficiency at the construction site and diminishes the duration of construction, potentially leading to a further decrease in construction expenses [11]. Compared to traditional construction methods, using additive manufacturing of concrete with structural optimisation has yielded a significant reduction of approximately 50% in environmental impact [12, 13]. Therefore, the construction industry experiences a significant influence from 3D printing technology, and it's essential to recognise its potential advantages.

Many concrete constructions have been successfully built utilising 3D printing technology for concrete, encompassing structures such as buildings, bridges, and walls [14]. Even with the array of varied demonstration construction endeavours, the utilisation of concrete 3D printing for regular building projects is infrequent due to technical complexities. The rheological requirements and the mechanical and enduring capabilities of 3D printed concrete are still in the phases of advancement. Ordinary and high-performance concrete mixes are not directly employable for 3D concrete printing construction due to the incongruity between their rheological properties and the requisites of the printing procedure across various stages.

3D printed concrete is characterised by a layered structure that results from the concrete being deposited in successive layers to achieve a three-dimensional concrete component. These printed concrete elements can manifest two types of connections:

- horizontal interface arises from extruding a concrete layer atop the prior one while,
- depositing layers adjacent to the same level form a vertical interface between them.

The core portion of the extruded concrete holds greater strength compared to the strength observed at the horizontal or vertical layer interfaces. The mechanical characteristics of

printed concrete elements are anisotropic, signifying that the performance of the component relies on the direction of load application relative to the printing orientation, as evident in *Fig. 1*. This anisotropic behaviour may be attributed to the layer-by-layer deposition of the concrete material and can have implications for the structural performance of the printed concrete elements [15–17]. Paul et al. [18] have noted a decline in the compressive strength of printed concrete in contrast to conventionally cast concrete.

Most reported values indicate that the compressive strength of printed concrete is lower when the compressive load is applied along the Z-axis compared to the X-axis and Y-axis. However, [9, 19, 20] reported a higher compressive strength for printed concrete along the Z-axis than the corresponding cast concrete. Notably, these researchers used fibre-containing concrete for printing, which could have contributed to the observed differences in compressive strength. Most tested specimens in the literature to evaluate the compressive strength were extracted from a printed element, ranging from 25-60 mm, containing only one or two printed layers. Therefore, the herein-presented study aims to fill the gap in the literature to achieve the following objectives:

1. Evaluating the compressive strength of printed cubes extracted from a 3D printed slab with a large size of 100 mm tested in three directions: X (load longitudinal to printing direction), Y (load lateral to printing direction), and Z (load perpendicular to the printing direction)
2. Investigate the effect of printing paths on the compressive strength by fully printed cubes in three different paths with a standard size of 150 mm and compared with cast cubes of the same size.
3. For comparison purposes, cast cubes of sizes 100 mm and 150 mm were tested.

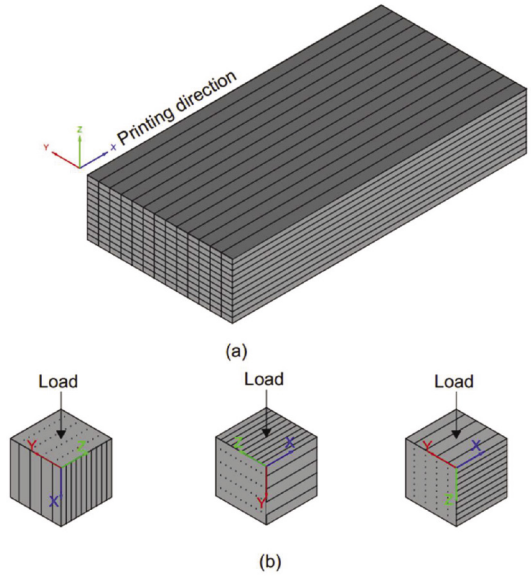

Fig. 1 (a) The anisotropic mechanical behaviour of 3D printed slab, (b) compressive strength measurements in different directions, X direction (layer length), Y direction (layer width), and Z direction (layer height)
1. ábra (a) 3D betonnyomtatással készült lemez anizotrop mechanikai viselkedése (b) nyomószilárdság különböző irányokban: X irány (réteg hosszirány), Y irány (réteg keresztirány) és Z irány (réteg magasság irány)

2. Experimental program

2.1 Materials

The Sikacrete®-751 3D pre-mix of cement containing dry powder, fillers, and specially selected additives was used to prepare the 3D printed and cast specimens. Sikacrete®-751 3D has a light grey-white colour with an accelerated setting suitable for cool climates with a maximum grain size 1 mm. As a 1-component material, it only needs to be mixed with water, providing ease of use. Its fast mixing feature, pumpability, and buildable workability simplify the construction process. Additionally, it exhibits good interlayer adhesion and maintains its shape after extrusion, ensuring dimensional accuracy. The material delivers a uniform and consistent appearance, meeting essential construction needs. *Table 1* shows the mixture properties provided by the producer [21].

Mix component	Cement, aggregate and additives
Max. grain size	1 mm
Density	2140 kg/m³
Compressive strength (DIN EN 196-1)	30 N/mm² (1 day) 40 N/mm² (7 days) 50 N/mm² (28 days)
Young's modulus (DIN EN 13412)	31 GPa (28 days)

Table 1 Mixture properties used in this study [21]
1. táblázat A kutatásban használt keverék jellemzői [21]

2.2 3D Printing System

Different construction methods have emerged to use 3D printing and leverage manufacturing capabilities. Among these techniques, extrusion-based and selective binding (also known as powder-based) methods have become prominent, serving as the foundation for these advancements. This study adopted an extrusion-based technique using a large-scale six-axis robotic system (*Fig. 2*) to perform 3D concrete printing.

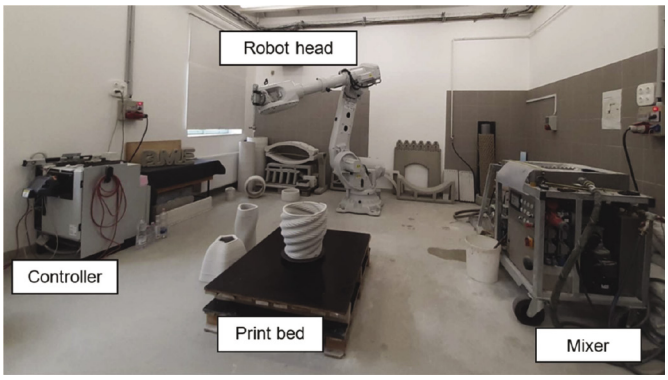

Fig. 2 3D concrete printing equipment (Budapest University of Technology and Economics, Laboratory of Department of Construction Materials)
2. ábra A 3D betonnyomtató komponensei (Budapesti Műszaki és Gazdaságtudományi Egyetem, Építőanyagok és Magasépítés Tanszék Laboratóriuma)

Industrial robotic arms can manifest as many as six rotational degrees of freedom (DOF), which proves advantageous in facilitating the fabrication of intricate and multifaceted geometries. The printing system consists of three essential parts: a mixing and extruder machine, a print head and a controller.

The used mixing machine was MAI®MULTIMIX-3D with a hopper capacity of 45 L, maximum pumping speed of 8 L/min, and maximum particle size of 2 mm. This 3D printing mixing pump is remarkably straightforward across diverse scenarios, allowing for loading from a transportation silo, a large bag, or manual placement using bagged materials. It has a controller, which controls the pumping speed and water amount. The utilised robot was IRB 6700. The robot can perform printing operations with a 360-degree rotational capability, encompassing a horizontal diameter of 3 m and a vertical height of 3 m, and with extension, can reach up to 6 m. The highest achievable printing speed reaches up to 200 mm/s. The robotic arm is connected to a controller that governs the movement of the robotic arm.

2.3 Preparation of the specimens

Printed samples are made using the robotic arm, as detailed in section 2.2. At first, the material was manually loaded to the mixing tank and then started to mix by choosing the appropriate water amount. Upon the finalisation of the mixing procedure, the material is loaded to a feeder system attached to a screw pump. The pump draws the material from the feeder and conveys it to the print head via a flexible hose conduit. The hose has dimensions of 25 mm in diameter and a length of 5 m. A stepper motor propels the pump, ensuring a uniform displacement rate for the material. The pump and the printer are integrated into the control system, which governs the printer's movements and the extrusion velocity at the print head. Ultimately, the material is extruded through a circular nozzle measuring 20 mm at the print head. The water amount, printing speed, pumping speed, layer height, and width were kept the same for all printed specimens: 0.145 L/kg 84 mm/s, 1.5 L/min, 10 mm and 22 mm, respectively.

Preparing printed cubes for studying the printing direction effect on the compressive strength was done by printing a 3D concrete slab with dimensions of 580 mm × 300 mm × 110 mm (L × W × H), as shown in *Fig. 3a*. The printed slab was stored in the lab condition, and before the 28 day testing day, the rectangular slab was cut and polished into nine cubes, each measuring 100 mm × 100 mm × 100 mm, *Fig. 3b*. For the printing paths effect, 150 mm cubes were printed in three different paths, as illustrated in *Fig. 4*. Three nominally identical cubes were printed for each path type. In Path 1, the layer is printed in a zigzag pattern in the odd layer and a zigzag pattern with 90 degrees rotation in the even layer. In Path 2, the layers are printed in a circular route, while in Path 3, the layers are printed in zigzag forms in the exact alignment in both odd and even layers. *Fig. 4a* shows the schematic of the three paths, while *Fig. 4b* shows the top and side views for each path. After printing, the printed cubes were stored in the lab condition and tested at the age of 28 days.

Furthermore, six cast cubes (100 mm) are manufactured for the printing direction test and five cubes with 150 mm dimensions for the printing path test. These specimens are compacted by a vibrating table as regulated in EN 12390-2:2009 [22]. After casting, the top surface of these cubes was covered by a plastic sheet to prevent excessive water evaporation. After 24 hours, these cubes were de-moulded, stored in the ambient temperature, and tested at 28 days.

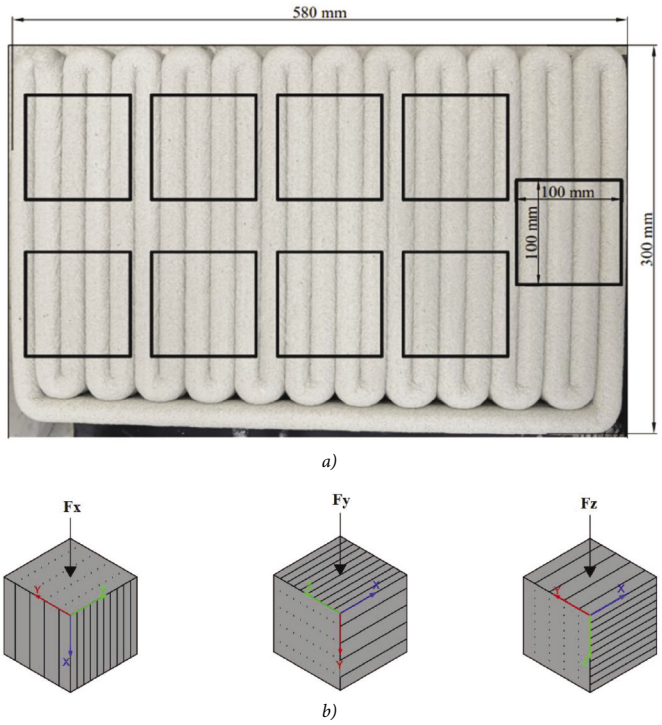

Fig. 3 Details of cut cube specimens with size 100 mm from the 3D printed slab a) Cube-cutting locations, b) Loading directions for compressive strength
3. ábra A 3D nyomtatással készült beton lemezből kivágott 100 mm élhosszúságú kockák a) A próbatestek kinyerésének helyei, b) Terhelési irányok nyomószilárdság mérések esetén

Table 2 outlines the specimens for the compressive strength test, where the nomenclature is as follows: the first three characters (3PC) refer to 3D printed cubes, the second symbol (S) refers to cubes sawed from the printed slab, and the characters (X), (Y) and (Z) refer to the longitudinal, lateral and perpendicular loading directions to the printing direction, respectively. The characters (3FPC) refer to the fully 3D printed cubes with a size of 150 mm, while the notes (P1), (P2), and (P3) represent the fully printed cubes in path direction one, path direction two, and path direction three, respectively. Meanwhile, the (CC) letter indicates the cast cubes.

Specimen Nomenclature	Specimen Size (mm)	No. of Specimen	Type
3PC-S-X	100×100×100	3	Cubes sawed from the printed slab and tested in X direction
3PC-S-Y	100×100×100	3	Cubes sawed from the printed slab and tested in Y direction
3PC-S-Z	100×100×100	3	Cubes sawed from the printed slab and tested in Z direction
3FPC-P1	150×150×150	3	Fully printed cubes in Path1
3FPC-P2	150×150×150	3	Fully printed cubes in Path2
3FPC-P3	150×150×150	3	Fully printed cubes in Path3
CC-100	100×100×100	5	Cast cubes
CC-150	150×150×150	5	Cast cubes

Table 2 Tested specimens.
2. táblázat Vizsgált próbatestek

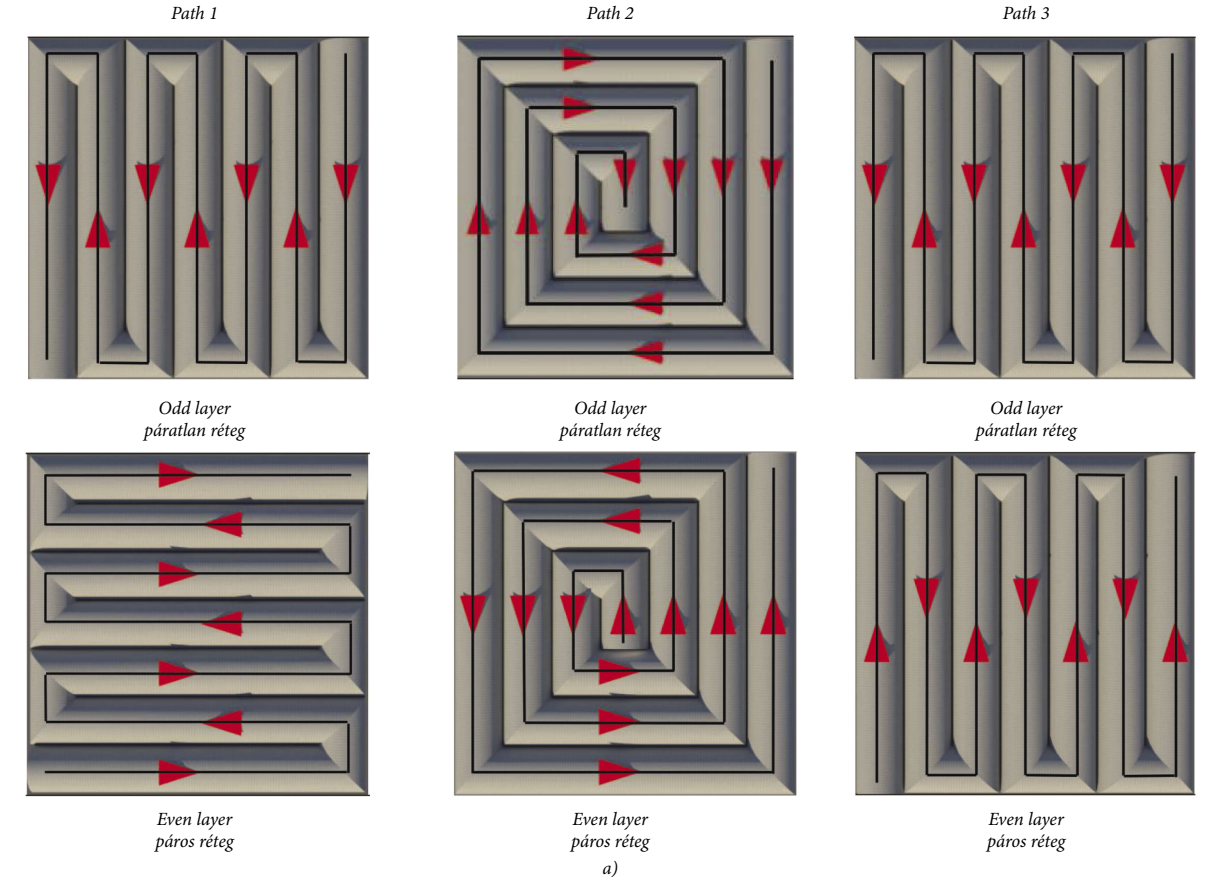

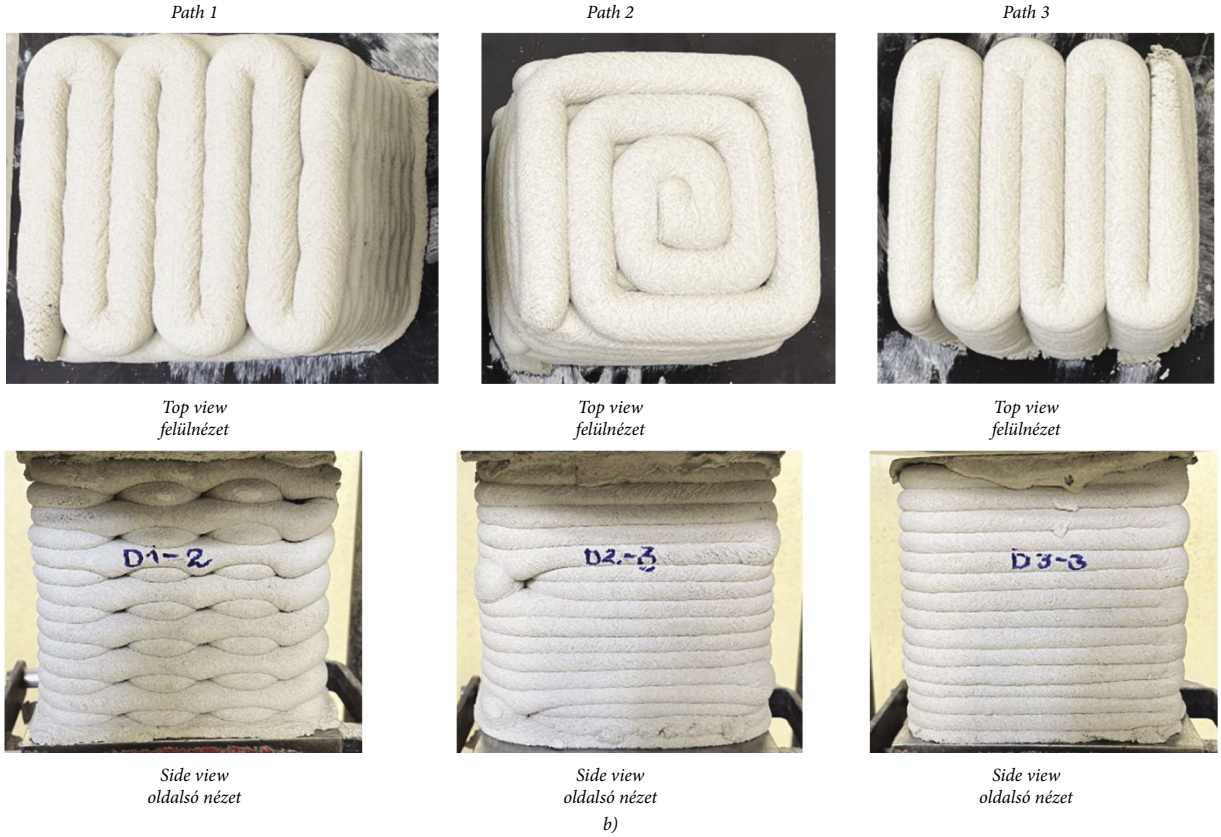

Fig. 4 Details of fully printed cubes with size 150 mm in three different paths. a) Print paths schematic, b) Prepared cubes for the compressive strength test.
4. ábra 150 mm élhosszúságú kockák három eltérő vonalvezetési móddal a) Nyomtatási vonal megadása, b) Kockák nyomószilárdság vizsgálathoz

2.4 Testing of the hardened properties of concrete

A total of nine printed cubes with a size 100 mm were tested to study the effect of printing directions. Three cubes were tested in the X direction (load parallel to the layer length), the second three cubes tested in Y direction (load parallel to the layer width), and the last three cubes were tested in the Z direction (load perpendicular to the layer length), *Fig. 3b*. Meanwhile, nine printed cubes with a size 150 mm were tested to investigate the effect of printing paths on the compressive strength, three cubes in each path. for comparison purposes, ten cast cubes were tested, five with size 100 mm and the other five with size 150 mm. After 28 days, the volume and mass were calculated for all cast cubes, printed cubes for density determination.

The compressive strength of cast and printed cubes was determined by using a compression testing machine with a loading capacity of 3000 kN at a load rate of 11.25 kN/s for 150 mm cubes and 5 kN/s for 100 mm cubes; *Fig. 5* shows the test setup. The compression test was conducted following the specifications of European Standard EN 12390-4:2009 [23]. The compressive strength test was carried out for all cast and printed samples at the age of 28 days.

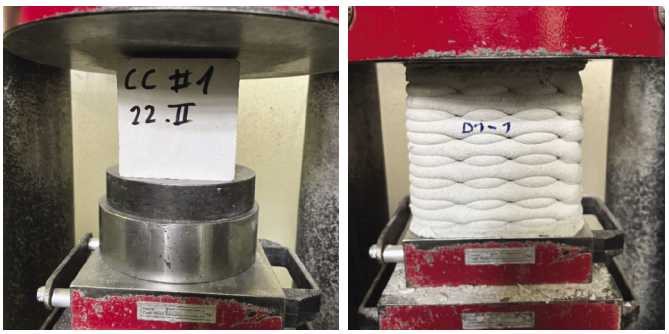

a) b)

Fig. 5 Compressive strength test setup
a) Cast cube, 100 mm, b) Fully printed cube in Path 1, 150 mm
5. ábra Kísérleti elrendezés a nyomószilárdság vizsgálatához
a) 100 mm élhosszúságú, öntött kocka, b) 150 mm élhosszúságú, a Path 1 nyomtatási vonalnak megfelelően

3. Results and discussion

The average compressive strength (f_{cm}) values of the cast cubes and cubes sawed from the 3D printed slab with dimensions of 100×100×100 mm tested in three directions, X, Y and Z directions are shown in *Fig. 6*. Based on the test results, it can be concluded that the cast cubes exhibited a higher average compressive strength of 65.7 MPa, while the printed cubes in the X, Y and Z directions had lower average compressive strengths, with values of 60.87 MPa, 50.07 MPa, and 56.25 MPa, respectively. It is clear from *Fig. 6* that the average compressive strength of the cast specimens is higher than the average compressive strength of 3D printed specimens in X, Y and Z directions by about 7%, 24%, and 14%, respectively.

As well as *Fig. 6* indicates that the printing directions considerably influence the compressive strength of the printed material. As shown, the compressive strength in the longitudinal direction (X direction) is higher by about 18%, and 8%, compared to the lateral direction (Y direction) and the perpendicular direction (Z direction), respectively. This might be explained by the material being compacted in the printing direction due to the extrusion process' mechanical pressure [24, 25]. Similar anisotropic behaviour for several types of printed concrete has been shown in earlier studies [26, 27].

However, the orthotropic behaviour of 3D printed concrete can be minimised by selecting the proper materials and mix design, using the correct nozzle speed, pumping speed, and nozzle shape and reducing the gap time between the layers. For instance, literature [18] indicated that the strength development of specimens printed using a rectangular nozzle was similar to that of conventional cast specimens.

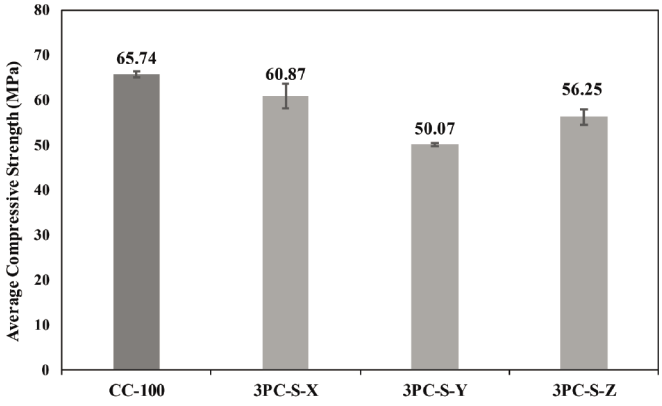

Fig. 6 Average compressive strength of cast and printed cubes with size 100 mm, sawed from printed slab and tested in X, Y and Z directions.
6. ábra 100 mm élhosszúságú nyomtatott és öntött kockák átlagos nyomószilárdsága, a nyomtatott kockák nyomtatott lemezből lettek kivágva és terhelve X, Y és Z irányban

Fig. 7 shows the compressive failure modes of the cast and printed cubes with a size of 100 mm extracted from the printed slab and tested in three different directions regarding the printing directions (longitudinal, lateral and perpendicular). The printed samples displayed a brittle failure mode like cast concrete specimens, with two failure planes extending from the upper and lower edges towards the centre of the sample.

Meanwhile, the average compressive strengths of the cast and fully printed in three different paths with dimensions of 150×150×150 mm are shown in *Fig. 8*. The test results showed that the cast cubes exhibited the highest average compressive strength at 52.1 MPa. In contrast, the fully printed cubes in Path1, Path2, and Path3 had progressively lower average compressive strengths of 46.6 MPa, 32.9 MPa, and 41.1 MPa, respectively. The cast specimen's average compressive strength is higher than that of 3D fully printed specimens in Path1, Path2 and Path3 by about 11%, 37%, and 21%, respectively.

The printing path significantly affects the compressive strength of the printed cubes. The highest compressive strength was achieved by Path1, followed by Path3 and then Path2. The strength of printed cubes in Path1 was higher than that of the strength of cubes printed in Path2 and Path3 by about 29% and 12%, respectively. Moreover, the results show higher variations in Path2 and Path3 by about 5.78 and 4.65, respectively. While the variation of the results in Path1 is much lower, 1.57 compared to the other paths.

Fig. 9 shows the compressive failure modes of the cast and fully printed cubes with a size of 150 mm in three different paths. The 3D printed specimens in Path1 and Path3 failed similarly to the cast specimens. Meanwhile, the printed specimens in Path2 had a vertical crack passed along the specimen.

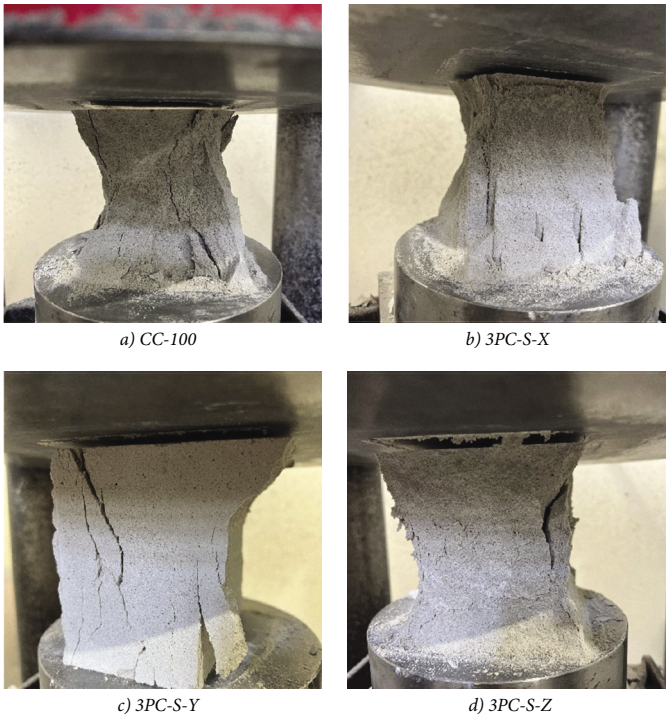

a) CC-100 *b) 3PC-S-X*

c) 3PC-S-Y *d) 3PC-S-Z*

Fig. 7 Compressive failure modes of cast and printed cubes with size 100 mm, sawed from printed slab and tested in X, Y and Z directions.
7. ábra Nyomási tönkremeneteli módok 100 mm élhosszúságú nyomtatott és öntött kockák esetén, a nyomtatott kockák nyomtatott lemezből lettek kivágva és terhelve X, Y és Z irányban

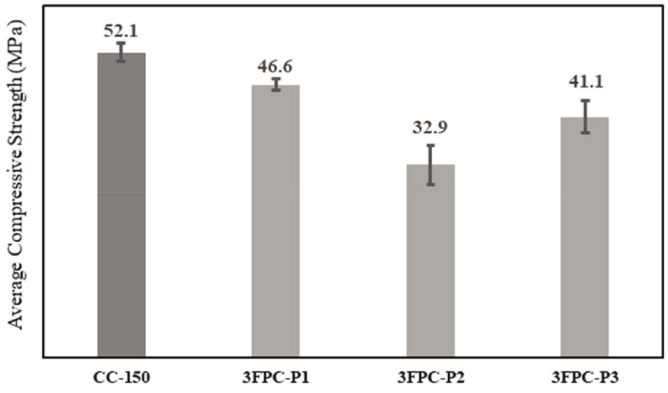

Fig. 8 Average Compressive strength of cast and 3D fully printed cubes in three paths with size 150 mm.
8. ábra 150 mm élhosszúságú öntött, ill. három nyomtatási vonalnak megfelelően nyomtatott kockák nyomószilárdsági vizsgálata

The results of the compressive strength (f_{cm}), and hardened density (HD), at 28 days for the cast cubes and printed cubes in different directions and different paths are presented in *Fig. 10* and *Fig. 11*, respectively. In this study, the density of conventionally cast cubes and 3D printed cubes were compared. The results showed that the average hardened density of printed cubes in X, Y and Z directions are 2150, 2149, and 2145 kg/m^3, respectively, which are slightly more than that of cast concrete with 2100 kg/m^3. The higher density of printed cubes, which also seen in [20, 26], is because it gets well compacted under the pressure during extrusion, as well as these cubes sawed from the middle part of the printed slab which compacted well compared to the outer layers.

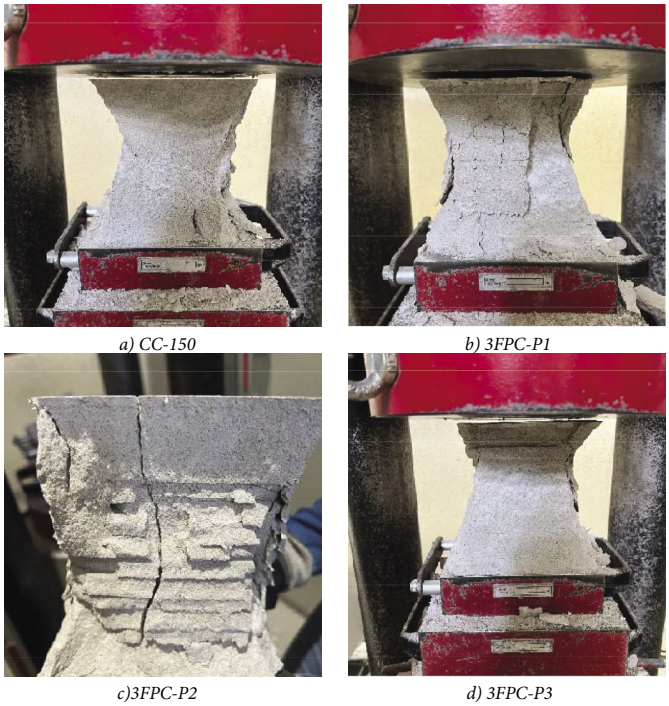

a) CC-150 *b) 3FPC-P1*

c)3FPC-P2 *d) 3FPC-P3*

Fig. 9 Compressive failure modes of the cast and 3D fully printed cubes in three paths with size 150 mm.
9. ábra 150 mm élhosszúságú öntött, ill. három nyomtatási vonalnak megfelelően nyomtatott kockák nyomószilárdsági vizsgálata – törésképek

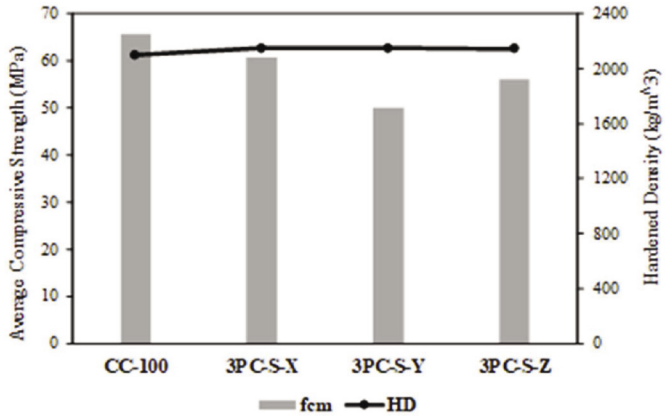

Fig. 10 Compressive strengths and hardened density results for cubes tested in X and Z directions.
10. ábra Nyomószilárdság és porozitás vizsgálati eredmények a kockák X és Z irányú vizsgálatából

In contrast, the average hardened density of cast cubes with size 150 mm is 2071 kg/m^3, which is higher than that of fully printed cubes in Path1, Path2, and Path3 with 2008, 1888, and 1930 kg/m^3, respectively. The density of cast cubes was considerably higher by about 3.04%, 8.84%, and 6.81%, compared to the density of printed cubes in Path1, Path2, and Path3, respectively. This can be explained by the characteristics of 3D printing, such as the free-flowing nature of the material in the lateral direction and the potential for entrapped air voids in the absence of vibration, as compared to the conventional

mould casting approach. As well as the printed layers in the middle has more restrictions from the outer layers. Moreover, due to layering the sides of the printed cubes are uneven thus the volume will be higher compared to the cast cubes, and it will effect on the density calculations.

These findings offer a potential explanation for the observed decrease in compressive strength in Path2, attributing it to a lower density along this circular route. This reduced density may arise from increased voids or insufficient bonding in the circular path, which could substantially impact the compressive strength of the 3D printed cube in this Path2.

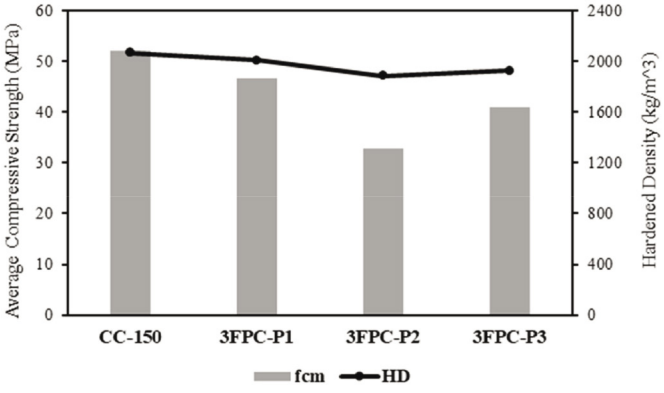

Fig. 11 Compressive strengths and hardened density results for cubes printed and tested in three different paths.
11.ábra Nyomószilárdság és porozitás eredmények a kockák vizsgálatából, ahol a nyomtatás három eltérő vonal mentén történt

4. Conclusions

The possibilities of 3D concrete printing in the construction industry are undeniably transformative. Nevertheless, the layer-by-layer printing process substantially impacts the orthotropic nature of the printed object, influencing its compressive strength in various directions. Therefore, the main purpose of the presented study is to investigate the effect of printing direction and printing paths on the compressive strength of 3D printed cubes.

Two different cube sizes were used in this study. Printed cubes with *size 100 mm* sawed from 3D printed slab and tested in X, Y and Z directions (loading parallel, lateral and perpendicular to the printing direction). Whole 3D printed cubes with a standard size of *150 mm* were printed in three different paths. In Path 1, the layer is printed in a zigzag pattern in the odd layer and a zigzag pattern with 90 degrees rotation in the even layer. In Path 2, the layers are printed in a circular route, and in Path 3, the layers are printed in zigzag forms in the exact alignment in both odd and even layers. Cast cubes with sizes 100 mm and 150 mm were also used for comparison purposes. Based on the results of our study, the following conclusions can be deduced.

Specimens sawed from *printed slab*:

1. The average compressive strength of the cast specimens is higher than the average compressive strength of 3D printed specimens in X, Y and Z directions by about 7%, 24%, and 14%, respectively.
2. The direction of loading considerably affects the strength of the printed material. The compressive strength in the X direction is higher by about 18%, and 8% compared to the Y, and Z directions, respectively. This can be explained by the orthotropic behaviour of 3D printed concrete can be minimised by selecting the proper materials and mix design, using the correct nozzle speed, pumping speed, and nozzle shape and reducing the gap time between the layers.
3. The density of the cast and printed cubes is approximately the same, and this can be attributed to printed cubes sawed from the middle part of the printed slab which compacted well compared to the outer layers.

Specimens printed with *different paths*:

1. The average compressive strength of the cast cube with the standard size 150 mm is higher than the compressive strength of 3D fully printed specimens in Path1, Path2 and Path3 by about 11%, 37%, and 21%, respectively.
2. *The printing path* significantly affects the compressive strength of the printed cubes. The highest compressive strength was achieved by Path1, followed by Path3 and then Path2. The strength of printed cubes in Path1 was higher than that of the strength of cubes printed in Path2 and Path3 by about 29% and 12%, respectively.
3. The average hardened density of cast cubes is considerably higher by about 3.04%, 8.84%, and 6.81%, compared to the average hardened density of fully printed cubes in Path1, Path2, and Path3, respectively. This can be explained by the characteristics of 3D printing, such as the free-flowing nature of the material in the lateral direction and the potential for entrapped air voids in the absence of vibration.

Though the studied printing directions and printing paths parameters in this paper show a considerable effect on the compressive properties of the concrete, further research is necessary to fully assess the impact of other printing parameters (e.g., printing speed, layer thickness, the gap time and the bond between the layers) on the mechanical properties of 3D printed elements.

5. Acknowledgements

The *Stipendium Hungaricum Scholarship* Program is highly acknowledged for supporting the PhD study and research work. Authors acknowledge the support by the Hungarian Research Grant VKE 2018-1-3-1_0003 "Development of advanced concrete elements". Thanks to Anna Szijártó and Balázs Burai for their help in the printing process and the laboratory measurements.

References

[1] Li, Z., Wang, L. and Ma, G. (2020). Mechanical improvement of continuous steel microcable reinforced geopolymer composites for 3D printing subjected to different loading conditions. *Compos B Eng* 187.
[2] Paolini, A., Kollmannsberger, S. and Rank, E. (2019). Additive manufacturing in construction: A review on processes, applications, and digital planning methods. *Addit Manuf* 30.
[3] Roussel, N. (2018). Rheological requirements for printable concretes. *Cem Concr Res* 112. 76–85.

[4] Chen, Y., He, S., Gan, Y., Çopuroğlu, O., Veer, F. and Schlangen, E. (2022). A review of printing strategies, sustainable cementitious materials and characterization methods in the context of extrusion-based 3D concrete printing. *Journal of Building Engineering* 45.

[5] Thajeel, M. M. and Balazs, G. L. (2022). 3D Printing-Challenges for Concrete Printing. In *Next Generation of Concrete Engineering for Post-Pandemic Europe* pp 110–3. 13th Central European Congress On Concrete Engineering, CCC 2022 Zakopane.

[6] Al Rashid, A., Khan, S. A., G. Al-Ghamdi, S. and Koç, M. (2020). Additive manufacturing: Technology, applications, markets, and opportunities for the built environment. *Autom Constr* 118.

[7] Apa) Chen, Y., Veer, F. ; and Copuroglu, O. (2017). *A critical review of 3D concrete printing as a low CO_2 concrete approach*.

[8] Menna, C., Mata-Falcón, J., Bos, F. P., Vantyghem, G., Ferrara, L., Asprone, D., Salet, T. and Kaufmann, W. (2020). Opportunities and challenges for structural engineering of digitally fabricated concrete. *Cem Concr Res* 133.

[9] Arunothayan, A. R., Nematollahi, B., Ranade, R., Bong, S. H., Sanjayan, J. G. and Khayat, K. H. (2021). Fiber orientation effects on ultra-high performance concrete formed by 3D printing. *Cem Concr Res* 143.

[10] Zhang, J., Wang, J., Dong, S., Yu, X. and Han, B. (2019). A review of the current progress and application of 3D printed concrete. *Compos Part A Appl Sci Manuf* 125.

[11] De Schutter, G., Lesage, K., Mechtcherine, V., Nerella, V. N., Habert, G. and Agusti-Juan, I. (2018). Vision of 3D printing with concrete — Technical, economic and environmental potentials. *Cem Concr Res* 112. 25–36.

[12] Agustí-Juan, I. and Habert, G. (2017). Environmental design guidelines for digital fabrication. *J Clean Prod* 142. 2780–91.

[13] Alimrani, N. S., Thajeel, M. M. and Balázs, G. L. (2022). Structural aspects of topology optimization in 3d printing of concrete. *Concrete Structures* 23. 41–6.

[14] Thajeel, M. M., Alimrani, N. S. and Balázs, G. L. (2022). 3D Concrete printing structural and non-structural solutions. *Concrete Structures* 23. 47–53.

[15] Ma, G., Li, Z., Wang, L., Wang, F. and Sanjayan, J. (2019). Mechanical anisotropy of aligned fiber reinforced composite for extrusion-based 3D printing. *Constr Build Mater* 202. 770–83.

[16] Feng, P., Meng, X., Chen, J. F. and Ye, L. (2015). Mechanical properties of structures 3D printed with cementitious powders. *Constr Build Mater* 93. 486–97.

[17] Ma, G., Zhang, J., Wang, L., Li, Z. and Sun, J. (2018). Mechanical characterization of 3D printed anisotropic cementitious material by the electromechanical transducer. *Smart Mater Struct* 27.

[18] Paul, S. C., Tay, Y. W. D., Panda, B. and Tan, M. J. (2018). Fresh and hardened properties of 3D printable cementitious materials for building and construction. *Archives of Civil and Mechanical Engineering* 18. 311–9.

[19] Soltan, D. G. and Li, V. C. (2018). A self-reinforced cementitious composite for building-scale 3D printing. *Cem Concr Compos* 90. 1–13.

[20] Pham, L., Tran, P. and Sanjayan, J. (2020). Steel fibres reinforced 3D printed concrete: Influence of fibre sizes on mechanical performance. *Constr Build Mater* 250.

[21] Available online: https://www.https://www.sika.com/en/serp.html?q=Sikacrete%C2%AE-751+3D+&box=Top. [Access date: 2023. 10. 29].

[22] EN 12390-2:2009. Testing hardened concrete - Part 2: Making and curing specimens for strength tests.

[23] EN 12390-3:2009. Testing hardened concrete - Part 3: Compressive strength of test specimens.

[24] Asprone, D., Menna, C., Bos, F. P., Salet, T. A. M., Mata-Falcón, J. and Kaufmann, W. (2018). Rethinking reinforcement for digital fabrication with concrete. *Cem Concr Res* 112. 111–21.

[25] Sanjayan, J. G., Nematollahi, B., Xia, M. and Marchment, T. (2018). Effect of surface moisture on inter-layer strength of 3D printed concrete. *Constr Build Mater* 172. 468–75.

[26] Le, T. T., Austin, S. A., Lim, S., Buswell, R. A., Law, R., Gibb, A. G. F. and Thorpe, T. (2012). Hardened properties of high-performance printing concrete. *Cem Concr Res* 42. 558–66.

[27] Bong, S. H., Nematollahi, B., Nazari, A., Xia, M. and Sanjayan, J. (2019). Method of optimisation for ambient temperature cured sustainable geopolymers for 3D printing construction applications. *Materials* 12.

Ref.:
Thajeel, Marwah M. – **Sólyom**, Sándor – **Balázs**, György L.: *Impact of Printing Directions and Printing Paths on the Compressive Strength of 3D Printed Concrete*
Építőanyag – Journal of Silicate Based and Composite Materials, Vol. 76, No. 1 (2024), 31–38 p.
https://doi.org/10.14382/epitoanyag-jsbcm.2024.4

GUIDELINE FOR AUTHORS

The manuscript must contain the followings: title; author's name, workplace, e-mail address; abstract, keywords; main text; acknowledgement (optional)**; references; figures, photos with notes; tables with notes; short biography** (information on the scientific works of the authors).

The full manuscript should not be more than 6 pages including figures, photos and tables. Settings of the word document are: 3 cm margin up and down, 2,5 cm margin left and right. Paper size: A4. Letter size 10 pt, type: Times New Roman. Lines: simple, justified.

TITLE, AUTHOR

The title of the article should be short and objective.

Under the title the name of the author(s), workplace, e-mail address.

If the text originally was a presentation or poster at a conference, it should be marked.

ABSTRACT, KEYWORDS

The abstract is a short summary of the manuscript, about a half page size. The author should give keywords to the text, which are the most important elements of the article.

MAIN TEXT

Contains: materials and experimental procedure (or something similar), results and discussion (or something similar), conclusions.

REFERENCES

References are marked with numbers, e.g. [6], and a bibliography is made by the reference's order. References should be provided together with the DOI if available.

Examples:

Journals:

[6] Mohamed, K. R. – El-Rashidy, Z. M. – Salama, A. A.: In vitro properties of nano-hydroxyapatite/chitosan biocomposites. *Ceramics International.* 37(8), December 2011, pp. 3265–3271, http://doi.org/10.1016/j.ceramint.2011.05.121

Books:

[6] Mehta, P. K. – Monteiro, P. J. M.: Concrete. Microstructure, properties, and materials. *McGraw-Hill*, 2006, 659 p.

FIGURES, TABLES

All drawings, diagrams and photos are figures. The **text should contain references to all figures and tables**. This shows the place of the figure in the text. Please send all the figures in attached files, and not as a part of the text. **All figures and tables should have a title**.

Authors are asked to submit color figures by submission. Black and white figures are suggested to be avoided, however, acceptable.

The figures should be: tiff, jpg or eps files, 300 dpi at least, photos are 600 dpi at least.

BIOGRAPHY

Max. 500 character size professional biography of the author(s).

CHECKING

The editing board checks the articles and informs the authors about suggested modifications. Since the author is responsible for the content of the article, the author is not liable to accept them.

CONTACT

Please send the manuscript in electronic format to the following e-mail address: femgomze@uni-miskolc.hu and epitoanyag@szte.org.hu or by post: Scientific Society of the Silicate Industry, Budapest, Bécsi út 122–124., H-1034, HUNGARY

We kindly ask the authors to give their e-mail address and phone number on behalf of the quick conciliation.

Építőanyag – *Journal of Silicate Based and Composite Materials*, Quarterly peer-reviewed periodical of the Hungarian Scientific Society of the Silicate Industry, SZTE.
http://epitoanyag.org.hu

14th International Conference on Ceramic Materials and Components for Energy and Environmental Systems

18–22 August 2024
Budapest Congress Center
Budapest, Hungary

Invitation to CMCEE-14

The 14th International Conference on Ceramic Materials and Components for Energy and Environmental Applications (CMCEE-14) will be held in the beautiful city of Budapest, Hungary. The conference series began in 1980s and has established a strong reputation for state-of-the-art presentations and information exchange on the latest emerging ceramic technologies and their wide ranging applications. CMCEE-14 will contain more than 30 symposia covering wide range of topics, which will facilitate global dialogue and discussion with leading world experts to ceramic technologies for sustainable development of society.

We would like to invite all of you to actively participate in the conference and visit the city of Budapest. We are quite hopeful that this conference will provide excellent forum for interaction and friendship with participants from various continents.

We hope to meet you all in 2024!

About Budapest

Budapest is famous not only for the monuments reflecting its own 1,000-year-old culture, but also for the relics of others who settled here. Remains from both Roman occupation and much later ruled by the Turks can still be seen in the city. After the Ottoman Empire the union with Austria has a particular influence on the city's form and style.

Conference venue

Budapest Congress Center & Novotel Budapest City****Budapest Congress Center is the largest, most convenient, modern event facility in Budapest. It has over 20 meeting rooms in various shapes and sizes, adjustable for every possible need, as well as an exhibition space of over a 4000 m^2, which means it can hold separate events at the same time without them interfering with each other. International congresses, exhibitions, professional conferences, corporate meetings, gala dinners, tradeshows, fairs, concerts, plays or graduation ceremonies – Budapest Congress Center is perfect for them all!

https://akcongress.com/cmcee14